STRUCTURE AND RHEOLOGY OF CUBIC PARTICLES IN SUSPENSIONS

A Dissertation

Presented to the Faculty of the Graduate School

of Cornell University

in Partial Fulfillment of the Requirements for the Degree of

Doctor of Philosophy

by

Rajesh Kumar Mallavajula

May 2014

STRUCTURE AND RHEOLOGY OF CUBIC PARTICLES IN SUSPENSIONS

Rajesh Kumar Mallavajula, Ph.D.

Cornell University 2014

It is well known that the shape of particles is an important factor that determines the fluid flow behavior of suspensions. Interactions of cubic particles with one another and with the flow medium are unique because of their sharp edges, corners and flat surfaces. Using theory, simulations and experiments, the structure and flow properties of cube-shaped particles in suspension over a range of volume fractions is studied to understand the effect of shape on fluid structure and rheology.

At very low volume fractions, the sharp edges and corners of cubes are found to profoundly alter the velocity field around the cube.The stresslet-strain relationship for a cube is anisotropic and depends on the orientation of the cube with respect to the velocity flow field. The effective viscosity of the suspension in a simple shear flow is obtained by computing the orientationaly averaged stresslet acting on cubes. These calculations yield a universal intrinsic viscosity, $[\eta] = 3.1$ for sharp cubes, which is higher than the corresponding value for spheres $[\eta] = 5/2$. Using the 2D velocity flow profile around sharp corners we further find that the pressure becomes singular near the edges of the cube, which results in the increased value of stress and hence the higher viscosity when compared with spherical particles.

In the presence of an external torque acting on each cube, the orientation distribution is no longer isotropic. This can be achieved by using magnetic cubes in magnetic field. The general expression for the stress in a suspension of mag-

netic cubes subjected to linear velocity field in presence of an external magnetic field is calculated. We find that the intrinsic viscosity for the weakly Brownian suspension in a simple shear flow can be varied between $[\eta] = 3.25$ to $[\eta] = 5.5$ by changing the strength and the direction of the applied magnetic field.

At low to moderate volume fractions, Brownian dynamics simulations were carried out to study the structure and flow behavior of suspensions. Simulations were performed over a wide range of volume fractions and Pe to study its rheological properties. Our equilibrium results show that cubic particles behave like spheres interacting with a soft repulsion potential function for volume fractions less than 0.25. This soft repulsion potential captures the orientationally averaged excluded volume of the cubes and produces identical probability distributions as that of for cubes at very low volume fractions. For higher volume fractions, cubic particles starts to lose their orientational freedom resulting in the deviation of equilibrium properties from that of soft spheres. We also found that suspension of cubic particles when subjected to simple shear will produce higher viscosity when compared with spherical particles in suspensions with equivalent volume. We show that the suspension rheology in this regime can be discussed in terms of ordering and collisions among hard cubic particles.

In order to gain insights from experiments, cubic particles of varying sizes (10nm to 5 micron sized cubes) and chemistries ($PbTe$,Fe_3O_4 and $MnCO_3$) were synthesized. Polymer brushes were also attached on the surfaces of $PbTe$ and Fe_3O_4 nanocubes to characterize the effect of particle surface chemistry on flow behavior. $MnCO_3$ spherical particles of similar sizes as that of $MnCO_3$ cubes were also synthesized and their suspension behavior studied to empirically characterize the effects of shape. A key result from this study is that irrespective of the cube size, size distribution, and surface chemistry, the intrinsic viscosity($[\eta]$)

for cube-shaped particles is $[\eta] = 3.1 \pm 0.2$ which agrees well with the value estimated from theory.

BIOGRAPHICAL SKETCH

Rajesh Kumar Mallavajula was born to parents M. Anjaneya Prasad and Vijaya Laxmi in Hyderabad, India on September 12, 1984. After completing his high school from Paramita High School, he passed the Joint Entrance Examination and joined Indian Institute of Technology Bombay in the field of Chemical Engineering. In his undergraduate studies, he developed his interests in transport phenomena and colloidal science. As a part of his undergraduate thesis, he evaluated the diffusion coefficient of sugar crystals in water using differential interference contrast microscopy. After working for a year in a consulting firm, he joined the PhD program in the department of Chemical and Biomolecular Engineering at Cornell University. His strong interest in understanding the fluid flow behavior using both theory and experiments has motivated him to work with Prof. Lynden Archer and Prof. Donald Koch at Cornell University since spring 2009.

Dedicated to my grand parents, parents and my dear brother

ACKNOWLEDGEMENTS

Firstly, I would like to thank both Professor Lynden Archer and Professor Donald Koch for being the ideal advisors that I hoped for. Prof. Archer is extremely enthusiastic and gave me the freedom to work on a range projects. I have worked on at least three different research topics. Weekly meetings with him have always renewed my enthusiasm towards my research goals. I inevitably left every meeting with some new avenues to explore and encouragement for my half-baked ideas. Prof. Koch is a clear thinker, extremely intuitive and has the ability to give insights into the problem in many different ways. He is such an approachable person that no matter how small the question is I can always find an answer from him. I will never forget how inspired I was when I took the advanced fluids course. Both of them have been very patient with me and motivated me when things did not seem to work out. Under their guidance, I feel that I have become more organized, better communicator and a mature researcher. I will forever treasure the advice that I have received in the past five years.

I am grateful to have Prof. Itai Cohen serve on my committee. His insights into colloids and suspension science have broadened my perspective. I enjoyed all the discussions in the rheology group meetings.

I am going to miss some of the intellectually stimulating discussions (and sometimes not so intellectual) with Kasyap and Indu, John Singh, Mukul, Arijeet, Anubhab and Senjuti. I would like to thank them for putting up with the unexpected ups and downs grad school brings.

I found Archer group lab to be extremely collaborative environment. I would like to thank Snehashis Choudary, Adam Hardimann, Ashwin Narayanan, Shekar Moganty, Shyamal Das, Jai Prakash, Zhengyuan Tu, Ying

Ying Lu for working with me on my research projects.

I have enjoyed my time with DFB housemates (Desi Frat Boys, as we call ourselves) which includes Praveen Agarwal, Shantanu Rajwade, Mihir Khadilkar, Umang Agarwal and Anirikh Chakraborthy. Some of our popular dinner table discussions would be related to philosophy, international and Indian politics or research outlook in various fields. Quick shout to CIA, (Cornell India Association) and all the people that I had met through it. They have all made my stay in Ithaca more enjoyable.

Even before my time at Cornell, my professors at IIT Bombay helped me understand and appreciate Chemical Engineering after which I have decided to pursue a PhD degree. I would like to particularly thank Prof. Mahesh Tirumkudulu for developing my interests in fluids.

Finally, and most importantly, I am very much indebted to my parents, my dear brother and my late grand parents for always being there for me. I have counted on their wisdom, encouragement and advice at every stage of my life and words cannot express my love and respect for them.

TABLE OF CONTENTS

LIST OF TABLES

LIST OF FIGURES

CHAPTER 1

INTRODUCTION

Suspensions are important in a large number of applications and in a variety of natural and industrial settings. Examples include handling and transportation of solid particulates and in manufacturing processes such as food processing, ceramics and paints. The flow behavior is often complex and depends on many factors such as the shape, size and concentration of particles, shear rate and medium viscosity. This work deals with understanding the importance of shape of the particle on the transport properties of suspensions. Currently, nanoparticles in a spectrum of sizes, shapes, mass distributions (e.g. hollow, rattles, core-shell), and chemistries are routinely synthesized using a growing set of wet chemistry approaches: sol-gel, solvothermal, ionothermal, soft and hard templating, to name a few. It is now possible to synthesize particles in variety of shapes, including tetrahedrons, cubes, rods, polyhedrals and non-convex shapes[1, 2, 3, 4] in bulk quantities.

Since Einstein[5] developed a theoretical expression for the viscosity of dilute suspension of spherical particles, a large number of studies have concentrated on theoretical prediction and experimental evaluation of transport properties of suspensions[6, 7, 8, 9]. For the most part, these studies have been restricted to spherical particles and axisymmetric particles such as ellipsoids, rods and discs in the medium[10, 11]. The effect of the shape of the particle is still not very clearly understood. The goal of my research is to develop more insights into this dependence. We restrict ourselves to cube shaped particles since they form an ideal geometry with sharp corners, edges, flat surfaces and yet no aspect ratio. We study the rheological properties of cubic particle suspensions

both using numerical simulations and experiments. We have synthesized cubic particles of various sizes and chemistries to study the flow behavior experimentally.

In the second chapter of my research, we analyze the distinct geometric properties of cube and define a fourth order tensor to define its symmetry properties. We have calculated the velocity profile of the fluid past a fixed cube using multipole and finite element method. The problem was solved for three imposed velocity fields: 1) constant velocity (v_i) at infinity 2) constant angular velocity ω at infinity ($v_i = \epsilon_{ijk}\omega_i r_j$) and 3) planar extensional flow field ($v_i = E_{ij}r_j$). Here r_i is any position vector. In multipole method, the velocity profile around a cube is written using multipole series expansion with unknown coefficients. Assuming that the contribution of higher ordered terms are negligible, the number of terms in the expansion are truncated to $O(\frac{1}{r^5})$ for constant velocity field problem and $O(\frac{1}{r^4})$ for extensional velocity field problem. Appropriate boundary conditions are applied to obtain these unknown coefficients. The obtained velocity profile is then used to calculate the stress acting on an isolated cube near the interface between the particle and fluid. This is in turn used to calculate some of the basic properties such as drag force, torque drag and stresslet on a cube in constant flow, rotational and planar extensional fields respectively. In the finite element method, a cube is placed at the center of another cubic enclosure and the region is meshed with many grid points. Required velocity conditions are imposed on the walls of the enclosure to generate the flow field in the medium. Since the disturbance velocity field due to the presence of walls produces an $O((\frac{a}{H})^3)$ scaling (H and a are the side lengths of the enclosure and the cube respectively), we obtain the results for various H/a and extrapolate the results for the infinite enclosure. The results from multipole series expansion

and finite element method are compared to validate the assumption that the higher order terms are negligible.

In the third chapter, we developed a theoretical expression for the viscosity of dilute suspension of cubic particles. We calculate the intrinsic viscosity, which measures the intrinsic ability of cubic particles to increase the viscosity. It is defined as the limit of the ratio of the fractional increase in viscosity to the volume fraction as the volume fraction goes to zero. Unlike spherical particles, intrinsic viscosity for cubic suspensions also depends on the orientation of each cube in the suspension. When there are no external forces/torques acting on hard cubic particles, the orientation distribution is isotropic. We calculate the dependence of viscosity as a function of the orientation of the cube and is orientationally averaged to get the bulk viscosity of the suspension. We solved the finite element solution of simple shear flow around an isolated cube for two specific orientations. Using the symmetry of the cube and the solutions for two specific orientations, we obtain the stresslet and the viscosity for any orientation of the cube. Geometric properties like the sharp edges and corners affect flow profile around the cube. In the finite element method, the sharpness of the edges and corners can be varied using the grid spacing on the surface of the cube. The stresslet acting on the particle was found to increase with the sharpness of the cube. A theoretical scaling for this increase was predicted using the 2D flow profile around edges. The results for the stresslet were fitted with this scaling to obtain the results for cubes with sharp edges and corners. The suspension viscosity, η_{eff}, in the limit of zero shear rate can be obtained from the orientational average of the stresslet acting on the cube, yielding a prediction of $\eta_{eff} = \eta_0(1 + 3.1\phi)$. Here η_0 is the solvent viscosity, ϕ is the volume fraction of cubic particles in suspension and the coefficient 3.1 is the intrinsic viscosity $[\eta]$ for

cubes. The calculated value of $[\eta]$ for cubes is larger than the computed value for spheres ($[\eta] = 5/2$). To validate our prediction using experiments, we have synthesized cube-shaped particles of various sizes, chemistries and measured their rheological properties in dilute suspensions. Experimentally, we have synthesized three different systems, lead telluride nanocubes (PbTe, 10nm) iron oxide nanocubes (Fe_3O_4, 20nm) and (Fe_3O_4, 100nm) as model hard cube particles. Polymer brushes were attached on the PbTe and Fe_3O_4 cube surfaces to characterize the effect of particle surface chemistry on flow behavior. These particles were suspended in polyethylene glycol (PEG, MW 250) and their intrinsic viscosity was measured. We found that irrespective of cube size, size distribution and surface chemistry, the intrinsic viscosity was $[\eta] = 3.1 \pm 0.2$, which is in excellent agreement with the theory.

When there is no external torque acting on the cubes, the dependence of stress on orientation is not apparent since the orientation distribution is isotropic. In the next chapter, we introduce anisotropy in orientation distribution, by studying the viscosity of dilute suspension of magnetic cubes in an external magnetic field. When a uniform external magnetic field is applied on the suspension, each cube experiences a net external torque whenever the magnetic dipole moment of the cube is not aligned with the applied magnetic field. The competition between the viscous torque and the magnetic torque will result in anisotropic orientation distribution. The degree of anisotropy was varied by changing the direction and the magnitude of the applied magnetic field and its effect on the viscosity was studied. We have calculated the general expression for the stress in the dilute suspension of magnetic cubes in presence of magnetic field, subjected to linear shear flow field. We have also obtained specific numerical results for the intrinsic viscosity of the suspension in a simple shear flow,

when the magnetic field is either parallel or perpendicular to the fluid vorticity vector. When the magnetic field is perpendicular to vorticity, we find that the intrinsic viscosity increases at first with increasing shear rate. It passes through a maximum and then shear thins. The intrinsic viscosity can vary from 3.25 to 5.5 in response to changes in the relative strengths of the shear and magnetic fields. The maximum value of 5.5 for the intrinsic viscosity was obtained, when the magnetic moment of the cube, which is parallel to one of the normals is in the flow gradient plane and is aligned at an angle of $\pi/4$ to the flow direction. The minimum value was obtained when the magnetic moment if parallel to the fluid vorticity.

The chapter five of my thesis is related to the flow behavior of cubic particle suspensions at low to moderate concentrations. Brownian dynamic simulations for hard cubic particles in a suspension were carried out to understand stresses in the medium for both equilibrium and sheared suspensions. These numerical simulations include contact stresses developed between two randomly oriented cubes colliding with each other. Inter-particle hydrodynamic interactions were not considered in these simulations. Instead, the anisotropic stress-strain relationship developed for a isolated cube was used to calculate the hydrodynamic stress in the suspensions. Simulations are performed over a wide range of volume fractions ϕ and Peclet numbers (Pe). Using radial distribution functions, osmotic pressure, viscosity, normal stresses, the structure and rheological properties of these suspensions was studied. Comparisons were made with the corresponding properties of spherical particles in suspension to study the influence of sharp edges, corners and flat surfaces.

In chapter six, we measure the rheological properties of cubic particles in

suspensions. We discuss the procedures used to synthesize cubic particles of various chemistries. We have used iron oxide ($Fe_3O_4, 100nm$) and $MnCO_3$ microcubes to study the rheology at low to moderate volume fractions. $MnCO_3$ spherical particles of similar sizes were also synthesized and their suspension behavior studied to empirically characterize the effects of shape. The rheological measurements at dilute and moderate volume fractions were correlated with the theory and simulations. We found that Fe_3O_4 cubic nanoparticles show shear thinning behavior due to inter-particle magnetic interactions, while $MnCO_3$ microcubes show Newtonian behavior up to volume fraction (ϕ) of 0.3. The second order correction, which is the coefficient of ϕ^2 for the relative viscosity was measured as 6.54, which is close to that of the value for spherical particles in suspensions [12].

BIBLIOGRAPHY

[1] D. Kim, N. Lee, M. Park, B. H. Kim, K. An, and T. Hyeon. Synthesis of uniform ferrimagnetic magnetite nanocubes. *Journal of the American Chemical Society*, 131(2):454, 2009.

[2] J. Joo, S. G. Kwon, J. H. Yu, and T. Hyeon. Synthesis of zno nanocrystals with cone, hexagonal cone, and rod shapes via non-hydrolytic ester elimination sol-gel reactions. *Advanced Materials*, 17(15):1873, 2005.

[3] L Manna, DJ Milliron, A Meisel, EC Scher, and AP Alivisatos. Controlled growth of tetrapod-branched inorganic nanocrystals. *Nature Materials*, 2(6):382–385, 2003.

[4] X. G. Peng, L. Manna, W. D. Yang, J. Wickham, E. Scher, A. Kadavanich, and A. P. Alivisatos. Shape control of cdse nanocrystals. *Nature*, 404(6773):59–61, 2000.

[5] A Einstein. *Investigation on the theory of the Brownian movement*. Dover Publications, 1956.

[6] K. C. Nunan and J. B. Keller. Effective viscosity of a periodic suspension. *Journal of Fluid Mechanics*, 142:269–287, 1984.

[7] S. R. Aragon and D. K. Hahn. Preaveraged hydrodynamic interaction revisited via boundary element computations. *Journal of Chemical Theory and Computation*, 2(1):12–17, 2006.

[8] J. F. Douglas and E. J. Garboczi. Intrinsic viscosity and the polarizability of particles having a wide range of shapes. *Advances in Chemical Physics, Vol 91*, 91:85–153, 1995.

[9] John F. Brady. Computer simulation of viscous suspensions. *Chemical Engineering Science*, 56(9):2921 – 2926, 2001.

[10] SB Chen and DL Koch. Rheology of dilute suspensions of charged fibers. *Physics of Fluids*, 8(11):2792–2807, 1996.

[11] Jan Mewis and Norman J. Wagner. Current trends in suspension rheology. *Journal of Non-Newtonian Fluid Mechanics*, 157(3):147 – 150, 2009.

[12] G. K. Batchelor and J. T. Green. The hydrodynamic interaction of two small freely-moving spheres in a linear flow field. *Journal of Fluid Mechanics*, 56:375–400, 10 1972.

CHAPTER 2

RESISTIVITY FOR AN ISOLATED CUBE IN A LINEAR FLOW FIELD

The goal of this chapter is to understand the unique symmetric properties of a cube and calculate some of the basic properties such as the translational and rotational resistivities for a cube. We know that the translational resistivity (R_t^s) for a sphere with radius a in a medium of viscosity η is given by $R_t^s = 6\pi a\eta$ and the rotational resistivity (R_ω^s) is $R_\omega^s = 8\pi\eta a^3$. It is a common practice to approximate any shape with a sphere of equivalent diameter. The resistivity for a cube is generally approximated as the resistivity of a sphere with an equivalent diameter that has same volume as the cube. This leads to the translational (R_t) and rotational resistivities(T_ω) for the cube as $R_t = 11.68a\eta$ and $R_\omega = 6\eta a^3$. These equations are generally used to calculate the approximate size of particles using dynamic light scattering experiments. However, accurate results for the cube resistivities to our knowledge are not available in the literature. In order to calculate the resistivities accurately, we begin by calculating the flow properties past an isolated cube in an external linear flow. The velocity profiles in the fluid is solved for two cases: 1) constant velocity at infinity and 2) constant rotational field at infinity. The velocity profile was calculated using both multipole and finite element method for the first case and only finite element method for the second case. The velocity profiles were then used to calculate the stress acting at the interface between the particle and the fluid. The drag force and torque drag acting on the cube for the respective cases are calculated from stress. Translational and rotational resistivities are the coefficients for the net force and the net torque on the cube.

2.1 Geometric properties of a cube

Cube is a platonic solid bounded by six square faces. Firstly, we wish to capture the symmetry properties of the cube mathematically by defining cube specific symmetric tensors. The defined tensor should adhere to the cubic symmetry operations which leave a cube invariant. Let us assume that a unit cube is placed in an arbitrary cartesian reference frame. For simplicity, let us define three normal vectors perpendicular to the adjacent sides of the cube, n_i, m_i, p_i though only two of the three vectors are sufficient to describe its orientation as shown in the figure 2.1. The property tensor, that defines the orientation of the cube must be a function of the above three vectors. The symmetry of the cube dictates that this property tensor should be an even function of n_i, m_i, p_i, since interchanging n_i, m_i or p_i with $-n_i, -m_i$ or $-p_i$ does not change its orientation. Similarly, it should be symmetric in n_i, m_i, p_i (i.e n_i, m_i, p_i are interchangeable with each other).

The second order symmetric tensor, which satisfies the above conditions is

$$\delta_{ij} = (n_i n_j + m_i m_j + p_i p_j) \tag{2.1}$$

Since, n_i, m_i, p_i are orthonormal, δ_{ij} is the identity tensor. Similarly, we can define two fourth order symmetric tensors which satisfy the symmetry properties of a cube:

$$A_{ijkl} = \quad (n_i n_j n_k n_l + m_i m_j m_k m_l + p_i p_j p_k p_l) \tag{2.2}$$

$$\begin{aligned} B_{ijkl} = \quad & (n_i n_j + m_i m_j + p_i p_j)(n_k n_l + m_k m_l + p_k p_l) \\ & +(n_i n_l + m_i m_l + p_i p_l)(n_k n_j + m_k m_j + p_k p_j) \\ & +(n_l n_j + m_l m_j + p_l p_j)(n_k n_i + m_k m_i + p_k p_i) \end{aligned} \tag{2.3}$$

Simplifying the above equations, we get

$$A_{ijkl} = \delta_{ijkl} = \quad 1, \text{ for } i = j = k = l; \tag{2.4}$$

$$= \quad 0, \text{ otherwise}$$

$$B_{ijkl} = \quad \delta_{ij}\delta_{kl} + \delta_{ik}\delta_{jl} + \delta_{il}\delta_{jk} \tag{2.5}$$

B_{ijkl} is a fourth order isotropic tensor which also satisfies other more symmetric shapes such as spheres. However, δ_{ijkl} is a fourth order tensor, which is specific to the cubic symmetry. Similarly, we can extend the analysis and obtain higher order tensors which satisfy the cubic symmetry. For example, the sixth order cube specific symmetry tensors are:

$$\begin{aligned}
\alpha_{ijklqr} &= \delta_{ijklqr} \\
\beta_{ijklqr} &= \delta_{ijkl}\delta_{qr} + \delta_{ijqr}\delta_{kl} + \delta_{klqr}\delta_{ij} + \delta_{ijkq}\delta_{lr} + \delta_{ijkr}\delta_{ql} \\
&+ \delta_{ijql}\delta_{kr} + \delta_{ijrl}\delta_{kq} + \delta_{iqkl}\delta_{jr} + \delta_{irkl}\delta_{qj} + \delta_{qjkl}\delta_{ir} \\
&+ \delta_{rjkl}\delta_{qi} + \delta_{kjqr}\delta_{il} + \delta_{ikqr}\delta_{jl} + \delta_{jlqr}\delta_{ik} + \delta_{ilqr}\delta_{kj}
\end{aligned} \tag{2.6}$$

The velocity profile around an isolated cube should be a function of these symmetry tensors. Similar symmetry tensors were used previously in defining the cubic symmetry in problems with periodic suspensions. [1] [2] [3]

2.2 Velocity profile around a cube using multipole series expansion

The equations of motion governing the fluid motion for steady flow past any object at low Reynolds number is given by incompressible Stokes equations.

$$\nabla p = \nabla^2 u \tag{2.7}$$

$$\nabla . u = 0 \tag{2.8}$$

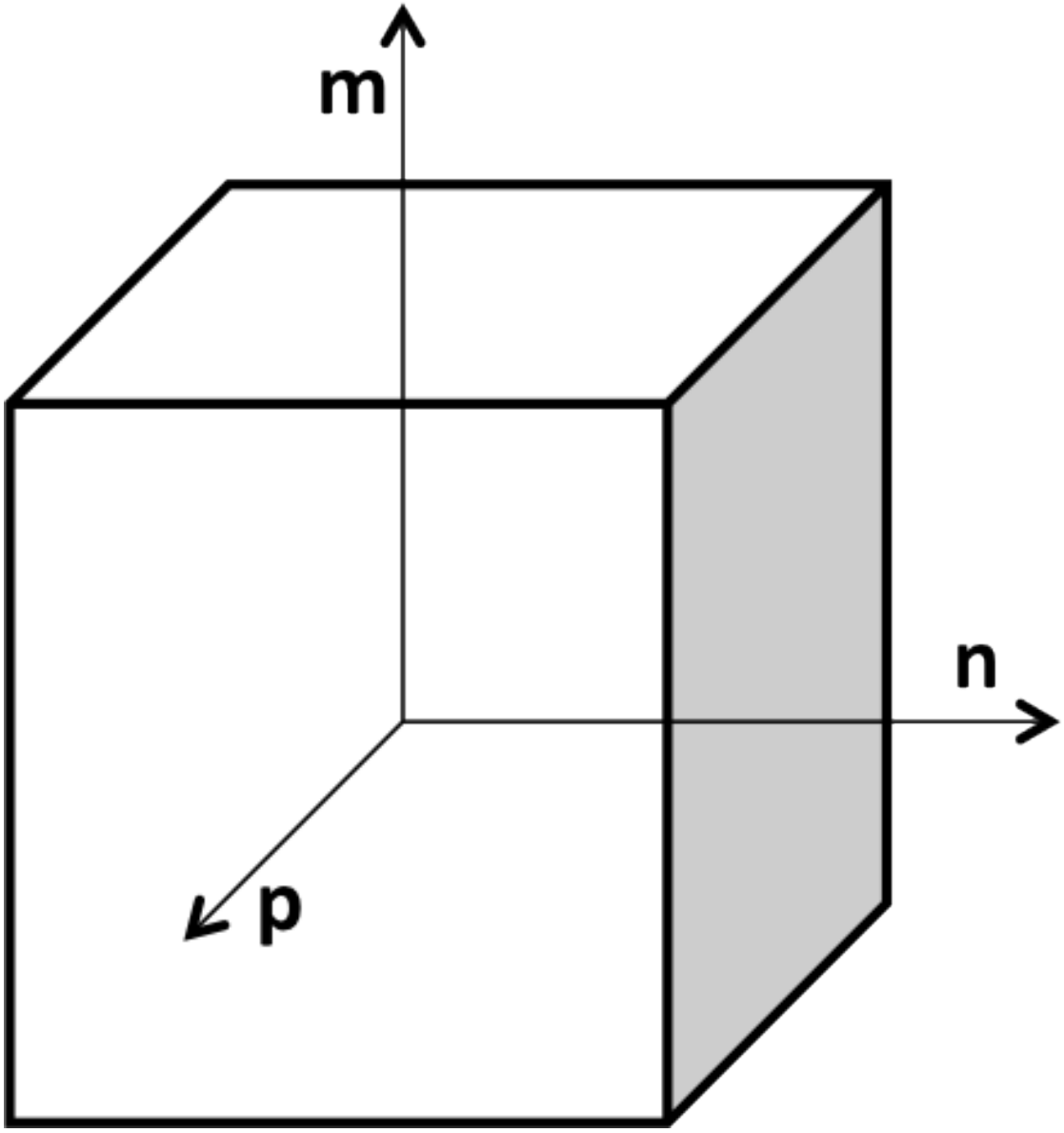

Figure 2.1: Orientation of a cube is defined by the three normal vectors n_i, m_i, p_i

The general solution for velocity (u_i) and pressure(p) at any point in the fluid is given by the infinite multipole series expansion [4], [5]

$$
\begin{aligned}
u_i &= \frac{\partial}{\partial r_i}\Phi + \epsilon_{ijk}\frac{\partial}{\partial r_j}\chi_k + A_j.J_{ij} + B_{jk}\frac{\partial}{\partial r_k}J_{ij} + C_{jkl}\frac{\partial}{\partial r_k}\frac{\partial}{\partial r_l}J_{ij} + D_{jklm}\frac{\partial}{\partial r_k}\frac{\partial}{\partial r_l}\frac{\partial}{\partial r_m}J_{ij} + ... \\
p &= A_iK_i + B_{ij}\frac{\partial}{\partial r_j}K_i + C_{ijk}\frac{\partial}{\partial r_j}\frac{\partial}{\partial r_k}K_i + ... \qquad (2.9) \\
\Phi &= A^{\Phi}\frac{1}{r} + B_i^{\Phi}\frac{\partial}{\partial r_i}\frac{1}{r} + C_{ij}^{\Phi}\frac{\partial}{\partial r_i}\frac{\partial}{\partial r_j}\frac{1}{r} + ... \\
J_{ij} &= \frac{1}{8\pi\mu}(\frac{\delta_{ij}}{r} + \frac{r_ir_j}{r^3}) \\
K_i &= \frac{1}{4\pi}\frac{r_i}{r^3} \qquad (2.10)
\end{aligned}
$$

Here, J_{ij} is the free-space Greens function, known alternatively as the Stokeslet or Oseen tensor. The tensor variables $A_j, B_{jk}, C_{jkl}, D_{jklm}, A^{\Phi}, B_i^{\Phi}, C_{ij}^{\Phi}$ are evaluated based on the flow and boundary conditions.

Consider an isolated cube in an externally applied uniform linear flow field. We use the above described solutions to obtain the pressure and velocity in the fluid. Since tensors are our friends, the unknown variables in the general solution should be only dependent on the symmetry tensors of the cube and the external flow field conditions. We exploit this relation and simplify the terms in the multipole series and finally truncate it to obtain the approximate velocity profile around the cube. This velocity profile is then used to calculate other bulk properties such as force, torque, stress and stresslet acting on the whole cube.

2.3 Translational and rotational resisitivies for a cube

We solve for the velocity profile around an isolated cube moving with a constant velocity (v_i) in a infinite quiescent fluid medium of viscosity η_0. The unknown

tensor variables in the multipole series should be only dependent on the following tensors: 1) v_i 2) δ_{ij}, 3)δ_{ijkl}, 4) α_{ijklqr}, 5) β_{ijklqr} and other higher order cubic symmetry tensors. Furthermore, due to the linearity of Stokes equation, the velocity profile around the cube should be a linear function of v_i. Since the even ordered tensor variables such as B_{ij}, D_{ijkl} cannot be expressed in terms of the above defined tensors, they should be equal to zero. The odd order tensor variables can be expressed as:

$$A_j = \lambda_1 v_j \tag{2.11}$$

$$C_{jkl} = \lambda_2(v_j\delta_{kl} + v_k\delta_{jl} + v_l\delta_{jk}) \tag{2.12}$$

$$\begin{aligned} E_{jklmn} &= \lambda_3(v_j\delta_{klmn} + v_k\delta_{jlmn} + v_l\delta_{kjmn} + v_m\delta_{kljn} + v_n\delta_{klmj}) \\ &+ \lambda_4(v_j(\delta_{kl}\delta_{mn} + \delta_{kn}\delta_{ml} + \delta_{km}\delta_{nl}) + v_k(\delta_{jl}\delta_{mn} + \delta_{jn}\delta_{ml} + \delta_{jm}\delta_{nl}) \\ &+ v_l(\delta_{kj}\delta_{mn} + \delta_{kn}\delta_{mj} + \delta_{km}\delta_{nj}) + v_m(\delta_{kl}\delta_{jn} + \delta_{kn}\delta_{jl} + \delta_{kj}\delta_{nl}) \\ &+ v_n(\delta_{kl}\delta_{mj} + \delta_{kj}\delta_{ml} + \delta_{km}\delta_{jl})) \end{aligned} \tag{2.13}$$

$$B_i^{\Phi} = \lambda_5 v_j \tag{2.14}$$

$$D_{ijk}^{\Phi} = \lambda_6(v_j\delta_k l + v_k\delta_{jl} + v_l\delta_{jk}) \tag{2.15}$$

The unknown scalar variables $\lambda_1, \lambda_2, \lambda_3, \lambda_4, \lambda_5, \lambda_6$ are evaluated by applying the no slip boundary conditions on the surface of the cube.

$$u_i = v_i, \text{ on the surface of the cube} \tag{2.16}$$

$$= 0, \text{ at infinity} \tag{2.17}$$

We assume that the higher order terms in the infinite series are negligible and the solution for the velocity is truncated to $O(1/r^5)$. Therefore, the velocity and the pressure profiles are given by

$$u_i = A_j.J_{ij} + C_{jkl}\frac{\partial}{\partial r_k}\frac{\partial}{\partial r_l}J_{ij} + E_{jklmn}\frac{\partial}{\partial r_k}\frac{\partial}{\partial r_l}\frac{\partial}{\partial r_m}\frac{\partial}{\partial r_n}J_{ij} + B_i^{\Phi}\frac{\partial}{\partial r_i}\frac{1}{r} + D_{ijk}^{\Phi}\frac{\partial}{\partial r_i}\frac{\partial}{\partial r_j}\frac{\partial}{\partial r_k}\frac{1}{r}$$

$$p = A_i K_i + C_{ijk}\frac{\partial}{\partial r_j}\frac{\partial}{\partial r_k}K_i + E_{ijklm}\frac{\partial}{\partial r_j}\frac{\partial}{\partial r_k}\frac{\partial}{\partial r_l}\frac{\partial}{\partial r_m}K_i \tag{2.18}$$

Equations 2.12 through 2.16 expresses the variables $A_i, C_{ijk}, D_{ijklm}, B_i^{\Phi}$ and C_{ijk}^{Φ} using unknown scalar variables: $\lambda_1, \lambda_2, \lambda_3, \lambda_4, \lambda_5$ and λ_6 . Since we have truncated the multipole series, we apply a relaxed boundary condition to calculate the scalar unknown variables:

$$\int u_i \frac{du_i}{d\lambda_j} dA = \int v_i \frac{du_i}{d\lambda_j} dA, \text{ for } j = 1, 2, 3, 4, 5, 6 \tag{2.19}$$

The integration is carried out over the surface of the cube. After solving these equations, we find that $\lambda_1 = 9.2$; $\lambda_2 = 0.07$; $\lambda_3 = 1.5$; $\lambda_4 = 2.2$; $\lambda_5 = -0.075$; and $\lambda_6 = -0.075$.

The stress in the medium is then calculated from the velocity profile. [6]

$$\sigma_{ij} = -p\delta_{ij} + \eta_0\left(\frac{\partial u_i}{\partial r_j} + \frac{\partial u_j}{\partial r_i}\right) \tag{2.20}$$

Net force acting on the cube is obtained by integrating the stress over the surface of the cube.

$$F_i = \int \sigma_{ij} n_j dA \tag{2.21}$$

Substituting the values of λ_1, λ_2, λ_3, λ_4, λ_5, and λ_6, we find that the force acting on the cube is given by

$$F_i = 12.4 a \eta v_i \tag{2.22}$$

We have also used finite element method to calculate the velocity profile around the cube. In this problem, we solve for the velocity profile around a stationary cube in a constant velocity field. COMSOL was employed to solve the Stokes equations of motion in the fluid around a cube of side length a centered in a cubic simulation cell of side length H. The region was meshed with many

grid points and constant velocity boundary conditions were imposed on the external walls of the cell. The velocity profile around the cube is shown in the figure 2.2. Integration of stress over the surface area of the cube yields the force acting on it. The finite domain size produces a fluid velocity disturbance which scales as $(a/H)^2$. The value of force was calculated by extrapolating to $a/H \to 0$. The force acting on the cube was found to be:

$$F_i = 13.94 a \eta v_i \tag{2.23}$$

Similarly, we calculate the torque on an isolated stationary cube placed in fluid which rotates with a constant angular velocity (ω) ($v_i = \epsilon_{ijk}\omega_j r_k$). Following the similar procedure used to calculate force, velocity profile was obtained using COMSOL by fixing a cube of side a at the centered of a cubic simulation cell of side H and imposed velocity boundary conditions are applied on the walls. Even for this case, the fluid velocity disturbance scales as $(a/H)^2$ and so the results were extrapolated for $(a/H) \to 0$. Figure 2.3 shows the velocity profile in the fluid near the surface and it the mid-plane of the cube. The magnitude of torque acting on the cube is given by

$$T_i = \int \epsilon_{ikl} r_k \sigma_{lj} n_j dA \tag{2.24}$$

We found that the torque acting on the cube fixed in a rotational flow field is

$$L_i = 7.39 a^3 \eta_0 \omega \tag{2.25}$$

Here η is the viscosity of the medium and ω_i is the imposed angular velocity.

2.4 Conclusions

The value of translational resistivity was found as $R_t = 12.4a\eta$ from multipole series and $R_t = 13.94a\eta$ from finite element method. The value of rotational resistivity was found to be $R_\omega = 7.39a^3\eta$ from finite element method. Assuming that the cube is a sphere with equivalent diameter, we get the diameter of the sphere as $1.24a$. Therefore the translational and rotational resistivities based on this diameter are $R_t = 11.68a\eta$ and $R_\omega = 6a^3\eta$. This approximation under estimates the translational diffusvity by 15% and about 18% for rotational diffusivity. The discrepancy in these values may be because of the presence of sharp edges in the cubes which leads to singular stresses around it. Using the values of resistivities, the translational tracer diiffusivity (D_t) and rotational tracer diffusivity (D_ω) can be evaluated with the help of Stokes- Einstein equation [7].

$$D_t = \frac{kT}{R_t} = \frac{kT}{13.94a\eta} \tag{2.26}$$

$$D_\omega = \frac{kT}{7.39a^3\eta} = \frac{kT}{7.39a^3\eta} \tag{2.27}$$

The tracer diffusivities and resisitivities are used as inputs in the Brownian dynamics simulations.

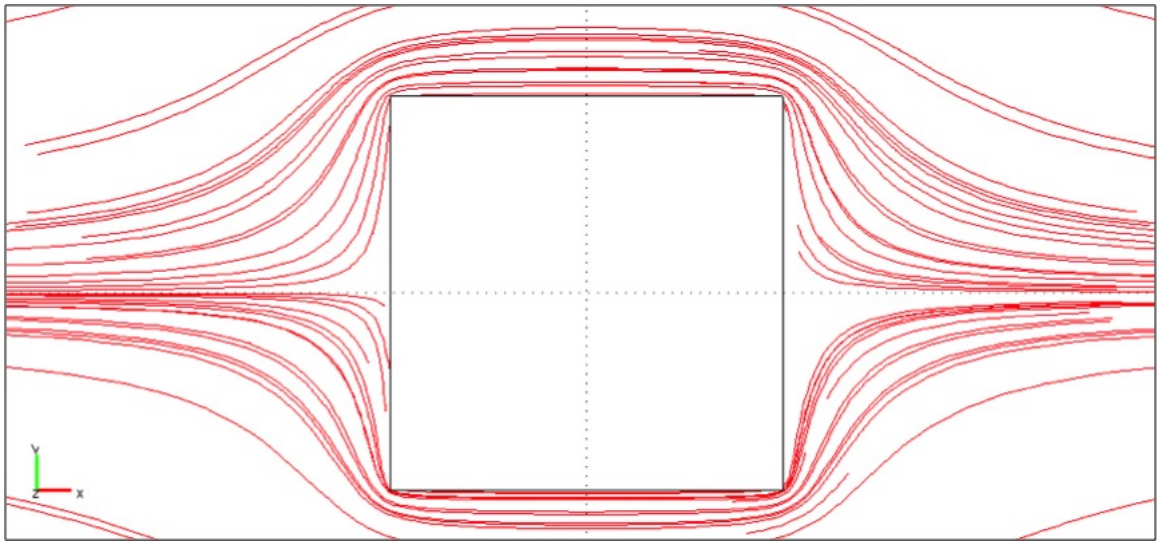

Figure 2.2: Velocity profile around the cube in a constant velocity field evaluated using COMSOL. The streamlines are plotted at the center plane of cube.

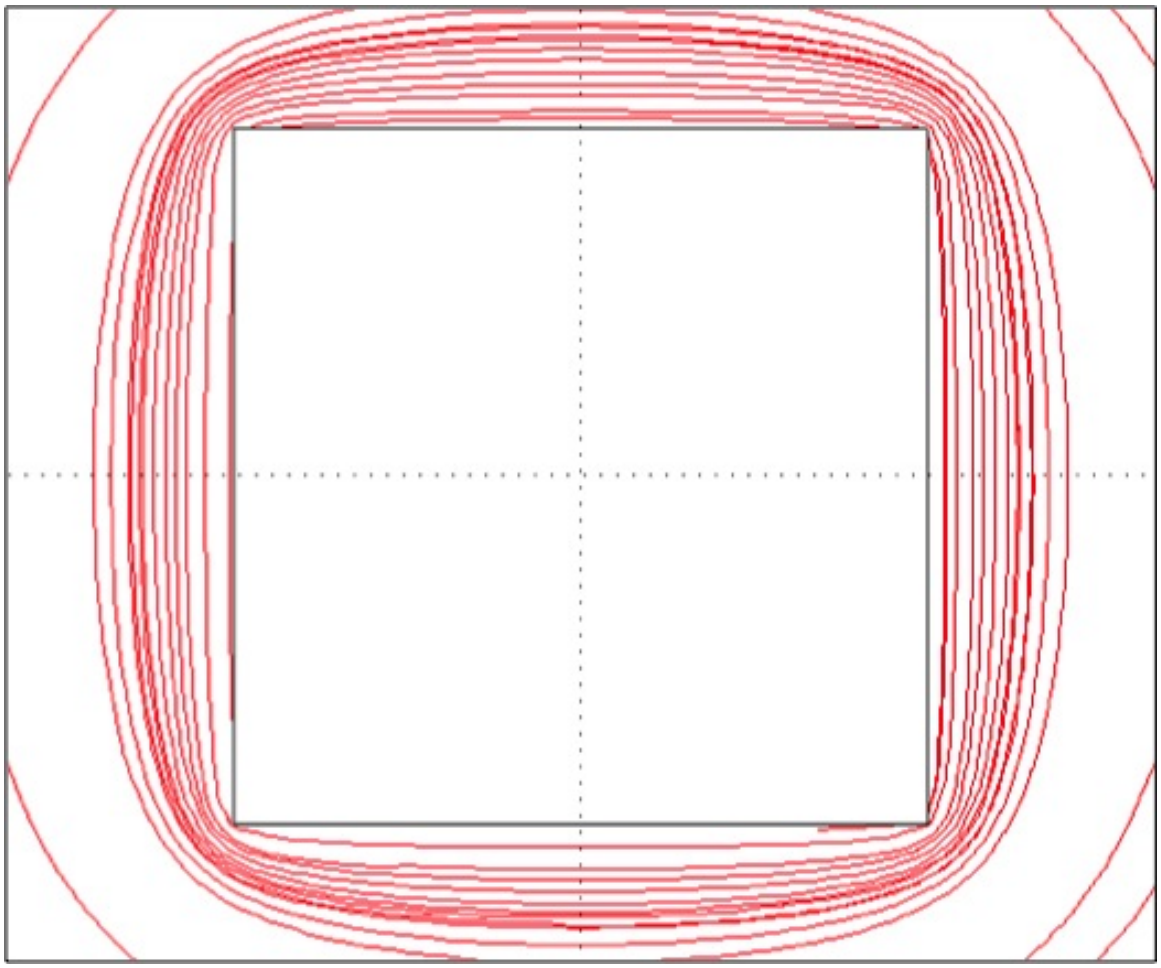

Figure 2.3: Velocity profile around a stationary cube placed in a constant angular velocity field. The streamlines are plotted for the center plane

BIBLIOGRAPHY

[1] K. C. Nunan and J. B. Keller. Effective viscosity of a periodic suspension. *Journal of Fluid Mechanics*, 142:269–287, 1984.

[2] E. J. Hinch. Note on the symmetries of certain material tensors for a particle in stokes flow. *Journal of Fluid Mechanics*, 54:423–425, 1972.

[3] A. S. Sangani; A. Acrivos. The effective conductivity of a periodic array of spheres. *Proceedings of the royal society A*, 386:263, 1983.

[4] W. B. Russel. *Colloidal Dispersions*. Cambdrige University Press, 1999.

[5] Sir Horace Lamb. *Hydrodynamics*. Dover Publications, 1932.

[6] G. K. Batchelor. The stress system in a suspension of force-free particles. *Journal of Fluid Mechanics*, 41:545–570, 4 1970.

[7] S. Kim and S.J. Karrila. *Microhydrodynamics: Principles and Selected Applications*. Butterworth-Heinemann, 1991.

CHAPTER 3

INTRINSIC VISCOSITY OF A SUSPENSION OF CUBES

3.1 Abstract

We report on the viscosity of a dilute suspension of cube-shaped particles. Irrespective of the particle size, size distribution and surface chemistry, we find empirically that cubes manifest an intrinsic viscosity $[\eta] = 3.1 \pm 0.2$, which is substantially higher than the well-known value for spheres, $[\eta] = 2.5$. The orientation-dependent intrinsic viscosity of cubic particles is determined theoretically using a finite element solution of the Stokes equations. For isotropically oriented cubes, these calculations show $[\eta] = 3.1$, in excellent agreement with our experimental observations.

3.2 Introduction

There has been an upsurge in recent interest in understanding how the shape, size, surface topology and chemistry of nanoparticles influence their assembly [1][2]. This interest is sustained by the promise such assemblies offer for creating novel particle-based, meta-materials in which particles, not atoms, are the fundamental building blocks [3][4]. Many methods have been proposed to synthesize particles in a variety of shapes, including tetrahedrons, cubes, rods, polyhedrals and non-convex shapes[5, 6, 7, 8]. And, it is now feasible to produce particles in bulk quantities[9] for many of these shapes. By varying the geometric and other attributes of the particles it is possible to manipulate electronic and

optical properties of materials [10, 11, 12] for applications.

Using Monte Carlo and molecular dynamics simulations it has been shown that shape plays an important role in both static and dynamic behavior of bulk nanoparticle assemblies [13]. For example, molecular simulations of 2D square shaped discs reveal self assembly to form tetratic and square crystal phases[13]. These results are notably different from experimental observations, where it has been reported that Brownian square-shaped particles do not form tetratic or square crystal phases, but instead assemble into a hexagonal rotor crystal phase or a rhombic crystal phase [14]. Molecular simulations by Avendano et. al., [15] show that slight rounding of the squares used in experiments are the source of the discrepancy. In particular, it was shown that the particles will self-assemble to form observed phases if the radius of curvature of the corners non-dimensionalized by the cube length is more than 0.165. There are few easily measurable properties that depend only on the shape of particles in a suspension, which would allow these subtle effects to be quantified apriori and their potential effects on assembly diagnosed.

3.3 Synthesis of nanocubes and suspension characterization

The intrinsic viscosity $[\eta] = \lim_{\phi \to 0} \frac{\eta - \eta_s}{\phi \eta_s}$, defined in the limit of zero volume fraction ϕ quantifies the contribution that the suspended phase makes to augment the viscosity η_s of the suspending phase and set the overall viscosity η. It is related to the fluid resistance incurred in the shear flow around a single suspended particle to maintain a bulk flow. The intrinsic viscosity therefore provides a simply measured physical quantity that can be used to diagnose even

subtle features of the suspended particle shapes. Unlike commonly used techniques such as transmission electron microscopy (TEM) and scattering which can characterize particle shape from femtoliter and smaller volumes within a bulk material, $[\eta]$ is determined from bulk measurements and involves averages over very large numbers of individual particles.

To quantify the intrinsic viscosity of cube-shaped particles, PbTe hard cubes were synthesized using a simple solution procedure [16]. The approach leads to particles with a mean edge length of 9.5 nm with the distribution shown in Figure 3.1. The particles have very high surface areas and would aggregate without steric stabilization. PbTe particles were stabilized by oleic acid or polymer brushes tethered to the particle surface. In order to study rheology, these particles were suspended in a low molar mass polyethylene glycol (PEG, MW 400), which exists as a neat viscous liquid at 25 °C. Cone-and plate (50 mm diameter, 5° gap angle) shear measurements in a Rheometrics Ares rheometer at 25 °C were used to characterize the shear viscosity of oleic-acid stabilized PbTe particles in PEG over a wide range of particle volume fractions ϕ. Figure 3.1(b) reports the relative viscosity, $\eta_r = \eta/\eta_s$ as a function of ϕ for these suspensions. It is apparent from the figure 3.1 that $\eta_r = 1 + k\phi$ over a rather broad range of ϕ. This indicates that inter-particle interactions and other multibody hydrodynamic effects are negligible at the measurement conditions. The linear slope of the straight line fitted to the data yields $[\eta] = 4.25 \pm 0.4$, which is evidently substantially higher than the well-known result $[\eta] = 2.5$ for suspensions of spheres. Because the PbTe cubes have oleic acid attached on their surface, the effective particle volume fraction, ϕ, is larger due to the size of the oleic acid brush. Assuming that the oleic acid chains are fully extended, the brush height on the particles is 0.56 nm. The open symbols in Figure 3.1(b) are the relative

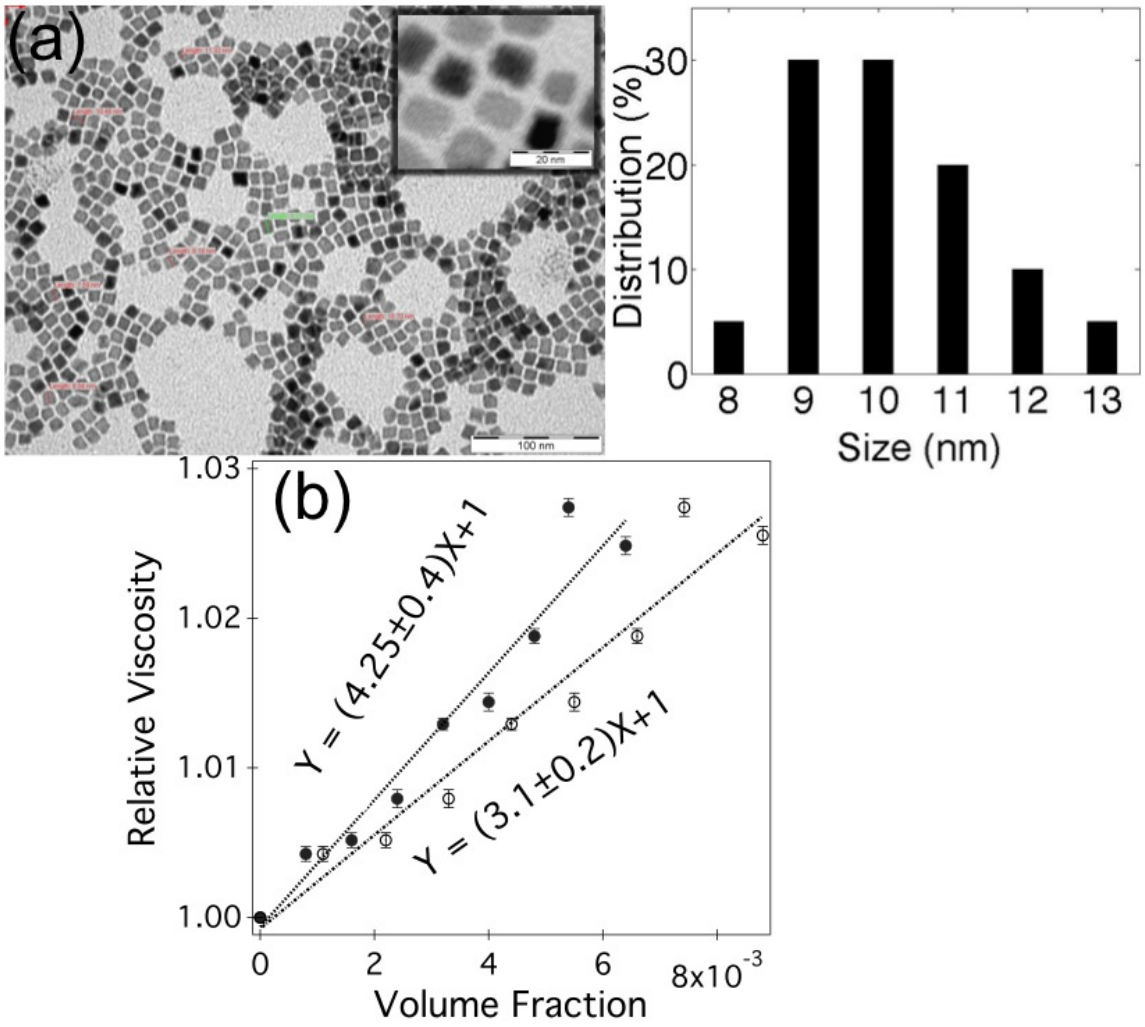

Figure 3.1: a)TEM images of PbTe nanocubes and their size distribution; b) Relative viscosity as a function of volume fraction for PbTe cubes, the closed circles represent cubes without size correction for the oleic acid brush height and the open circles are for size corrected cubes

viscosities obtained after correcting the size for the oleic acid brush. It is again apparent from the plot that η_r is a linear function of ϕ. And, a straight line fit of the relative viscosity versus ϕ data yields $[\eta] = 3.1 \pm 0.2$, which is again higher than the corresponding result for spheres.

To assess the generality of the observations made using the PbTe nanocubes, cube shaped particles in a range of other chemistries were synthesized and their intrinsic viscosity measured. Specifically, iron oxide (Fe_3O_4) nanocubes of two different sizes 20 nm and 100 nm were synthesized to study the effect of size and size distribution on intrinsic viscosity. A procedure described in [5] was used for the synthesis of the 100 nm cubes and the procedure reported in [17] was employed for the 20 nm cubes. The TEM images and size distribution of these particles are shown in figure 3.2. Suspensions containing 1:1 volume mixture of 20 nm and 100nm nanocubes at all volume fractions were also created to study the effect of size polydispersity. In order to assess the effects of the interactions between the polymer brush layer on the cubes and the suspending medium, oleic acid and PEG brushes were used to stabilize the 100nm Fe_3O_4 nanocubes [18]. Figure 3.3 is the composite plot of η_r versus effective ϕ for all of the suspensions studied. The height of the PEG brush is assumed to be 3 nm. It is apparent from the plot that irrespective of the particle size, size-distribution, and the chemistry of the chains used to impart steric stabilization, $[\eta] = 3.1 \pm 0.2$ for cubes.

3.4 Theoretical estimation of intrinsic viscosity

Einstein in his seminal paper determined how the introduction of spherical particles in a fluid increases its viscosity at low volume fractions [19]. He found that the relative viscosity η_r is given by $\eta_r = (1 + [\eta]\phi)$ where $[\eta] = 2.5$, irrespective of the sphere sizes. To estimate the intrinsic viscosity for non-spherical particles, Douglas et. al pre-averaged the orientationally dependent hydrodynamic stresses in a shear flow and related the polarizability to the intrinsic viscosity[20]. Aragon et.al calculated the intrinsic viscosity by implementing the boundary element method solution of the exact integral equation formulation of the resistance problem [21]. We take a somewhat different approach for computing the intrinsic viscosity for a suspension of cubes. The inherent symmetry in the cube is exploited to write the stress in terms of a fourth rank tensor defined using Einstein index notation as $\delta_{ijkl} = 1, \text{for}\, i = j = k = l; 0, \text{otherwise}$. We then calculate the intrinsic viscosity for any orientation of the cubes and average it over all the orientations. An important advantage of this approach is that it allows us to analyze the dependence on radius of curvature of edges and corners for every orientation of the cube.

Our starting point is to compute the stress in a sheared fluid produced by a single, isolated particle. We will take advantage of the fact that any shear flow can be decomposed into purely rotational and purely straining/extensional components. We will also focus on the limit of Stokes flow where the particle inertia is unimportant. Since the viscosity at the low volume fractions relevant for computing $[\eta]$ does not depend on the inter-particle interactions, the average stress in suspension ($< \sigma >$) can related to the stresslet (S) on an isolated particle by $< \sigma >= 2\eta E = 2\eta_s E + nS$ [22]. Here, the stresslet is defined

as $S = \int \frac{1}{2}((\boldsymbol{\sigma} \cdot \boldsymbol{n})\boldsymbol{r} + \boldsymbol{r}(\boldsymbol{\sigma} \cdot \boldsymbol{n}))d\boldsymbol{A}$ Here r is the position vector measured from the center of the cube and the integral is performed over the surface. In general, for any non-spherical particle, this stresslet has two components: a hydrodynamic stress acting on a torque-free particle and a Brownian stress due to Brownian torques acting to restore the isotropy of the orientation distribution of particles. Any extensional flow field can be written as a linear combination of planar extensional flow fields whose neutral directions are along three orthogonal axes. Since a cube is stable in a planar extensional flow field with the neutral direction along its normal, cubic particles will not experience any torque in an extensional flow. Therefore, in the absence of an external torque, the particles are torque free and rotate freely with the fluid vorticity and maintain an isotropic distribution. As a result, the Brownian torque is zero and the intrinsic viscosity results solely from the hydrodynamic stress caused by the extensional flow relative to the cube.

The relationship between the stresslet and the strain rate for a non-spherical particle in Stokes flow is linear but anisotropic and can be written as $S_{ij} = \eta_{ijkl}E_{kl}$. Here η_{ijkl} is a fourth rank viscosity tensor, which depends on the orientation of the cube. Specifying the particle's orientation in terms of n_i, m_i and p_i, the three unit normal vectors to its faces, and taking advantage of the inherent symmetry of the cube, η_{ijkl} can be written as a function of the following fourth ranked tensors: 1) $(n_in_j + m_im_j + p_ip_j)(n_kn_l + m_km_l + p_kp_l) = \delta_{ij}\delta_{kl}$ and its permutations and 2) $(n_in_jn_kn_l + m_im_jm_km_l + p_ip_jp_kp_l) = \delta_{ijkl}$. The fourth rank tensor δ_{ijkl} has been used previously in defining the cubic symmetry in problems with periodic boundary conditions[23]. Thus, the viscosity tensor η_{ijkl} can be specified in terms of two coefficients λ_1 and λ_2, i.e., $\eta_{ijkl} = \lambda_1(\delta_{ik}\delta_{jl} + \delta_{il}\delta_{jk} - \frac{2}{3}\delta_{ij}\delta_{kl}) + \lambda_2(\delta_{ijkl} - \frac{1}{3}\delta_{ij}\delta_{kl})$. Computation of the stresslet for any two specific cube orientations relative to the

straining flow can be used to evaluate the two constants and we have chosen the cases where the strain rate in a coordinate system aligned with the cube is given by E^a and E^b, where $E^a_{11} = -E^a_{22} = 1$ and $E^b_{12} = E^b_{21} = 1$ and the other components are zero, corresponding to the extensional axis perpendicular to one of the faces and parallel to a diagonal of one of the faces, respectively.

The finite element method implemented with COMSOL was employed to solve Stokes equations of motion in the fluid around a cube of side a centered in a cubic simulation cell side H with no slip boundary conditions on the cube surface and an undisturbed extensional velocity field $\mathbf{v} = \mathbf{r} \cdot \mathbf{E}$ on the outer boundary. The symmetric first moment of the force distribution then yielded the particle stresslet. The boundary effects due to the finite domain size produce a fluid velocity disturbance, which decays with separation r from the particle center as $1/r^2$. The velocity gradient and pressure should then decay as $1/r^3$. Figure 3.4 shows the variation of intrinsic viscosity with the variation of $(a/H)^3$ for both E^a and E^b. By varying the domain sizes, we found that the stresslet decayed linearly with $(a/H)^3$. Accurate results for the stresslet were obtained by fitting simulations with this scaling and extrapolating to $a/H \to 0$.

To visualize the fluid velocity field, Figure 3.5 shows the streamlines in the 1-2 plane near the particles. The flow $\mathbf{E}^a$ with the extensional axis normal to the face leads to a much larger distortion of the streamlines from the hyperbolic shape of the undisturbed streamlines. This distortion requires a larger pressure field.

The stress exerted on the convex edges of a cube is singular as one approaches the edge. As a result the sharpness of the edges and corners may have a significant influence on the intrinsic viscosity. Simulations for cubes with

rounded edges having different radii of curvature R (non-dimensionalized by the cube side) are presented in figure 3.6. The sharpness of the edges is varied by changing the resolution of the grids on the surface of the cube. In finite element simulations, the edges and corners are effectively rounded within the adjacent elements. The spacing between the grids is taken as the radius of curvature of the cubes. We have verified that higher grid resolution implies lower radius of curvature by comparing the results of a rounded cube with specific radius of curvature and a resolved simulation with a purposely rounded edge (figure 3.6).

The scaling of the velocity and pressure fields near the edges can be understood by studying the two-dimensional Stokes flow near a corner as outlined by Moffat[24]. Using the general solution for the stream function ψ for a two-dimensional Stokes flow in polar coordinates, the symmetry of the streamlines far from the cube and the no slip boundary conditions on the cube surface, the slowest decaying contribution to the stream function as the radial distance r from the corner goes to zero is found to take the form $\psi = r^{1.544}(A\cos(1.544\theta) + B\cos(0.456\theta))$ for the flow E^a. Here θ is the angle defined such that $\theta = \pm 3\pi/4$ represents the two no slip surfaces. As a result, the fluid velocity scales as $r^{0.544}$ and the shear stress and pressure as $1/r^{0.456}$. Because the stresslet involves an integral over the cube surface that converges on radial distances from the edge of the order of the radius of curvature R, the stresslet is a constant minus an edge-induced correction of order $R^{0.544}$. In a similar manner, we find $\psi = r^{1.908}(A\sin(1.908\theta) + B\sin(0.092\theta))$ near the edge for the strain rate E^b leading to an $O(R^{0.908})$ edge correction to the stresslet.

As shown in figure 3.6, the scaling obtained from the two dimensional

Stokes flow near corners fits very well with the intrinsic viscosity for cubes with different radii of curvature in large computational domains. The intrinsic viscosity fits extrapolated for very sharp cubes give $\eta_a = 3.8$ and $\eta_b = 2.7$ for flow fields E^a and E^b, respectively. Using the intrinsic viscosities for the two orientations, we find $\lambda_1 = 2.7$ and $\lambda_2 = 2.2$. The viscosity tensor yielding the stresslet for any cube orientation in any linear flow field is therefore $\eta_{ijkl} = 2.7(\delta_{ik}\delta_{jl} + \delta_{il}\delta_{jk}\frac{2}{3}\delta_{ij}\delta_{kl}) + 2.2(\delta_{ijkl}\frac{1}{3}\delta_{ij}\delta_{kl})$. Since the particles are Brownian and torque-free, all orientations of the cube are equally probable. Averaging the viscosity tensor over these orientations yields $< \eta_{ijkl} >= \int \eta_{ijkl} \sin\theta d\theta d\phi = 3.1(\delta_{ik}\delta_{jl} + \delta_{il}\delta_{jk} - \frac{2}{3}\delta_{ij}\delta_{kl})$, which is in excellent accord with the results deduced from experiments and around 25% larger than the result for spheres.

The stronger influence of the radius of curvature on the stresslet or the intrinsic viscosity for cubes in the flow E^a compared with E^b arises because of the large pressure gradient produced by the streamline curvature as the fluid flows around the corners (see figure 3.5a). Figure 3.7 shows the variation of the pressure on the surface of the cube by changing the sharpness of the edges for the flow E^a. It is well known that 2/5 of the stresslet on a spherical particle arises from the pressure with the remaining 3/5 resulting from the shear stress. In contrast, pressure causes majority (63%) of the stresslet on a cube with orientation A and is largely responsible for the higher intrinsic viscosity (3.8) for cubes with this orientation. In the streamlined orientation in figure 3.5b, the shear stress dominates providing 77% of the relatively small intrinsic viscosity (2.7). The orientationally averaged stresslet (3.1) has contributions from pressure (43%) and shear stress (57%) in nearly the same proportions as for a spherical particle.

In summary, we have used a combination of shear rheology experiments

and finite element simulations to determine the intrinsic viscosity of a suspension of cube-shaped particles. Both approaches report an intrinsic viscosity for cubes of approximately 3.1, i.e. substantially higher than the well-known result for spheres. An analysis of the velocity profile and pressure distribution in the fluid near the particles, shows that the high pressure near the sharp edges of a cube is largely responsible for the enhanced intrinsic viscosity relative to spheres. Our results also indicate that even slight rounding of the edges of cube-shaped particles leads to substantial reduction in intrinsic viscosity. In the case of self-assembly of 2D square crystals, the cross over from disc-like to square-like phase behavior occurs at the non-dimensional radius of curvature of 0.166. For cubic particles, when the edges are rounded to the radius of curvature of 0.166, the value of intrinsic viscosity decreases significantly to 2.725, indicating the sensitivity of the roundness of the edges. These values are easily accessible using experiments which suggests that the measurements of $[\eta]$ for dilute suspensions of particles of known polyhedral shape can be used in conjunction with theoretical analysis to characterize even subtle geometric imperfections in particle suspensions.

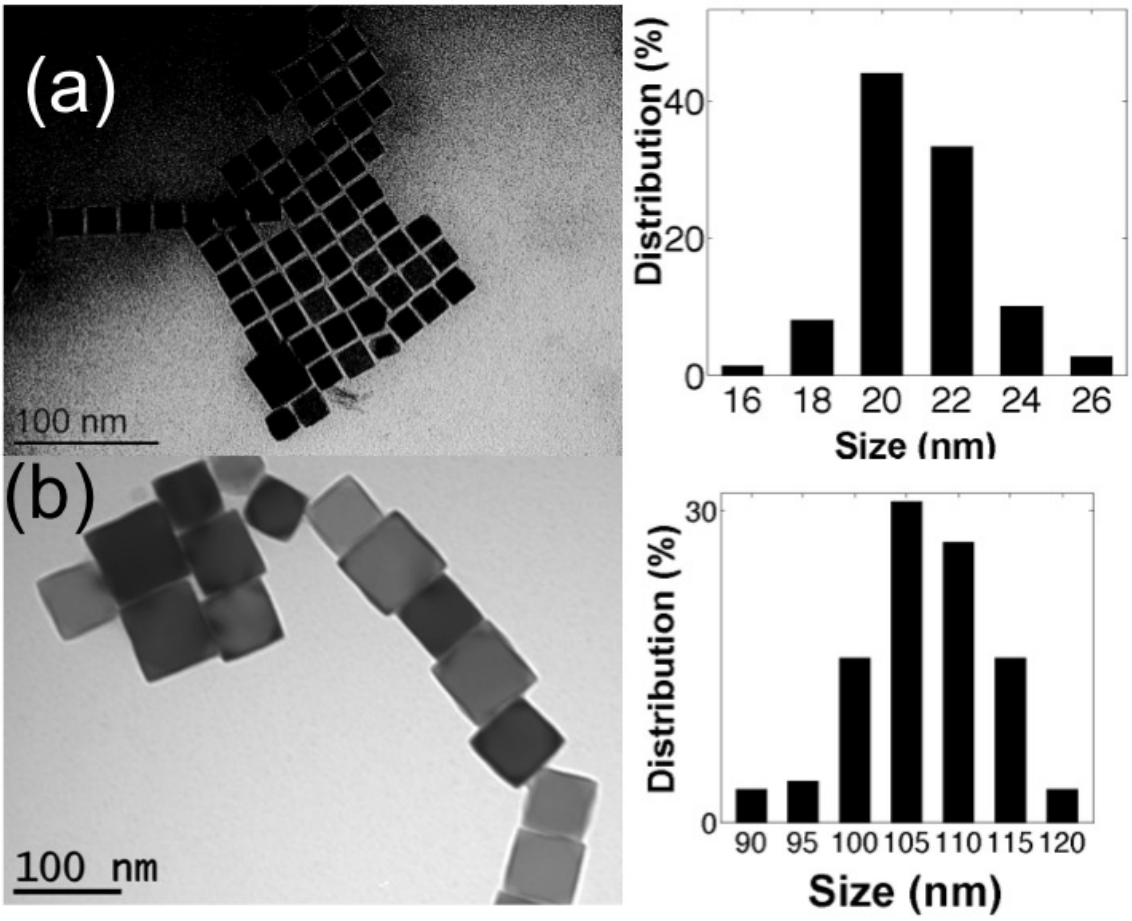

Figure 3.2: TEM images of iron oxide nanoparticles of size (a) 20 nm and (b) 100 nm

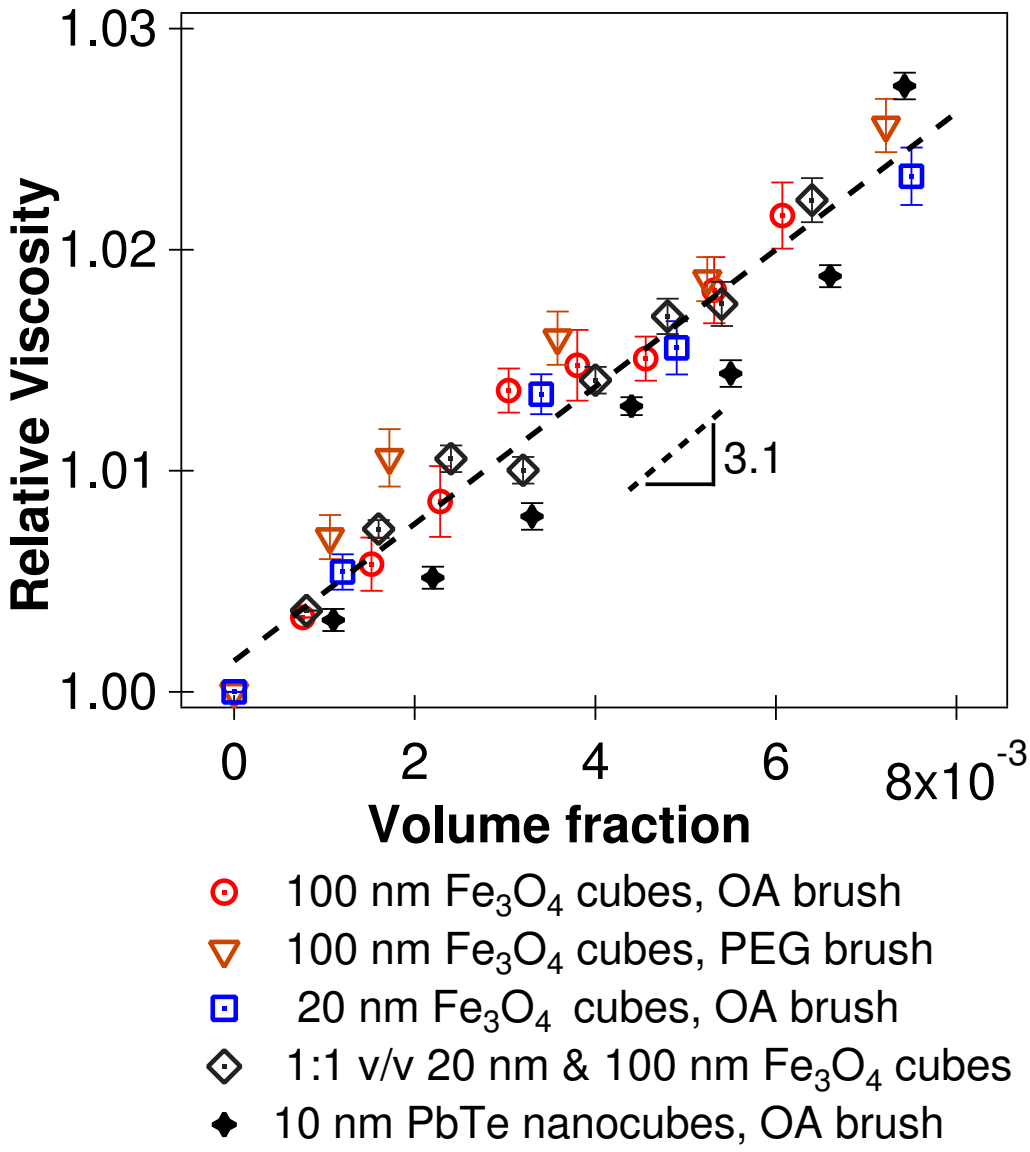

Figure 3.3: (color online) Intrinsic viscosity for cubic nanoparticles of various sizes and chemistries. Here the volume fractions are corrected by including the brush height on the cubes. The brush heights for oleic acid attached cubes and PEG attached cubes is assumed to be 0.56 nm and 3 nm respectively.

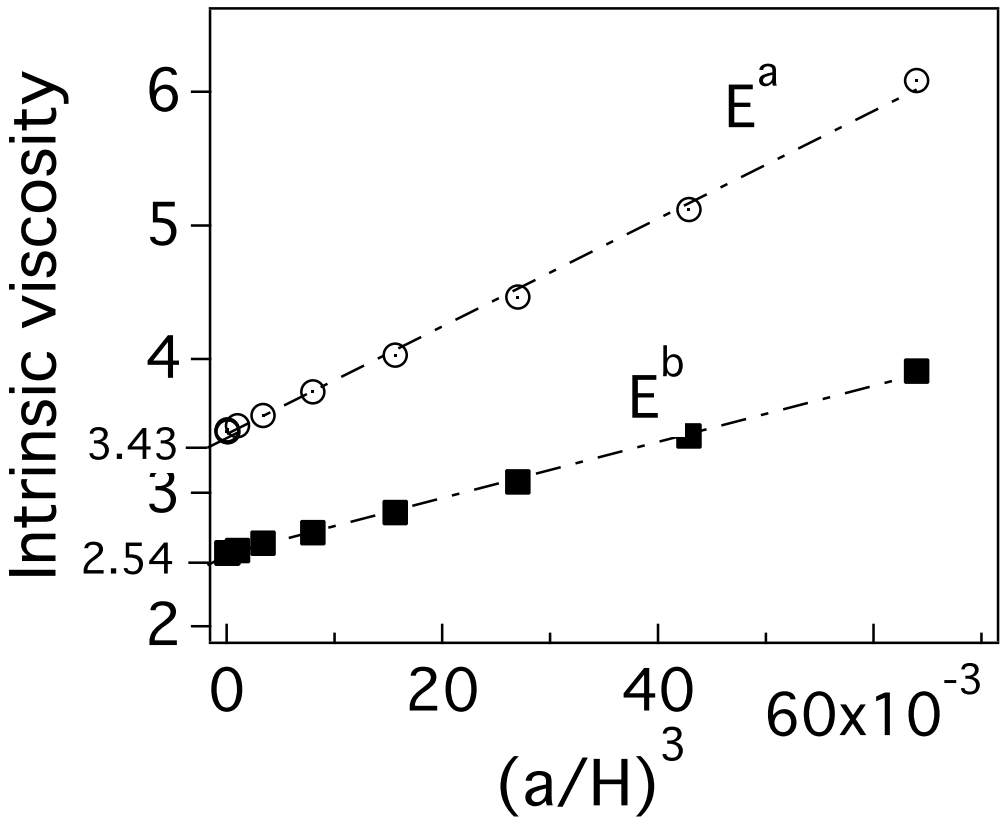

Figure 3.4: Dependence of intrinsic viscosity on a/H for E^a and E^b

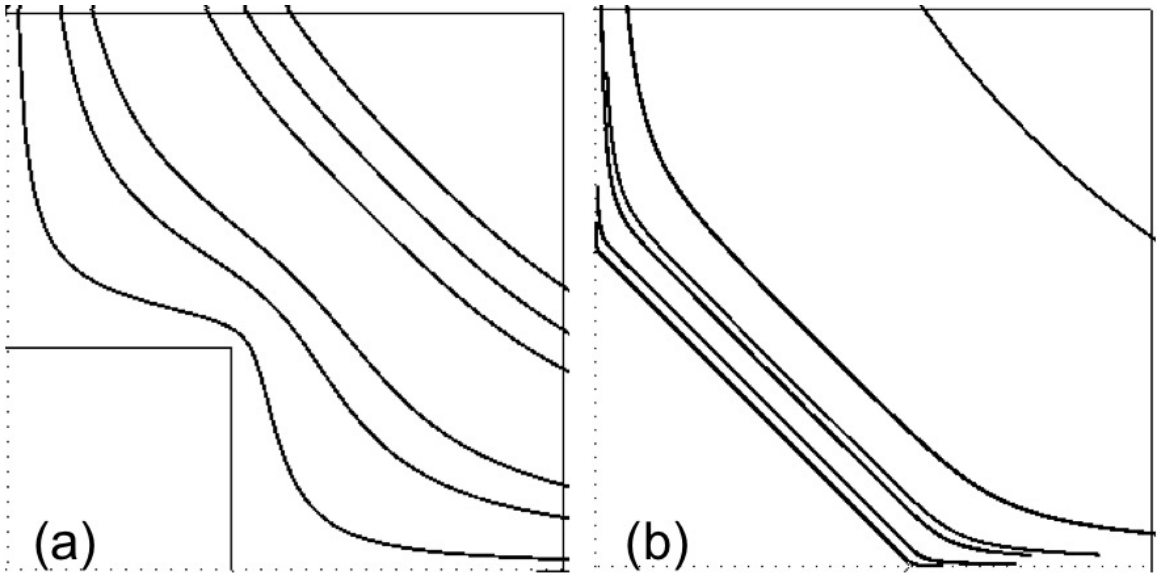

Figure 3.5: Velocity profiles around the cube for the two orientations a) E^a and b) E^b

in one quarter of the 1-2 plane.

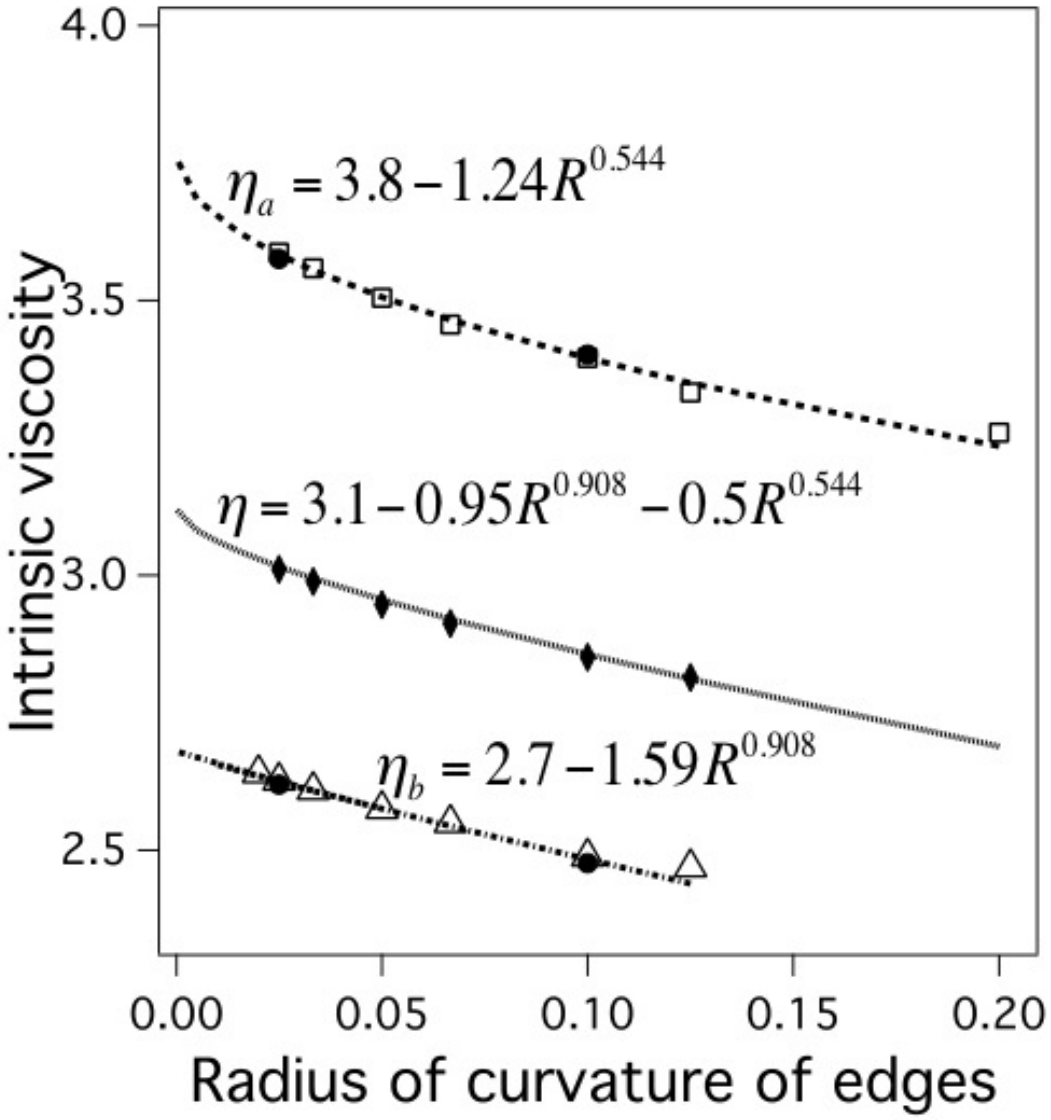

Figure 3.6: Variation of intrinsic viscosity with the radius of curvature of the edges. (□) is for E^a, (△) is for E^b and (⧫) for orientationally averaged cube, (•) are the data points for rounded cubes with high grid resolutions. The scaling for the fits are obtained from an analysis of two dimensional Stokes flow near corners.

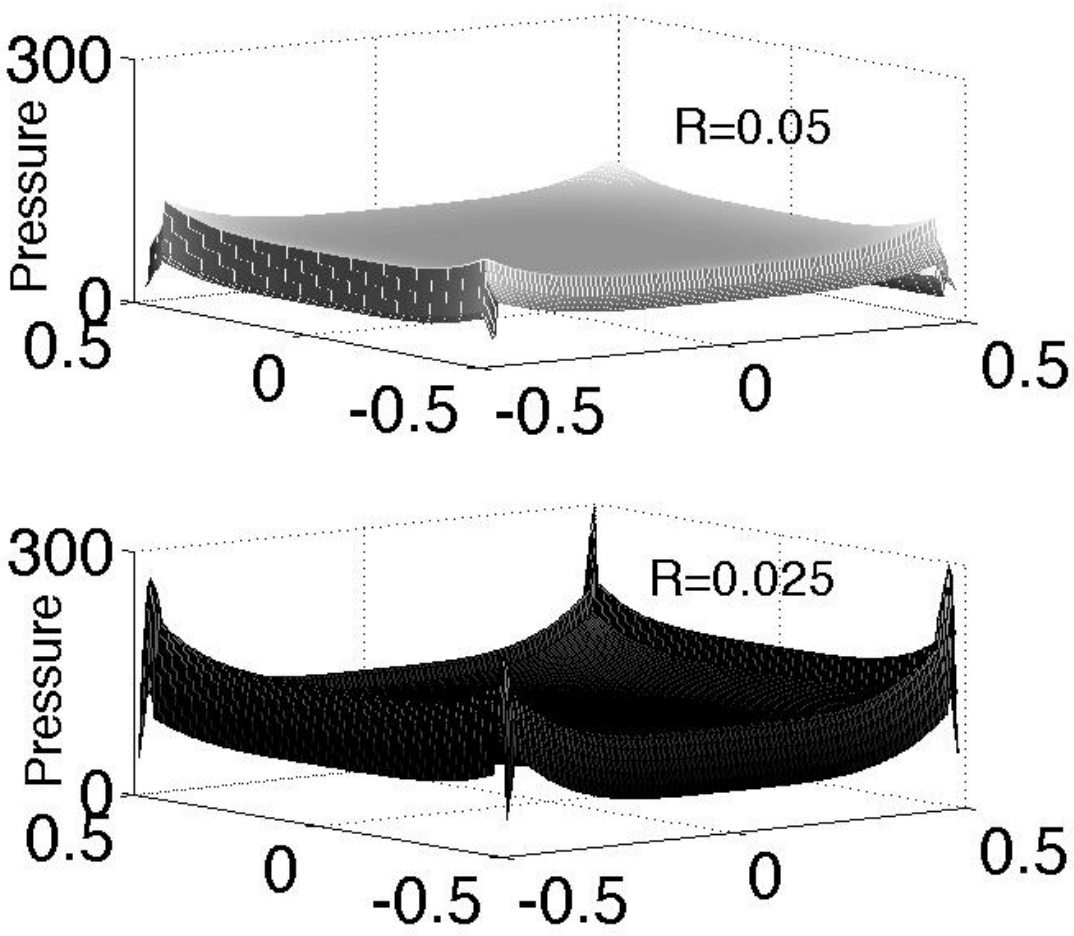

Figure 3.7: Variation of pressure on the surface of the cube for the flow E^a.

BIBLIOGRAPHY

[1] Umang Agarwal and Fernando A. Escobedo. Mesophase behaviour of polyhedral particles. *Nature Materials*, 10(3):230–235, 2011.

[2] S. C. Glotzer and M. J. Solomon. Anisotropy of building blocks and their assembly into complex structures. *Nature Materials*, 6(8):557–562, 2007.

[3] Dmitri V. Talapin, Jong-Soo Lee, Maksym V. Kovalenko, and Elena V. Shevchenko. Prospects of colloidal nanocrystals for electronic and optoelectronic applications. *Chemical Reviews*, 110(1):389–458, 2010.

[4] Clemens Burda, Xiaobo Chen, Radha Narayanan, and Mostafa A. El-Sayed. Chemistry and properties of nanocrystals of different shapes. *Chemical Reviews*, 105(4):1025–1102, 2005.

[5] D. Kim, N. Lee, M. Park, B. H. Kim, K. An, and T. Hyeon. Synthesis of uniform ferrimagnetic magnetite nanocubes. *Journal of the American Chemical Society*, 131(2):454, 2009.

[6] J. Joo, S. G. Kwon, J. H. Yu, and T. Hyeon. Synthesis of zno nanocrystals with cone, hexagonal cone, and rod shapes via non-hydrolytic ester elimination sol-gel reactions. *Advanced Materials*, 17(15):1873, 2005.

[7] L Manna, DJ Milliron, A Meisel, EC Scher, and AP Alivisatos. Controlled growth of tetrapod-branched inorganic nanocrystals. *Nature Materials*, 2(6):382–385, 2003.

[8] X. G. Peng, L. Manna, W. D. Yang, J. Wickham, E. Scher, A. Kadavanich, and A. P. Alivisatos. Shape control of cdse nanocrystals. *Nature*, 404(6773):59–61, 2000.

[9] J. Park, K. J. An, Y. S. Hwang, J. G. Park, H. J. Noh, J. Y. Kim, J. H. Park, N. M. Hwang, and T. Hyeon. Ultra-large-scale syntheses of monodisperse nanocrystals. *Nature Materials*, 3(12):891–895, 2004.

[10] G. M. Whitesides and M. Boncheva. Beyond molecules: Self-assembly of mesoscopic and macroscopic components. *Proceedings of the National Academy of Sciences of the United States of America*, 99(8):4769–4774, 2002.

[11] R. G. Egres and N. J. Wagner. The rheology and microstructure of acicular precipitated calcium carbonate colloidal suspensions through the shear thickening transition. *Journal of Rheology*, 49(3):719–746, 2005.

[12] E. Brown, H. J. Zhang, N. A. Forman, B. W. Maynor, D. E. Betts, J. M. DeSimone, and H. M. Jaeger. Shear thickening and jamming in densely packed suspensions of different particle shapes. *Physical Review E*, 84(3), 2011.

[13] KW Wojciechowski and D. Frenkel. Tetratic phase in the planar hard square system? *Comp. Met. Sci. Technol.*, 10:235, 2004.

[14] K. Zhao, R. Bruinsma, and T. G. Mason. Entropic crystal-crystal transitions of brownian squares. *Proceedings of the National Academy of Sciences of the United States of America*, 108(7):2684–2687, 2011.

[15] Carlos Avendano and Fernando A. Escobedo. Phase behavior of rounded hard-squares. *Soft Matter*, 8(17):4675–4681, 2012.

[16] Jun Zhang, Amar Kumbhar, Jibao He, Narayan Chandra Das, Kaikun Yang, Jian-Qing Wang, Howard Wang, Kevin L. Stokes, and Jiye Fang. Simple cubic super crystals containing pbte nanocubes and their core?shell building blocks. *Journal of the American Chemical Society*, 130(45):15203–15209, 2008.

[17] H. T. Yang, T. Ogawa, D. Hasegawa, and M. Takahashi. Synthesis and magnetic properties of monodisperse magnetite nanocubes. *Journal of Applied Physics*, 103(7), 2008.

[18] J. Xie, C. Xu, N. Kohler, Y. Hou, and S. Sun. Controlled pegylation of monodisperse fe3o4 nanoparticles for reduced non-specific uptake by macrophage cells. *Advanced Materials*, 19(20):3163–3166, 2007.

[19] A Einstein. *Investigation on the theory of the Brownian movement*. Dover Publications, 1956.

[20] J. F. Douglas and E. J. Garboczi. Intrinsic viscosity and the polarizability of particles having a wide range of shapes. *Advances in Chemical Physics, Vol 91*, 91:85–153, 1995.

[21] S. R. Aragon and D. K. Hahn. Preaveraged hydrodynamic interaction revisited via boundary element computations. *Journal of Chemical Theory and Computation*, 2(1):12–17, 2006.

[22] G. K. Batchelor and J. T. Green. The hydrodynamic interaction of two small freely-moving spheres in a linear flow field. *Journal of Fluid Mechanics*, 56:375–400, 10 1972.

[23] K. C. Nunan and J. B. Keller. Effective viscosity of a periodic suspension. *Journal of Fluid Mechanics*, 142:269–287, 1984.

[24] H. K. Moffatt. Viscous and resistive eddies near a sharp corner. *Journal of Fluid Mechanics*, 18(01):1–18, 1964.

CHAPTER 4

STRESS IN A SUSPENSION OF CUBE-SHAPED MAGNETIC PARTICLES SUBJECT TO SHEAR AND MAGNETIC FIELDS

4.1 Abstract

The effect of a homogenous magnetic field (**H**) on the bulk stress in a dilute suspension of weakly Brownian magnetic cubes suspended in a Newtonian fluid subjected to a linear shear flow is studied. The stresslet on each cube is anisotropic and depends on its orientation. Application of a magnetic field to the suspension results in anisotropy in the orientational distribution of cubic particles. The steady-state orientation distribution is derived as a function of the angle between the directions of the magnetic field and the fluid vorticity vector and the strength of the magnetic torque non-dimensionalized by the viscous torque. Knowledge of the distribution function is used to derive a general result for the bulk stress in a linear flow field in a magnetic field when the magnetic field is either parallel or perpendicular to the vorticity. Specific numerical results are obtained for the intrinsic viscosity of the suspension in a simple shear flow. When the magnetic field is perpendicular to vorticity, we find that the intrinsic viscosity increases at first with increasing shear rate passes through a maximum and then shear thins. The intrinsic viscosity can vary from 3.25 to 5.5 in response to changes in the relative strengths of the shear and magnetic fields. The maximum value of 5.5 for the intrinsic viscosity was obtained, when the magnetic moment of the cube, which is parallel to one of the normals is in the flow gradient plane and is aligned at an angle of $\pi/4$ to the flow direction.

4.2 Introduction

Suspensions of ferromagnetic or ferrimagnetic nanoparticles in a Newtonian fluid (ferrofluids) have been observed to show interesting rheological properties in the presence of external magnetic fields including antisymmetric stresses and a complex shear-dependent rheology resulting from the competition between magnetic and viscous torques in controlling particle orientation. Such suspensions are used in the design of numerous devices and applications dealing with magnetic fluid seals, viscous dampers, actuation and robotics. Previous studies of ferrofluids have considered spherical particles or axisymmetric particles. A third category of interest is polygonal particles which may arise from a number of crystallization synthesis methods. As an example, we study the dependence of bulk stress in a dilute suspension of weakly Brownian magnetic cubic particles in a magnetic field.

It is well known that in the presence of a uniform magnetic field, a magnetic particle in a suspension subjected to simple shear flow experiences a net angular velocity relative to the fluid. When the particle's angular velocity does not coincide with the local rotational velocity of the fluid, the viscous dissipation of the medium increases. This phenomenon is known as the magnetoviscous effect. Experimentally, this effect was first observed by McTague [1] and Rosensweig et. al.[2]. McTague observed that the increase in the viscosity for dilute suspensions is greater when the magnetic field($\mathbf{H}$) is applied parallel to the flow than with it in perpendicular direction. Rosensweig studied the dependence of viscosity on the shear rate in the presence of a magnetic field perpendicular to the flow and observed Newtonian and shear thinning regimes depending on the relative strength of hydrodynamic and magnetic torques.

Hall and Busenberg [3] theoretically estimated the viscosity of a dilute suspension of non-Brownian, magnetic spherical particles in shear flow as a function of both direction and the magnitude of **H**. The steady state motion of these particles was derived using torque balance and the effective viscosity of the suspension was calculated using conservation of energy. They predicted that the effective viscosity (η_{eff}) of the suspension depends on both the direction and magnitude of the external magnetic field and is given by:

$$\eta_{eff} = \eta_0\left(1 + \frac{5\phi}{2} + \frac{3\phi}{4}(1+\xi^2) - \frac{3\phi}{2}\left(\frac{1}{4}(1+\xi^2)^2 - \xi^2\sin^2\alpha\right)^{1/2}\right) \tag{4.1}$$

$$\tag{4.2}$$

Here ϕ is the particle volume fraction, η_0 is the viscosity of the carrier liquid, $\xi = (\mu_0|\mathbf{M}||\mathbf{H}|)/(4\pi\eta_0 a^3\dot{\gamma})$ represents the ratio between the magnetic torque and the hydrodynamic torque acting on a particle, and α is the angle between the magnetic field and vorticity as shown in figure 4.2. Here μ_0 is the permeability of free space, $|\mathbf{M}|$ is the magnitude of particle magnetic dipole, **H** is the magnetic field, a is the particle radius, and $\dot{\gamma}$ is the shear rate. Later, Shliomis [4] derived an expression for a suspension of magnetized Brownian spherical particles for the case of low shear rate and short magnetization relaxation time which is given by

$$\eta_{eff} = \frac{3}{2}\phi\eta_0\left(1 + \frac{5}{2}\phi\right)\left[\frac{\kappa - \tanh\kappa}{\kappa + \tanh\kappa}\right]\sin^2\theta \tag{4.3}$$

Here $\kappa = \mu_0|\mathbf{M}||\mathbf{H}|/k_BT$, with k_B being Boltzmann constant and T the absolute temperature, is the Langevin parameter, and θ is the angle between the magnetic field and vorticity.

Brenner and Weissman [5] numerically solved the Smoluchowski equation for the orientational distribution function and developed a dynamical theory of the rheology of suspensions of noninteracting dipolar Brownian spherical parti-

cles. They derived expressions for the stress tensor and showed the effect on the intrinsic viscosity of both the external field strength and shear rate, parameterized through the rotational Peclet number $Pe_r = \dot{\gamma}/D_r$, where D_r is the rotational diffusion coefficient of the particle.

In this paper we will consider magnetic cube-shaped particles in a magnetic field in the limits of very weak rotary Brownian motion relative to the shear induced rotation $Pe_r \gg 1$ and the magnetic field induced rotation ($\zeta = \mu_0|\mathbf{M}||\mathbf{H}|/kT \gg 1$). Thus, among the aforementioned work on spherical particles, our study is most closely related to that of Hall and Busenberg [3]. A small amount of Brownian motion allows cubic particles undergoing rotational motion to sample all possible phase angles of their orbits. As a representative example, this theory can be used to understand the dilute rheological behavior of 100nm Fe_3O_4 cubic particles synthesized using the procedure described by Hyeon et. al. ([6]), suspended in a fluid with viscosity of 100 cp (for example motor oil used to make ferro fluids) being sheared at a shear rate ($\dot{\gamma} = 50s^{-1}$) in the presence of a magnetic field of 1000 Oe. For this case, we have $Pe_r = 150$ and $\zeta > 1000$.

Non-spherical particles which are axisymmetric such as rods, spheroids, etc. have been extensively studied in the literature [7][8] [9] [10]. The net torque acting on stationary axisymmetric particles in an extensional flow is non-zero and depends on their orientation. As a result, the orientation distribution is non-isotropic and the particles undergo trajectories called Jeffrey's orbits in the absence of a magnetic field. When external magnetic fields are applied, the orientation distribution becomes much more complex. Almog and Frenkel [11] studied the motion of a dilute suspension of weakly Brownian axisymmetric

dipolar magnetic particles under shear in the presence of an external magnetic field. They show that the long time behavior of the orientation distribution function in linear shear flow can in general exhibit multiple stable equilibria. Depending on their initial orientations, particles may remain in a family of periodic orbits or converge to a stable equilibrium orientation. They discuss the implications of these results on the rheology of these suspensions. They then provide specific calculations for the bulk stresses in the medium for the cases where there is a single stable node.

Cubic particles are the simplest polyhedral particles with flat surfaces, sharp corners and edges. Due to its symmetric shape, a cube does not experience any torque in an extensional flow. As a result, when cubic particles are subjected to simple shear flow in the absence of a magnetic field, they rotate freely with the applied vorticity. The rotational behavior of cubes in the presence of a magnetic field is equivalent to that described by Hall and Busenberg [3]. Unlike a sphere, however, the symmetric first moment of stress acting on a cube depends on the orientation of the cube with respect to the rate of strain. The rotational motion of the cube in the presence of competing vorticity and magnetic fields results in an anisotropic orientation distribution of the cubes altering the symmetric part of the stress in the ferrofluid. The symmetric part of the stress tensor in a suspension of weakly Brownian spheres is independent of the ratio of the magnetic and viscous torques and the shear thinning of the suspension results solely from the antisymmetric part of the stress. In contrast, both the symmetric and antisymmetric parts of the stress in a suspension of cubic particles are modulated by the ratio of magnetic to viscous torques. In this way, cubic particles exhibit a behavior intermediate between axisymmetric non-spherical particles and spherical particles. Like other non-spherical particles their stresslet responds to

extensional flow in an anisotropic fashion that responds to the magnetic field, but unlike axisymmetric particles they do not exhibit an anisotropic distribution in a linear shear flow in the absence of a magnetic field. Thus, the study of cubic particles provides a simple illustration of the influence of magnetic field induced anisotropy of the particle orientation distribution on both the symmetric and antisymmetric stress in a suspension.

This chapter is divided into three sections. In the first section, we use the symmetric properties of the cube to calculate the symmetric stress as a function of the cube's orientation. We identify the orientations which produce the maximum and minimum stresslet and show that the stresslet for any orientation can be determined from a computation of the stresslet in these two orientations. In the second section, we solve for the motion of the cube to obtain the cube's orientation as a function of applied magnetic and shear fields. At steady state, cubes either have a fixed orientation or rotate with constant angular velocity. This angular velocity vector is dependent on the relative direction and magnitude of applied magnetic and shear fields. The trajectories for the cube are analyzed when the magnetic field is either parallel or perpendicular to vorticity direction. In the last section, we calculate the anti-symmetric stress and use the results from previous sections to calculate the total stress as a function of applied magnetic and shear fields. The dependence of viscosity on the relative strengths of magnetic and shear fields is studied when magnetic field is parallel and perpendicular to vorticity direction.

4.3 Stress in a dilute suspension of force-free particles

Batchelor derived the general expression for the bulk stress in a Newtonian fluid at any instantaneous particle orientation in the presence of a net external torque on the particles[12]. Following the derivation carried out by Batchelor [12], the average deviatoric stress $\left(< \sigma_{ij} >\right)$ generated in the suspension can be written as

$$< \sigma_{ij} >= \frac{1}{V} \int_{V_f} {\sigma^f}_{ij} dV + \frac{N}{V} \int_{V_p} {\sigma^p}_{ij} dV \tag{4.4}$$

Here ${\sigma^p}_{ij}$ and ${\sigma^f}_{ij}$ are the particle and fluid deviatoric stresses, N is number of particles, V is the total volume, V_f is the fluid volume, and V_p is the volume of each particle. Since the fluid is Newtonian and ${\sigma^f}_{ij}$ inside the particle is zero, the first term in equation (4.4) can be integrated over the whole volume. Also, using divergence theorem, the second term can be transformed to a surface integral which results in

$$< \sigma_{ij} >= (2\eta_0 E_{ij}) + n \int_{A_p} ({\sigma^p}_{ik} n_k) r_j dA \tag{4.5}$$

E_{ij} is the imposed rate of strain and n is the number of particles per unit volume. The external torque (L_i) acting on each particle is given by $L_i = \int_{A_p} \epsilon_{ijl} r_j \sigma_{lk} n_k dA$. Using this relation in equation(4.5) and writing the symmetric and anti-symmetric components of stress separately leads to

$$< \sigma_{ij} > = < \sigma_{ij}^{sym} > + < \sigma_{ij}^{anti} > \tag{4.6}$$

$$< \sigma_{ij}^{sym} > = 2\eta_0 E_{ij} + n S_{ij} \tag{4.7}$$

$$< \sigma_{ij}^{anti} > = n \epsilon_{ijk} L_k \tag{4.8}$$

S_{ij} is the stresslet acting on each particle and is defined as

$$S_{ij} = \tfrac{1}{2} \int_{A_p} (\sigma_{ik}^{sym} n_k r_j + \sigma_{jk}^{sym} n_k r_i) dA. \tag{4.9}$$

We have previously calculated the intrinsic viscosity for an isotropic suspension of cubic particles ([13]) and verified the predictions with experimental measurements. However, since the present application highlights the stress that arises when a magnetic field induces an anisotropic orientation distribution of the cubes, we will review this aspect of the calculations here. The relationship between the stresslet and the strain rate for a cubic particle in Stokes flow is linear but anisotropic and can be written as

$$S_{ij} = \eta_{ijkl} E_{kl} \tag{4.10}$$

Here η_{ijkl} is a fourth rank viscosity tensor, which depends on the orientation of the cube. Let us define the orientation of a cube by the three unit normal vectors to its faces n_i, m_i, p_i. The symmetry of the cube dictates that η_{ijkl} should be an even function of three normal vectors n_i, m_i, p_i and symmetric in n_i, m_i, p_i. As a result, η_{ijkl} can be written as a function of the following fourth ranked tensors:

$$\begin{aligned}
\eta_{ijkl} &= \lambda_1(n_i n_j + m_i m_j + p_i p_j)(n_k n_l + m_k m_l + p_k p_l) && (4.11)\\
&+ \lambda_2(n_i n_j + m_i m_j + p_i p_j)(n_k n_l + m_k m_l + p_k p_l) \\
&+ \lambda_3(n_i n_j + m_i m_j + p_i p_j)(n_k n_l + m_k m_l + p_k p_l) && (4.12)\\
&+ \lambda_4(n_i n_j + m_i m_j + p_i p_j)(n_k n_l + m_k m_l + p_k p_l) \\
&+ \lambda_5(n_i n_j n_k n_l + m_i m_j m_k m_l + p_i p_j p_k p_l) && (4.13)
\end{aligned}$$

Here $\lambda_1, \lambda_2, \lambda_3, \lambda_4$ and λ_5 are unknown constants. Using $S_{ii} = 0$, and the symmetric properties of the cube, η_{ijkl} can be simplified to just two unknowns (λ_a and λ_b)

$$\eta_{ijkl} = \lambda_a(\delta_{ik}\delta_{jl} + \delta_{il}\delta_{jk} - \frac{2}{3}\delta_{ij}\delta_{kl}) + \lambda_b(\delta_{ijkl} - \frac{1}{3}\delta_{ij}\delta_{kl}) \tag{4.14}$$

Here $\delta_{ij}\delta_{kl} = (n_i n_j + m_i m_j + p_i p_j)(n_k n_l + m_k m_l + p_k p_l)$ and $\delta_{ijkl} = (n_i n_j n_k n_l + m_i m_j m_k m_l + p_i p_j p_k p_l)$. The fourth rank tensor δ_{ijkl} has been used previously in defining the

cubic symmetry in problems with periodic boundary conditions[14]. The two unknowns can be evaluated by computing the stresslet for any two specific cube orientations relative to the straining flow.

We have chosen the cases where the strain rate in a coordinate system whose axes are aligned with unit normal vectors to the cube is given by E^a_{ij} and E^b_{ij}

$$\begin{aligned} E^a_{ij} &= 1, \text{ for } i = j = 1, \\ &= -1, \text{ for } i = j = 2, \\ &= 0, \text{ otherwise} \end{aligned} \tag{4.15}$$

$$\begin{aligned} E^b_{ij} &= 1, \text{ for } i = 1, j = 2 \\ &= 1, \text{ for } i = 2, j = 1 \\ &= 0, \text{otherwise} \end{aligned} \tag{4.16}$$

These orientations correspond to the maximum and minimum possible stresslet, respectively.

A finite element method implemented with COMSOL was used to obtain the fluid velocity and pressure profiles surrounding the cube. The stresslet S_{ij} on the cube, subjected to the extensional flows E^a_{ij} and E^b_{ij} is determined from these profiles. These calculations were carried out within a cubic domain of side length L with a cube of side length a at its center. Specified velocity $v_i = r_j E_{ij}$ was imposed on the outer boundaries of the domain. The boundary effects due to the finite domain size produce a fluid velocity disturbance, which decays with separation r from the particle center as $1/r^2$. The velocity gradient and pressure should then decay as $1/r^3$. By varying the domain sizes, we found that the stresslet decayed as $(a/L)^3$. Accurate results for the stresslet were obtained by fitting simulations with this scaling and extrapolating to $L/a \to \infty$.

The stress exerted on each convex edge of a cube is singular as one approaches the edge. As a result the sharpness of the edges and corners may have a significant influence on the stresslet. Simulations for cubes with rounded edges having different radii of curvature R (non-dimensionalized by the cube side) are presented in figure 4.1 The scaling of the velocity and pressure fields near the edges can be understood by studying the two-dimensional Stokes flow near a corner as outlined by Moffat[15]. Using the general solution for the stream function ψ for a two-dimensional Stokes flow in polar coordinates, the symmetry of the streamlines far from the cube and the no slip boundary conditions on the cube surface, the slowest decaying contribution to the stream function as the radial distance r from the corner goes to zero is found to take the form $\psi = r^{1.544}(A\cos(1.544\theta) + B\cos(0.456\theta))$ for the flow $\mathbf{E}^a$. Here θ is the angle defined such that $\theta = \pm 3\pi/4$ represents the two surfaces. As a result, the fluid velocity scales as $r^{0.544}$ and the shear stress and pressure as $1/r^{0.456}$. Because the stresslet involves an integral over the cube surface that converges on radial distances from the edge of the order of the radius of curvature R, the stresslet is a constant minus an edge-induced correction of order $R^{0.544}$. In a similar manner, we find $\psi = r^{1.908}(A\sin(1.908\theta) + B\sin(0.092\theta))$ near the edge for the strain rate $\mathbf{E}^b$ leading to an $O(R^{0.908})$ edge correction.

As shown in the figure 4.1, the scaling obtained from the two dimensional Stokes flow near corners fits very well with the appropriate component of the stresslet (S_{ij}). S^a_{12} and S^b_{11} for cubes were plotted with different radii of curvature in large computational domains and the fits were extrapolated for very sharp cubes. We get $S^a_{12} = 7.6$ and $S^b_{11} = 5.4$ for flow fields $\mathbf{E}^a$ and $\mathbf{E}^b$ respectively. Using these values in the general expression for the stresslet, we get $\lambda_a = 2.7$ and $\lambda_b = 2.2$. The viscosity tensor yielding the stresslet for any cube orientation

in any linear flow field is therefore

$$\eta_{ijkl} = 2.7(\delta_{ik}\delta_{jl} + \delta_{il}\delta_{jk} - \frac{2}{3}\delta_{ij}\delta_{kl}) + 2.2(\delta_{ijkl} - \frac{1}{3}\delta_{ij}\delta_{kl}) \tag{4.17}$$

This expression along with equation 4.10 provides the stresslet for any orientation of the cube in any linear velocity field.

For a simple shear flow problem, the minimum value of viscosity from symmetric stress can be evaluated from previous equation. This value is 2.7 and it occurs when the normals to the cube are aligned along the flow, gradient and vorticity directions. Similarly, the maximum value of viscosity from symmetric stress which is 3.8 occurs when two of the normals to the cube are at an angle of $\pi/4$ with the flow direction and the third is parallel to vorticity. If the cubic particles have a magnetic moment parallel to one normal and an external magnetic field is applied, we will see that the direction of one of the normals to the cube will be independent of time and fixed at an orientation that depends on the relative strength of the magnetic and shear fields and the direction of the magnetic field. The particle will rotate about this axis leading the other normals to be isotropically averaged over the plane perpendicular to the magnetic moment. Therefore, the viscosity contribution from the symmetric stress can be varied using magnetic field although the absolute maximum value of viscosities from symmetric stress will not be realizable.

4.4 Motion of a cube in a linear flow field

The rotation of a cube in a linear shear flow field in the presence of a magnetic field is similar to that of a spherical particle, because neither cubes nor spheres

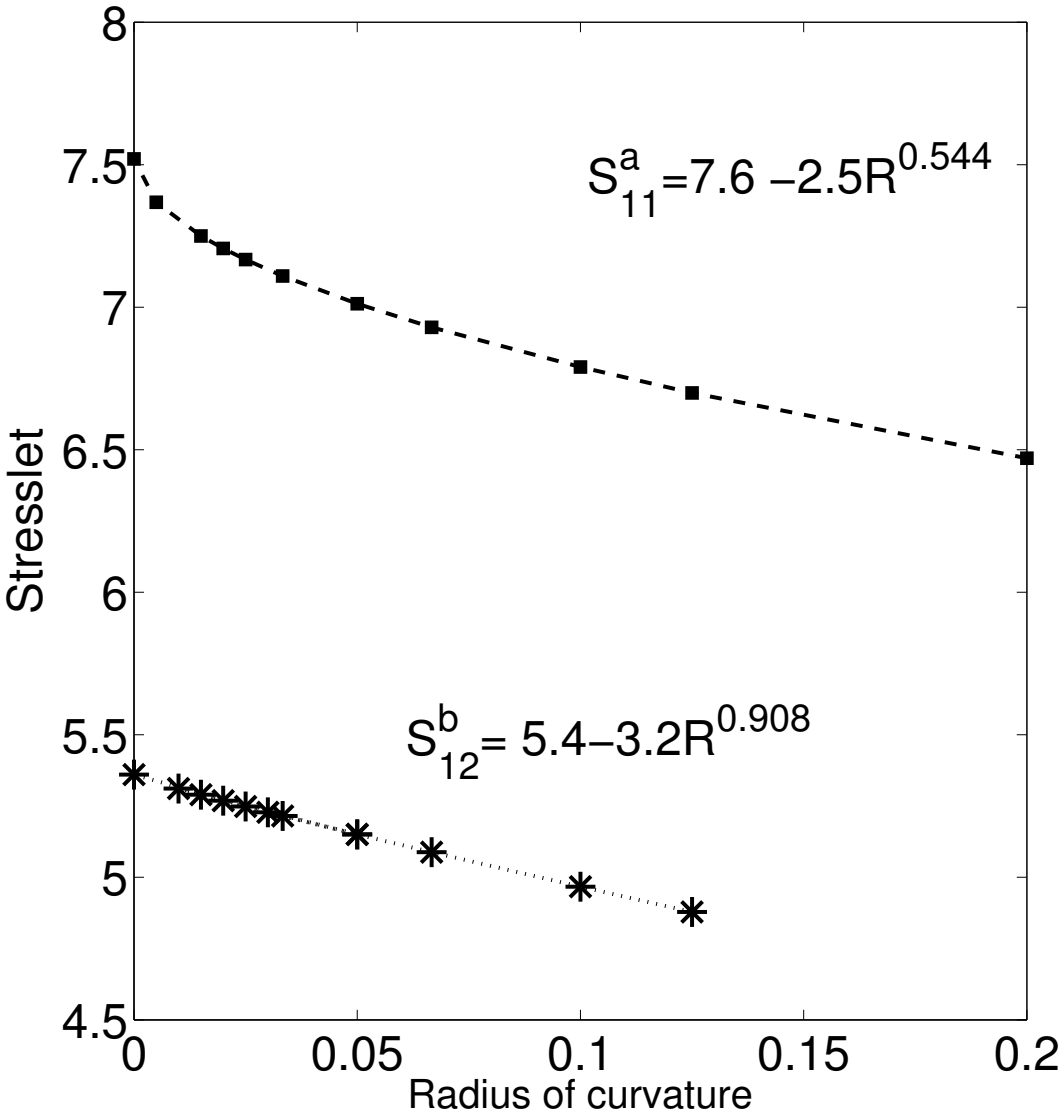

Figure 4.1: Dependence of stresslet (both S^b_{12} and S^a_{11}) on the radius of curvature of the edges of the cube. The fits are the scaling obtained from flow near 2D sharp corners.

rotate due to the extensional component of the flow. Therefore, the development here follows Hall and Busenberg's ([3]) analysis for spherical particles. Here, we have explicitly written down the equation for particle's angular velocity vector as a function of ξ and the angle between the magnetic field and vorticity direction.

Consider a cube with magnetic moment $\mathbf{M}$ aligned with one of the side normals that is suspended in a Newtonian fluid with viscosity η and subjected to a linear shear flow in the presence of an external magnetic field. Due to the symmetric shape of the cube, the net torque acting on it in a purely extensional flow is zero. In the absence of an external magnetic field, cubic particles are torque free and will rotate with the applied vorticity (ω). However when an external magnetic field ($\mathbf{H}$) is applied, cubic particles will have a net angular velocity ($\mathbf{\Omega} - \omega$) relative to the fluid. We assume that the Brownian torques are weak compared to both hydrodynamic and magnetic torques. In this case, the motion of the cube is governed by balancing the net magnetic torque acting on the cube ($\mu_0 \mathbf{M} \times \mathbf{H}$) with the torque produced due to the non-zero relative angular velocity of the cube ($R_\omega(\mathbf{\Omega} - \omega)$). Also, since the magnetic moment is fixed with one of the normals, it rotates along with the net angular velocity of the cube. The non-dimensionalized equations of motion for the cube are:

$$\xi(\bar{\mathbf{\Omega}} - \hat{\omega}) = (\hat{\mathbf{M}} \times \hat{\mathbf{H}}) \tag{4.18}$$

$$\frac{d\hat{\mathbf{M}}}{dt} = \bar{\mathbf{\Omega}} \times \hat{\mathbf{M}} \tag{4.19}$$

$\bar{\mathbf{\Omega}} = \mathbf{\Omega}/|\omega|$ is the non-dimensionalized angular velocity of the cube, $\hat{\omega} = |\omega|$ is the nondimensionalized vorticity of the cube and $\xi = \frac{R_\omega|\omega|}{\mu_0|\mathbf{M}||\mathbf{H}|}$ is the ratio of the strength of the hydrodynamic torque to the external magnetic torque, and μ_0 is the permeability. The hydrodynamic resistivity for rotation, R_ω, was calcu-

lated using finite element analysis and found to be $R_\omega = 7.39a^3\eta_0$. It has been shown by Hall and Busenberg [3] that the magnetic moment will reach a steady alignment and the particle will rotate with a constant angular velocity about the direction of the magnetic moment when it satisfies the above equations of motion, i.e.,

$$\hat{\mathbf{M}} = \frac{\bar{\mathbf{\Omega}}}{|\bar{\mathbf{\Omega}}|} \tag{4.20}$$

The stresslet of a sphere undergoing this motion is independent of time. For a cube, however, the unit normals **m** and **p** continue to rotate leading to temporal variations of the orientation of the cube relative to the extensional axes and an associated temporal variation of the stresslet. Our first aim would be to calculate the time dependent orientation of the cube as a function of ξ and the relative orientation of applied magnetic field with the vorticity direction. This will then be used to understand the dependence of average stress acting on the cube. Solving the equations of motion for steady state, the general solution for the net angular velocity and the magnetic moment of the cube is given by:

$$\hat{\mathbf{M}} = \frac{1}{1 + |\bar{\mathbf{\Omega}}|^2\xi^2}\left(\xi^2|\bar{\mathbf{\Omega}}|\hat{\omega} + \left(\frac{cos\theta}{|\bar{\mathbf{\Omega}}|}\right)\hat{\mathbf{H}} + (\xi)\hat{\omega}\times\hat{\mathbf{H}}\right) \tag{4.21}$$

$$|\bar{\mathbf{\Omega}}| = \left(\frac{\xi^2 - 1 + \sqrt{(\xi^2-1)^2 + 4\xi^2 cos^2\theta}}{2\xi^2}\right)^{1/2} \tag{4.22}$$

Here θ is the angle between applied magnetic field and the applied vorticity.

The orientation of the magnetic moment of the cube and its angular velocity are determined by the competition between magnetic and viscous torques. The magnitude and the orientation of the net angular velocity depends on both ξ and θ. Let us consider a specific case of $\theta = \pi/2$ to understand this dependence. For a simple shear flow, this value of θ would correspond to the applied magnetic field lying in the flow-gradient plane. This is particularly relevant

because in typical rheology experiments, magnetic field is applied along the velocity gradient direction ($\theta = \pi/2$) to measure the effect of magnetic field on viscosity. When $\theta \to \pi/2$, two different limiting solutions are feasible from the above equations based on the magnitude of ξ. For $\xi < 1$, the magnetic torque is always sufficient to balance viscous torque and the net angular velocity of the cube is zero. When $\xi > 1$, the magnetic torque cannot compensate for the applied viscous torque and the cube will have a non-zero angular velocity.

$$\begin{aligned} \text{When} \quad \xi < \quad & 1 \\ |\bar{\mathbf{\Omega}}| \quad = \quad & 0 \qquad (4.23) \\ \hat{\mathbf{M}} \quad = \quad & \left(\hat{\mathbf{H}}(1-\xi^2)^{1/2} + \xi(\hat{\omega} \times \hat{\mathbf{H}})\right) \qquad (4.24) \\ \text{When} \quad \xi \geq 1 & \\ |\bar{\mathbf{\Omega}}| \quad = \quad & \left(1 - \frac{1}{\xi^2}\right)^{1/2} \qquad (4.25) \\ \hat{\mathbf{M}} \quad = \quad & \left(\left(1 - \frac{1}{\xi^2}\right)^{1/2} \hat{\omega} + \frac{1}{\xi}\hat{\omega} \times \hat{\mathbf{H}}\right) \qquad (4.26) \end{aligned}$$

The schematic illustration of these results is shown in the figure 4.3. Let β be the angle between $\mathbf{H}$ and magnetic moment $\mathbf{M}$ and α be the angle between $\mathbf{M}$ and applied vorticity as shown in figure 4.2. For $\xi << 1$, the external torque is large compared hydrodynamic torque. As a result, the direction of the magnetic moment coincides with the direction of the applied magnetic field and the angular velocity of the cube is zero($\beta = 0$, $\alpha = \pi/2$ and $|\mathbf{\Omega}| = 0$). For $\xi < 1$, the angular velocity is still zero ($|\mathbf{\Omega}| = 0$) and $\alpha = \pi/2$ but β increases from 0 to $\pi/2$ as ξ increases from 0 to 1. When $\xi = 1$, the external magnetic torque is just sufficient to balance the hydrodynamic torque($\alpha = \pi/2, \beta = \pi/2$ and $|\mathbf{\Omega}| = 0$). When $\xi > 1$, the external magnetic torque is smaller than the hydrodynamic torque due to the imposed vorticity and the particle begins to rotate, i.e., $|\mathbf{\Omega}| \neq 0$, $\beta = \pi/2$ and α decreases from 0 to $\pi/2$ as ξ increases from 1 to ∞.

The plots of magnitude and the orientation of the angular velocity for any θ are shown in the figure 4.4. It is clear that for very small ξ, the magnetic moment is aligned along the magnetic field $\alpha = \theta$ and $\beta = 0$. However, the magnitude of angular velocity depends on θ. When $\theta = 0$, that is $\mathbf{H}$ is parallel to $\hat{\omega}$, the magnetic moment aligns along $\mathbf{H}$ and the cube rotates freely with the vorticity. Therefore $|\mathbf{\Omega}|$ is independent of ξ. As ξ increases from 0 to ∞, α decreases from θ to 0 and β increases from 0 to θ.

When $\theta = 0$, the applied magnetic field, vorticity and the resultant direction of the magnetic moment are all along the same direction. As a result, there is no net external torque on the cube and it rotates freely with the applied vorticity. This result is independent of the magnitude of ξ.

4.5 Calculation of symmetric and anti-symmetric stress in the suspension

Let the three normal vectors to the sides of the cube be $\mathbf{n}, \mathbf{m}, \mathbf{p}$. One of vectors $\mathbf{m}$ is aligned parallel to $\bar{\mathbf{M}}$ and the other two normals $\mathbf{n}$ and $\mathbf{p}$ rotate about $\mathbf{m}$ with the angular velocity $|\mathbf{\Omega}|$. Each cube undergoes periodic rotation so that the unit normal satisfy

$$\mathbf{n}(t) = \mathbf{n}_0 \cos(\Omega t) - \mathbf{p}_0 \sin(\Omega t) \tag{4.27}$$

$$\mathbf{m}(t) = \hat{\mathbf{M}} \tag{4.28}$$

$$\mathbf{p}(t) = \mathbf{n}_0 \sin(\Omega t) + \mathbf{p}_0 \cos(\Omega t) \tag{4.29}$$

However, in a suspension of many cubic particles with weak Brownian motion, there will be mixing among phase angles for $\mathbf{n}_0$ and $\mathbf{p}_0$, which results in

uniform distribution of all orientations in a 2D plane at any given time. Therefore, we can write the orientation of any cube in a dilute suspension as

$$\mathbf{n}(t) = \mathbf{n}_0 \cos(\Omega t + \varphi) - \mathbf{p}_0 \sin(\Omega t + \varphi) \tag{4.30}$$

$$\mathbf{m}(t) = \hat{\mathbf{M}} \tag{4.31}$$

$$\mathbf{p}(t) = \mathbf{n}_0 \sin(\Omega t + \varphi) + \mathbf{p}_0 \cos(\Omega t + \varphi) \tag{4.32}$$

where φ is a phase angle. Weak Brownian motion will lead to a uniform distribution of φ from 0 to 2π in the suspension. The bulk stress consisting of both symmetric and anti-symmetric stresses depend on the orientation of the cube and correspond to stress contributions averaged over all φ.

$$< S_{ij} >= \frac{1}{T}\int_0^T S_{ij}dt = \frac{1}{T}\int_0^T [2.7(\delta_{il}\delta_{jk}+\delta_{ik}\delta_{jl}-\frac{2}{3}\delta_{ij}\delta_{kl})+2.2(\delta_{ijkl}-\frac{1}{3}\delta_{ij}\delta_{ij})]E_{kl}dt \tag{4.33}$$

Here $T = 2\pi/\Omega$, the tensors $\delta_{ij}\delta_{kl}$,$\delta_{il}\delta_{jk}$ and $\delta_{ik}\delta_{jl}$ are isotropic and do not change with the rotation of n_i, m_i and p_i, while δ_{ijkl} changes with the rotation of the cube.

$$< \delta_{ijkl} >= \frac{1}{2\pi/\Omega}\int_0^{2\pi/\Omega} (n_i n_j n_k n_l + m_i m_j m_k m_l + p_i p_j p_k p_l)dt \tag{4.34}$$

Using symmetry and simplifying, we get

$$< \delta_{ijkl} > = m_i m_j m_k m_l + \frac{1}{4}(\delta^{(2)}_{ij}\delta^{(2)}_{kl} + \delta^{(2)}_{il}\delta^{(2)}_{kj} + \delta^{(2)}_{ik}\delta^{(2)}_{jl}) \tag{4.35}$$

$$\delta^{(2)}_{ij} = (\delta_{ij} - m_i m_j) \tag{4.36}$$

Simplifying the above equations, the final expression for $< S_{ij} >$ is

$$< S_{ij} >= 6.15E_{ij} + 0.375E_{kl}m_k m_l(7m_i m_j - \delta_{ij}) - 0.75(m_i m_k E_{kj} + m_j m_k E_{ki}) \tag{4.37}$$

Here m_i is a normal vector parallel to the magnetic moment. Eqn (4.37) together with the solution for the direction of the magnetic moment provides a general

result for the symmetric stress in any linear flow when the magnetic field is perpendicular to the vorticity axis. When the magnetic field is parallel to the vorticity axis Eqn (4.37) applies with **m** being parallel to the vorticity axis.

The anti symmetric stress acting on the cube in case (i) is given by

$$\sigma_{ij}^{anti} = n\epsilon_{ijk}L_k \tag{4.38}$$

$$L_k = R_\omega(\Omega_k - \omega_k) \tag{4.39}$$

$$\sigma_{ij}^{anti} = \frac{nR_\omega}{1+\xi^2|\Omega|^2}\left(cos(\phi)\epsilon_{ijk}\hat{H}_k - \epsilon_{ijk}\hat{\omega}_k - \xi(\hat{H}_i\hat{\omega}_j - \hat{H}_j\hat{\omega}_i)\right) \tag{4.40}$$

The above equations gives the general result for any linear velocity flow problem. The total stress in the medium in any linear velocity field will be the sum of symmetric and anti-symmetric stress in the medium.

4.6 Dilute suspension viscosity

We have calculated the general expression for both symmetric and anti-symmetric stress in any linear flow. We now simplify this solution for a simple shear flow problem and specific orientations of the magnetic field. The effective viscosity η_{eff} of the suspension depends on both the symmetric and the antisymmetric components of stress:

$$< \sigma_{ij} >= 2\eta_{eff}E_{ij} =< \sigma_{ij}^{sym} > + < \sigma_{ij}^{anti} >= 2\eta_f E_{ij} + n < S_{ij>} + n < \epsilon_{ijk}L_k > \tag{4.41}$$

Intrinsic viscosity is defined as the

$$\lim_{\phi\to 0}\frac{\eta_{eff} - \eta_0}{\eta_0\phi} \tag{4.42}$$

In case (i) we consider a magnetic field that is perpendicular to the vorticity (i.e $\theta = \pi/2$), the contributions to the viscosity from the symmetric stress (η^{sym}) and

anti-symmetric stress (η^{anti}) are dependent on the magnitude of ξ

$$\text{When} \quad \xi < 1$$

$$< \eta^{sym} > \quad = \quad \eta_0 \left(1 + 2.7\phi + \left(3.85 sin^2(\delta + \arcsin\xi) cos^2(\delta + \arcsin\xi)\right)\phi\right) \quad (4.43)$$

$$\text{When} \quad \xi \geq 1$$

$$< \eta^{sym} > \quad = \quad \eta_0 \left(1 + 3.25\phi - \frac{0.55}{\xi^2}\phi + \frac{3.85 cos^2\delta sin^2\delta}{\xi^4}\right) \quad (4.44)$$

Here $\arcsin\xi = \beta$, with β as the angle between magnetic moment and H for $\xi < 1$ (figure 4.2). This result clearly shows that the viscosity from symmetric stress is maximum when $\delta + \beta = \pi/4$. Where δ is the angle between the velocity gradient and the project of magnetic field on the flow-gradient plane. In this case, one of the normals is at an angle of $\pi/4$ with respect to the flow direction and the other two normals are orientationally averaged in the perpendicular plane. The symmetric stress is minimum when $\delta + \beta = 0$ or $\delta + \beta = \pi/2$. In this case, one of the normals is along the flow direction and the other two normals are averaged in the vorticity-gradient plane. It is important to note that the symmetric stress depends only on the direction of the magnetic moment with respect to the applied shear. The plot of η^{sym} as a function of ξ is plotted for $\delta = 0$ in figure 4.5. As ξ goes from 0 to $1/\sqrt{2}$, η^{sym} shows a shear thickening behavior with the value increasing from 2.7 to 3.65. When $\xi = 1/\sqrt{2}$, $\beta = \pi/4$, therefore the viscosity from symmetric stress is maximum. As ξ increases from $1/\sqrt{2}$ to 1, η^{sym} shear thins reaching a minimum value of 2.7, when $\beta = \pi/2$. As ξ increases from 1 to ∞, the angular velocity of the cube is non-zero and it approaches the applied vorticity as ξ increases. The value of η^{sym} increases from 2.7 and asymptotes towards 3.25 as $\xi \to \infty$.

In the case of viscosity contribution from anti-symmetric stress, when $\xi < 1$, $|\boldsymbol{\Omega}| = 0$ producing the maximum possible viscous torque and antisymmetric

stress. As ξ increases from 1 to , $|\bar{\Omega}|$ increases from 0 to 1. As a result, the angular velocity of the particle relative to the fluid, $(\bar{\Omega} - \hat{\omega})$, decreases and hence the antisymmetric stress decreases.

$$\eta_{ij}^{anti} = 1.85\eta_0\phi, \text{ when } \xi < 1 \tag{4.45}$$

$$\eta_{ij}^{anti} = \frac{1.85\eta_0\phi}{\xi^2}, \text{ when } \xi \geq 1 \tag{4.46}$$

The effective viscosity of the suspension is the sum of contributions of viscosity from both symmetric and anti-symmetric stresses:

$$\begin{aligned} &\text{When} \quad \xi < 1 \\ &\frac{\eta_{eff}}{\eta_0} = 1 + 2.7\phi + 3.85\sin^2(\delta+\beta)\cos^2(\delta+\beta)\phi + 1.85\phi \\ &\sin\beta = \xi \end{aligned} \tag{4.47}$$

$$\begin{aligned} &\text{When} \quad \xi \geq 1 \\ &\frac{\eta_{eff}}{\eta_0} = 1 + 3.25\phi - \frac{0.55}{\xi^2}\phi + \frac{3.85\sin^2\delta\cos^2\delta}{\xi^4} + \frac{1.85}{\xi^2}\phi \end{aligned} \tag{4.48}$$

In case (ii), we consider a magnetic field is aligned along the vorticity direction and find that

$$< \eta^{sym} > = \eta_0 (1 + 3.25\phi) \tag{4.49}$$

At steady state, the magnetic moment of the cube aligns along the magnetic field or the vorticity direction. The net external magnetic torque on the cube is zero. As a result, the cube rotates freely with the applied vorticity. The steady state configuration is independent of ξ and η_{sym} is constant and is equal to the isotropically averaged contributions from the orientations with the magnetic moment along vorticity direction. Also, since the magnetic moment aligns with the applied magnetic field which results in no external magnetic torque on the particle.

Therefore, when the magnetic field is aligned along the vorticity direction.

$$\frac{\eta_{eff}}{\eta_0} = 1 + 3.25\phi \tag{4.50}$$

The variation of intrinsic viscosity with ξ when $\theta = \pi/2$ and $\delta = 0$ is shown in figure 4.5. The maximum value of intrinsic viscosity is 5.5 and it is produced when magnetic moment is aligned at an angle of $\pi/4$ in the flow gradient plane. It is interesting to note that the minimum value of intrinsic viscosity 3.25 when $\xi \to \infty$, i.e. very weak magnetic field while the isotropically averaged intrinsic viscosity in the absence of any magnetic field is 3.1. Our analysis is based on the assumption that Brownian torques are weak compared to both the viscous and magnetic torques and therefore corresponds to the limits $Pe_r \gg 1$ and $Pe_r/\xi \gg 1$. The intrinsic viscosity of an isotropic suspension would be recovered when the magnetic torque is much weaker than the viscous torque, corresponding to $Pe_r/\xi \ll 1$.

The plot showing the variation of intrinsic viscosity on δ and ξ are shown in the figure 4.6. It is clear that the minimum and maximum value of intrinsic viscosity does not change on δ. For $\xi < 1$, the angular velocity of cube is zero and the anti-symmetric component is maximum. The symmetric component of stress depends on the equilibrium orientation of the cube with respect to the applied shear flow. The orientation is decided by both δ and ξ. The angle between velocity gradient and the magnetic momenet is $\delta + \beta$ with $\sin\beta = \xi$. As it is clear from the above equations, the intrinsic viscosity curves fall on the same curve if plotted against $\delta + \beta$. The maximum value of intrinsic viscosity is obtained when $\delta + \beta = \pi/4$ and the minimum value is obtained when $\delta + \beta = 0$ or $\pi/2$. For $\delta = \pi/6$, as ξ increases from 0 to 1, the angle between velocity gradient and the magnetic moment changes from $\pi/6$ to $2\pi/3$. The intrinsic viscosity increases as

this angle increases from $\pi/6$ to $\pi/4$. The value of intrinsic viscosity decreases from $\pi/4$ to $\pi/2$ and then it increases again until $2\pi/3$.

4.7 Conclusions

In this chapter, we have calculated the major effects of magnetic field on the viscosity of magnetic suspension. We found that the effective viscosity of the magnetic suspension increases in the presence of magnetic field by an amount dependent on the magnitude and the direction of applied shear. This increase is comparable in magnitude to the amount by which the solution viscosity in the absence of any field exceeds the viscosity of the solvent. Consequently, this field dependence should produce significant effects on the flow. When the magnetic field is perpendicular to the vorticity direction, with the increase in magnetic field, cubes exhibit either shear thickening or shear thinning behavior based on the magnitude of magnetic field strength

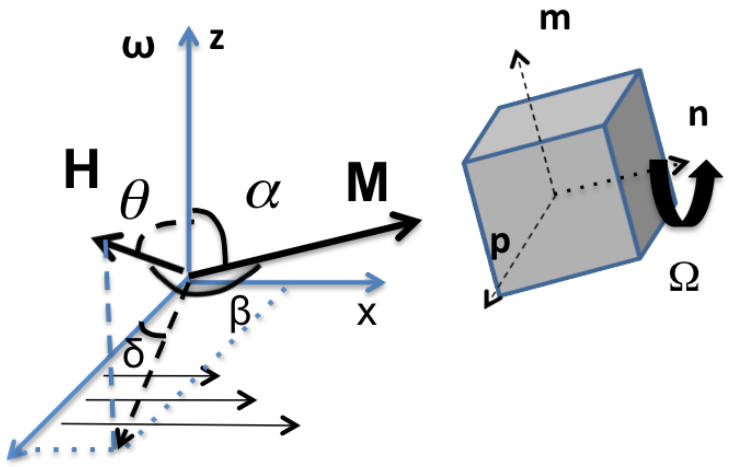

Figure 4.2: Schematic figure showing the orientation of the cube with respect to the applied shear and magnetic field. θ is the angle between **H** and vorticity vector (ω); δ is the angle the projection of **H** on the velocity-gradient plane makes with the gradient direction; α is the angle between magnetic moment and ω and β is the angle between **H** and **M**

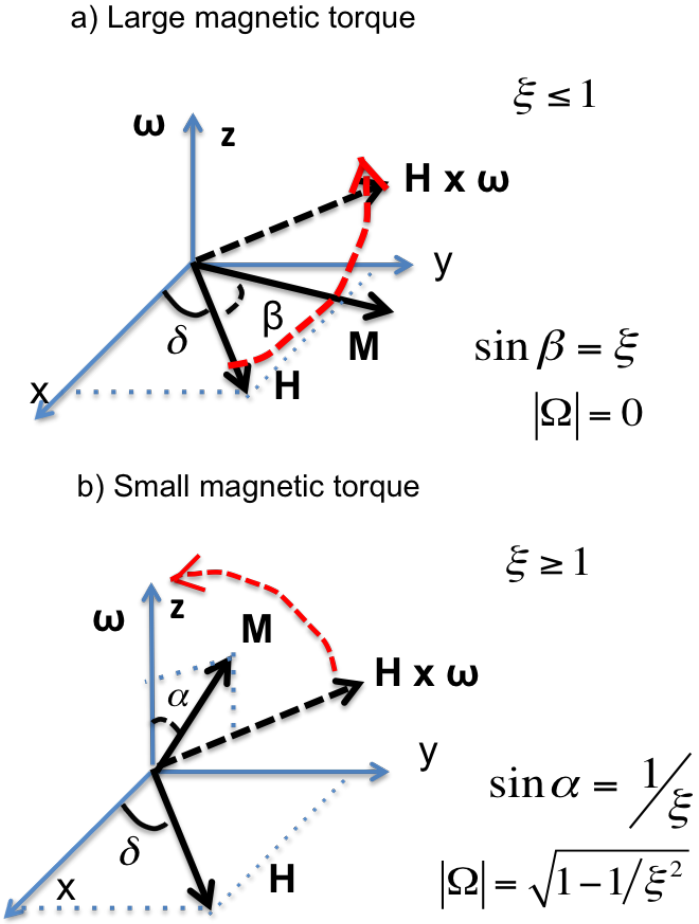

Figure 4.3: Schematic figure illustrating the evolution of orientation of the magnetic moment with increasing ξ. The dotted red arrow indicates the evolution of the direction of magnetic moment **M** with increasing ξ

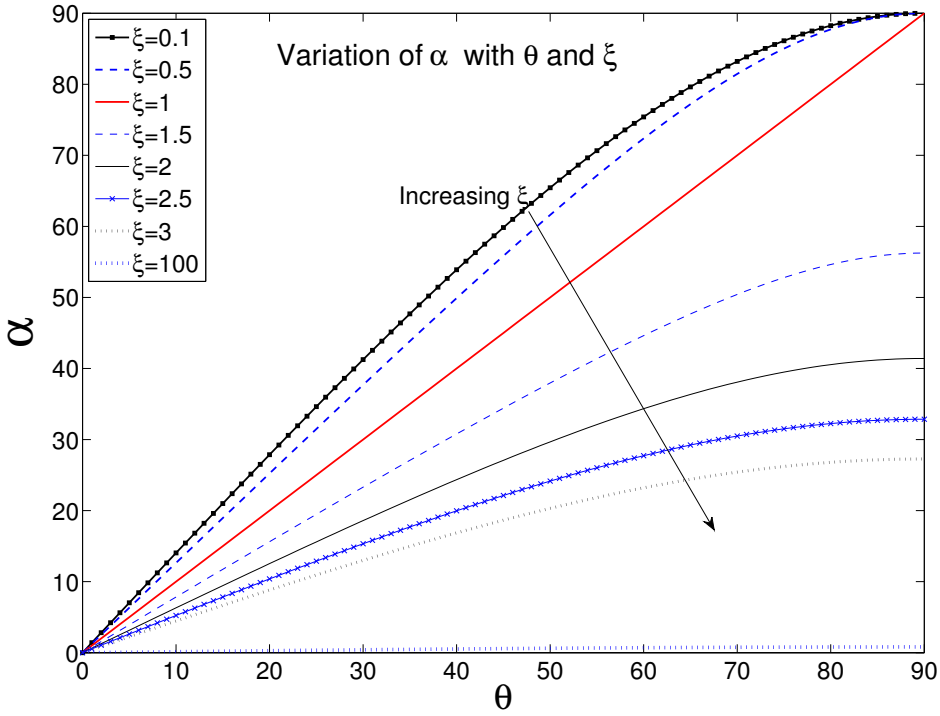

Figure 4.4: Plot shows the variation of α with θ and ξ. α is the angle between magnetic moment and the vorticity direction. As ξ increases, the strength of the magnetic field decreases and α decreases

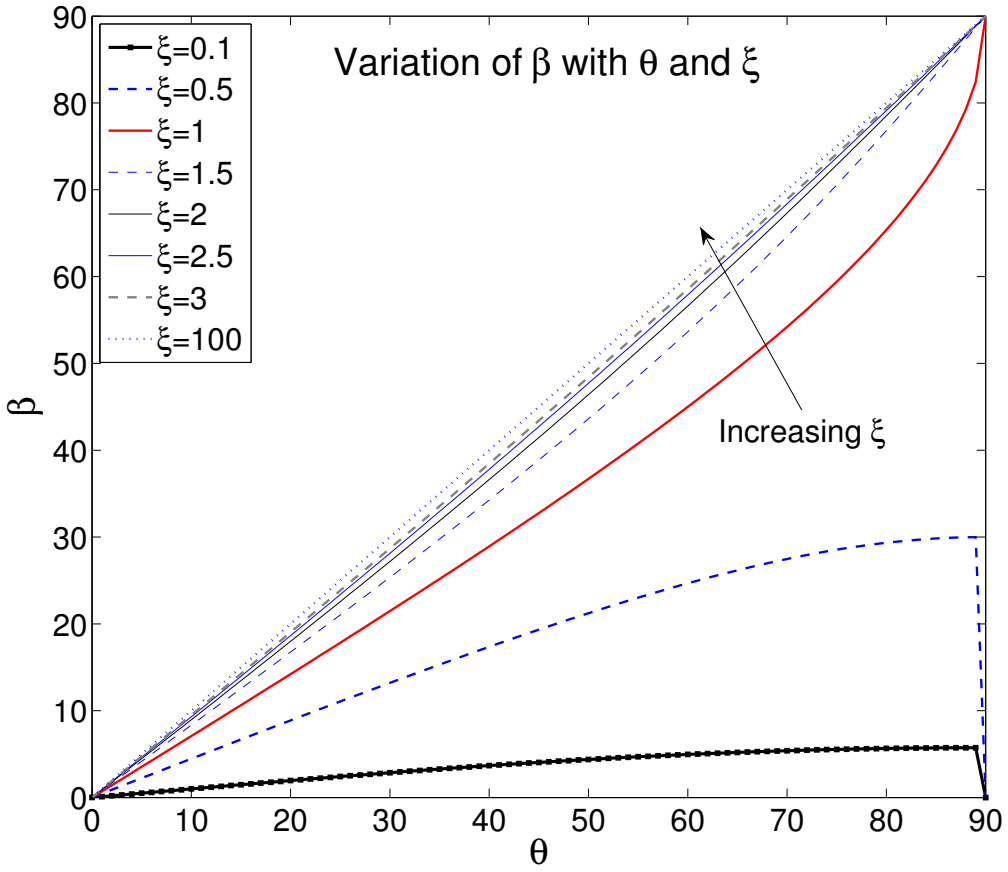

Figure 4.5: Plot shows the variation of β with θ and ξ. β is the angle between magnetic moment and the applied magnetic field. As ξ decreases, the strength of the magnetic field increases and β decreases

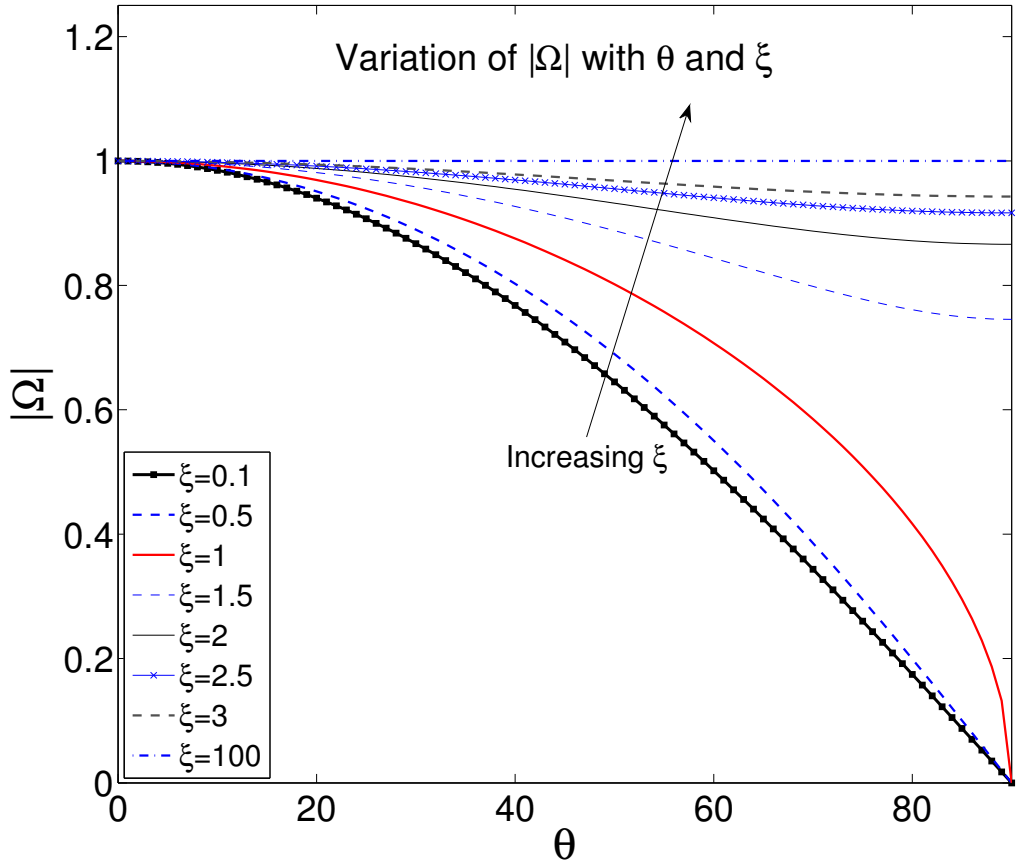

Figure 4.6: Plot shows the variation of Ω with θ and ξ. Ω is the magnitude of resultant angular velocity. As ξ increases, the strength of the magnetic field decreases and Ω becomes closer to 1

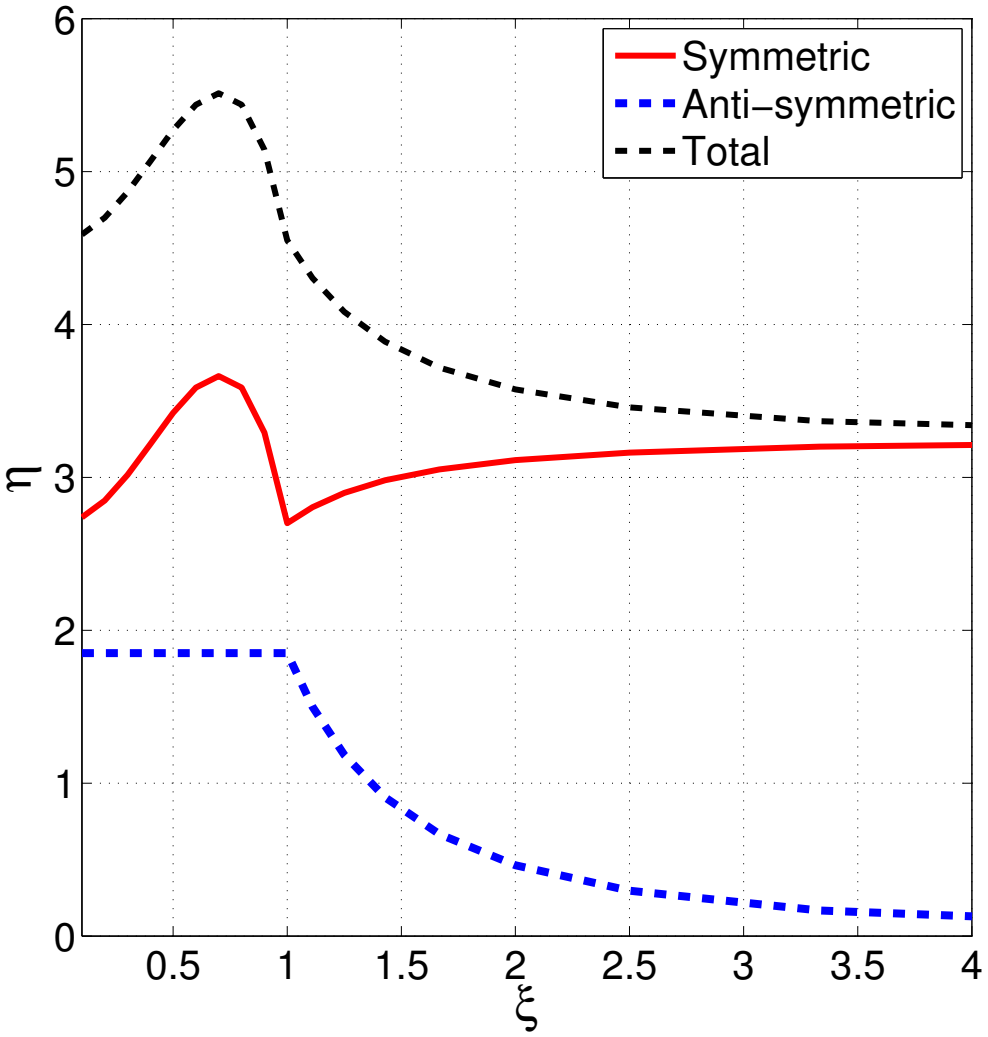

Figure 4.7: ξ dependence of the different contributions to the intrinsic viscosity of suspensions when the magnetic field is along the velocity gradient direction

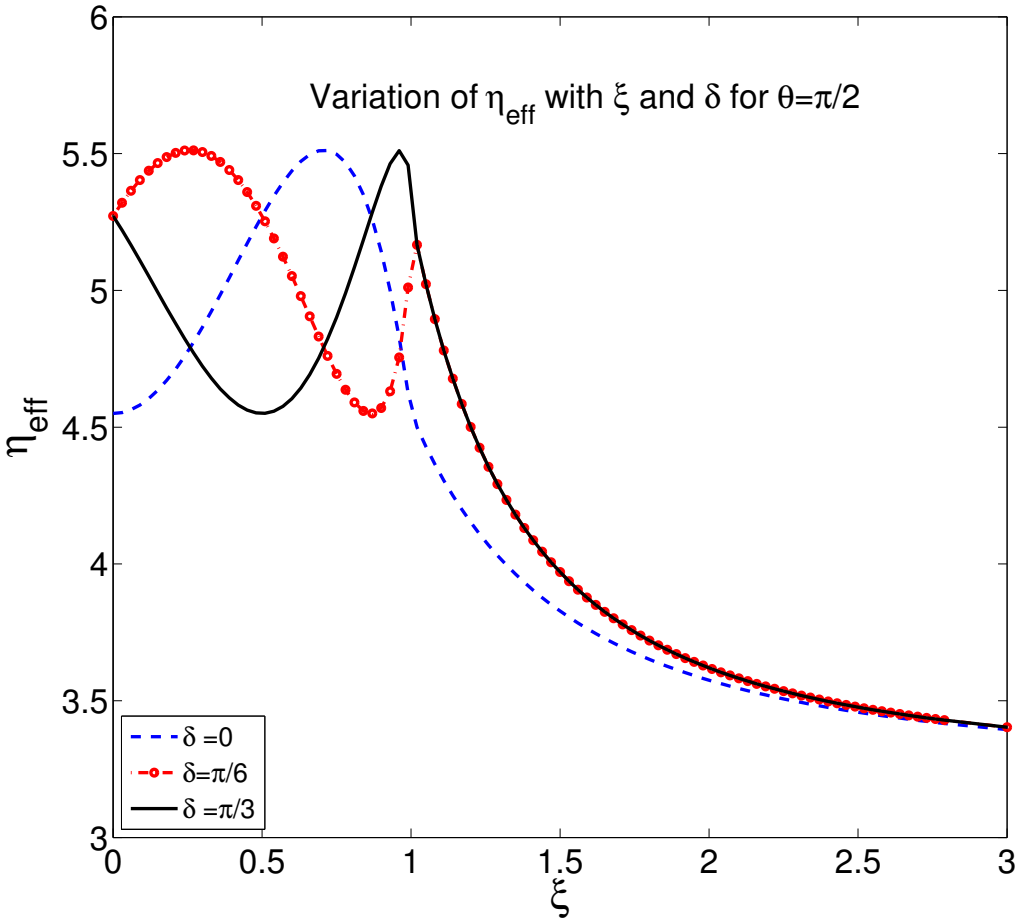

Figure 4.8: ξ Dependence of the different contributions to the intrinsic viscosity of suspensions when the magnetic field is at an angle δ to the flow direction.

BIBLIOGRAPHY

[1] John P. McTague. Magnetoviscosity of magnetic colloids. *The Journal of chemical Physics*, 51(1):153, 1969.

[2] R.E. Rosensweig. Viscosity of magnetic fluid in a magnetic field. *Journal of Colloid and Interface Science*, 29(4):680, 1969.

[3] W.F. Hall and S. N Busenberg. Viscosity of magnetic suspensions. *The Journal of chemical Physics*, 51(1), 1969.

[4] M.I. Shliomis. Effective viscosity of magnetic suspensions. *Soviet Physics JETP*, 34(6):1291, 1972.

[5] Howard Brenner and Michael H. Weissman. Rheology of a dilute suspension of dipolar spherical particles in an external field ii. effects of rotary brownian motion. *Journal of Colloid and Interface Science*, 41(3):499, 1972.

[6] D. Kim, N. Lee, M. Park, B. H. Kim, K. An, and T. Hyeon. Synthesis of uniform ferrimagnetic magnetite nanocubes. *Journal of the American Chemical Society*, 131(2):454, 2009.

[7] S.R. Strand and S. Kim. Dynamics and rheology of a dilute suspension of dipolar nonspherical particles in an external field: part 1. steady shear flows. *Rheologica Acta*, 31:94, 1992.

[8] K. Asokan and T.R. Ramamohan. The rheology of a dilute suspension of brownian dipolar spheroids in a simple shear flow under the action of an external force. *Physics of Fluids*, 16(2):433, 2004.

[9] J.H. Sanchez and C. Rinaldi. Magnetoviscosity of dilute suspension of magnetic ellipsoids obtained through rotational browniandynamics simulations. *Journal of Colloid and Interface Science*, 331:500–506, 2009.

[10] Akira Satoh. Rheological properties and orientational distribution of dilute ferromagnetic spherocylinder particle dispersions: Approximate solutions by means of galerkin's method. *Journal of Colloid and Interface Science*, 234:425, 2001.

[11] Y. Almog and I. Frenkel. The motion of axisymmetric dipolar particles in homogeneous shear flow. *Journal of Fluid Mechanics*, 289:243, 1995.

[12] G. K. Batchelor. The stress system in a suspension of force-free particles. *Journal of Fluid Mechanics*, 41:545–570, 4 1970.

[13] Rajesh K Mallavajula, Donald L. Koch, and Lynden A. Archer. Intrinsic viscosity of a suspension of cubes. *Physical Review E*, 88:052302, 2013.

[14] K. C. Nunan and J. B. Keller. Effective viscosity of a periodic suspension. *Journal of Fluid Mechanics*, 142:269–287, 1984.

[15] H. K. Moffatt. Viscous and resistive eddies near a sharp corner. *Journal of Fluid Mechanics*, 18(01):1–18, 1964.

CHAPTER 5

BROWNIAN DYNAMICS SIMULATIONS OF HARD CUBIC PARTICLES IN SUSPENSIONS UNDER SHEAR

5.1 Introduction

This chapter addresses the structure, diffusion, and rheology of colloidal dispersions of hard cubes in the absence of inter-particle hydrodynamic interactions using Brownian dynamics simulations. Interactions between cubic particles is unique due to the presence of flat surfaces, sharp corners and edges. Since a cube is a regular polyhedron with no aspect ratio, the force/velocity and torque/rotation rate resistivities are independent of its orientation. These resistivities were calculated in chapter 2 and they differ from the sphere only by a scalar constant. As a result the long range interactions between cubes will be similar to that of spherical particles. However, unlike spheres, cubic particles have anisotropic in stress. The stress acting on the cube depends on the orientation and was calculated in chapter 3. Also, in the case of hard spheres, inter-particle lubrication forces are sufficient to prevent them from overlapping with each other even before spheres actually collide. For cubic particles, most of the collisions are either edge-edge collisions or corner-face collisions at low to moderate volume fractions. The lubrication interaction between cubes is much weaker (or almost negligible) than for spheres since a sharp corner does not have a nearly parallel surface except when two cubes have nearly the same orientation. Therefore, unlike spheres inter-particle lubrication stresses do not play a major role in the rheology of cubic suspensions. Collisional stresses generated due to hard cubic interactions are calculated to understand the rheology of these

suspensions. Interestingly, collisions between cubes depends on the relative orientation and the distance between them and unlike spheres, the contact forces are not along the line of centers of the particles. This results in the coupling between translational and rotational motion through collisional forces and torques acting between them which leads to distinct rheological properties.

In collolidal suspensions the particles are large enough so that the suspending fluid can be treated as a continuum, yet small enough so that the particles are affected by Brownian motion arising from the thermal fluctuations in the surrounding fluid. Thus, the behavior of the particles in the dispersion is governed by the many-body Langevin equation. Brownian dynamics simulation studies the motion of particles without considering hydrodynamic interactions between the particles.

The theory of Brownian motion originated with the works of Einstein[1], Smoluchowski, Langevin, Fokker, Planck [2], Batchelor[3]. A method for simulating Brownian particles with hydrodynamic interactions was first presented by Ermak and Mc- Cammon [4]. There has been extensive work utilizing Brownian Dynamics to simulate particles with a variety of different interparticle potentials Heyes[5], Xue and Grest[6], Rastogi et al[7]. Durlofsky et al. [8] developed a method to include hydrodynamic interactions, both the strong short-range lubrication forces and the long-range many- body interaction called as Stokesian dynamics simulations. Foss and Brady implemented Stokesian dynamics simulatons and compared the results with the Brownian dynamics without hydrodynamic interactions[9][10]. The Stokesian Dynamics method as currently implemented is computationally intensive and there is interest in using a simpler algorithm. Elimination of hydrodynamic interactions between particles

greatly simplifies these computations.

Hard-sphere dispersions have proven difficult to simulate due to the singular and discontinuous nature of the hard-sphere interparticle potential. Heyes and Melrose [5]and Schaertl and Sillescu [11] independently developed a method for simulation of hard spheres for measuring shear thinning and self-diffusion, respectively. Brady and foss extended this method and obtained the simulation results for hard sphere suspensions. We have extended this method to include the non-spherical behavior of particles.

In the next section, Brownian Dynamics algorithm used in this work is explained and the method to determine the pairwise interparticle forces responsible for the hard- sphere-like behavior is described. These interparticle forces facilitates in calculation of instantaneous values of all components of the particle contribution to the bulk stress tensor. In Section 3 we present and discuss the results of these simulations.

5.2 Simulation Methodology

For N rigid cubic particles suspended in an incompressible Newtonian fluid of viscosity η and density ρ, the fluid motion is governed by the Navier-Stokes equations, while the particle motion is described by the coupled N-body Langevin equation:

$$m\frac{d\mathbf{U}}{dt} = \mathbf{F^h} + \mathbf{F^b} + \mathbf{F^p} \tag{5.1}$$

$$I\frac{d\mathbf{\Omega}}{dt} = \mathbf{T^h} + \mathbf{T^b} + \mathbf{T^p} \tag{5.2}$$

Here $\mathbf{F^h}$, $\mathbf{F^b}$ and $\mathbf{F}^p$ are the hydrodynamic, Brownian and interparticle forces acting on each cube and $\mathbf{T^h}$, $\mathbf{T^b}$ and $\mathbf{T}^p$ are the corresponding torques on each cube. m is the mass and I is the moment of inertia of the cube. Interaction between cubes are considered as hard cubic interactions. The hydrodynamic particle-particle interactions are neglected and the particle-fluid interactions give rise to the net force and torque acting on an isolated cube in a shear flow field.

$$\mathbf{F^h} = -R_f(\mathbf{U} - < \mathbf{U} >) \tag{5.3}$$

$$\mathbf{T}^h = -R_\omega(\mathbf{\Omega} - \omega) \tag{5.4}$$

$< \mathbf{U} >$ is the imposed shear flow at the center of the cube. For a linear shear flow $< \mathbf{U} > = \dot{\mathbf{\Gamma}}.\mathbf{r}$ Here $\mathbf{T}$ is the velocity gradient tensor of the bulk flow. $\mathbf{\Omega}$ is the net angular velocity of the cube and ω is the applied vorticity at the center of the cube. R_f and R_ω are the resistivity tensors to translation and the rotation of the cube. The resistivities R_f and R_ω are calculated using finite element simulations by imposing constant velocity field and constant rotational field around an isolated cube respectively. The values of R_f and R_ω are found to be $R_f = 13.94a\eta$ and $R_\omega = 7.39a^3\eta$.

The Brownian forces are due to the thermal fluctuations of the cubic particles. When Reynolds number based on the cube size is small, for the shear flows considered here, the cubic particles move in a force free and torque free environment. Due to the stochastic nature of particles, we assume that the correlation time in the force and torque fluctuations are rapid compared to the particle relaxation time. Applying fluctuation-dissipation theorem, we have

$$< \mathbf{F^b} > \; = \; < \mathbf{T^b} >= \mathbf{0} \tag{5.5}$$

$$< \mathbf{F}^b(0)\mathbf{F}^b(t) > \; = \; 2kTR_f\delta(t) \tag{5.6}$$

$$< \mathbf{T}^b(0)\mathbf{T}^b(t) > \; = \; 2kTR_\omega\delta(t) \tag{5.7}$$

Here the < . >denote the ensemble average of the interactions, k is the Boltzman constant and T is the temperature.

Upon integrating the above equation over a time step Δt larger than the inertial relaxation time of the cubes but small compared with the time over which the configuration changes, we get

$$\mathbf{r}(t+\Delta t) = \mathbf{r}(t) + < \mathbf{U} > \Delta t + \Delta \mathbf{X}^t_{HC} + \mathbf{X}^t(\Delta t) \tag{5.8}$$

$$\mathbf{n}(t+\Delta t) = (\mathbf{n}(t) \times \mathbf{\Omega})\Delta t \tag{5.9}$$

$$\mathbf{m}(t+\Delta t) = (\mathbf{m}(t) \times \mathbf{\Omega})\Delta t \tag{5.10}$$

$$\mathbf{p}(t+\Delta t) = (\mathbf{p}(t) \times \mathbf{\Omega})\Delta t \tag{5.11}$$

$$\mathbf{\Omega} = \omega + \frac{\Delta \mathbf{X}^r_{HC}}{\Delta t} + \frac{\mathbf{X}^r(\Delta t)}{\Delta t} \tag{5.12}$$

$$\Delta \mathbf{X}^t_{HC} = \frac{\mathbf{F}^p}{R_f}\Delta t \tag{5.13}$$

$$\Delta \mathbf{X}^r_{HC} = \frac{(\mathbf{r} \times \mathbf{F^p})}{R_\omega}\Delta t \tag{5.14}$$

Here, $\mathbf{r}(t)$ is the position vector of the cube at time t, $\mathbf{n}(t), \mathbf{m}(t), \mathbf{p}(t)$ are the three unit normals to the sides of the cube at time t. $\mathbf{X}^t_{HC}$ and $\mathbf{X}^r_{HC}$ are the translational and rotational displacements due to the inter-particle hard cube interactions. $\mathbf{X}^t(t)$ and $\mathbf{X}^r(t)$ are the translational and rotational displacements of the cube due to Brownian motion. Since the inter-particle hydrodynamic interactions are neglected rotational motion is completely decoupled from the translational motion and $\mathbf{X}^t(t)$ and $\mathbf{X}^r(t)$ has zero mean and covariance given by the corresponding short-time self diffusivities,

$$< \mathbf{X^t} > = < \mathbf{X^r} >= \mathbf{0} \tag{5.15}$$

$$< \mathbf{X}^t(0)\mathbf{X}^t(\Delta t) > = 2D_t\Delta t\mathbf{I} \tag{5.16}$$

$$< \mathbf{X}^r(0)\mathbf{X}^r(\Delta t) > = 2D_\omega\Delta t\mathbf{I} \tag{5.17}$$

D_t and D_ω are the tracer translational and rotational diffusivity of a cube, given by $D_t = kT/R_f$ and $D_\omega = kT/R_\omega$

Non-dimensionalizing the above equations leads to

$$\Delta\bar{\mathbf{r}} = Pe < \bar{\mathbf{U}} > \Delta\bar{t} + \bar{\mathbf{F}}^p\Delta\bar{t} + \bar{\mathbf{X}}^t(\Delta\bar{t}) \tag{5.18}$$

$$\mathbf{n}(t + \Delta t) = (\mathbf{n}(\bar{t}) \times \bar{\mathbf{\Omega}})\Delta\bar{t} \tag{5.19}$$

$$\mathbf{m}(t + \Delta t) = (\mathbf{m}(\bar{t}) \times \bar{\mathbf{\Omega}})\Delta\bar{t} \tag{5.20}$$

$$\mathbf{p}(t + \Delta t) = (\mathbf{p}(\bar{t}) \times \bar{\mathbf{\Omega}})\Delta\bar{t} \tag{5.21}$$

$$< \bar{\mathbf{X}}^{\mathbf{t}} > = \mathbf{0} \tag{5.22}$$

$$< \bar{\mathbf{X}}^t(0)\bar{\mathbf{X}}^t(\Delta\bar{t}) > = 2\Delta\bar{t}\mathbf{I} \tag{5.23}$$

$$\bar{\mathbf{\Omega}} = \bar{\omega} + \frac{D_\omega}{D_t}\frac{(\bar{\mathbf{r}} \times \bar{\mathbf{F}}^{\mathbf{p}})}{\Delta\bar{t}} + \frac{D_\omega}{D_t}\frac{\bar{\mathbf{X}}^{\mathbf{r}}(\Delta\bar{t})}{\Delta\bar{t}} \tag{5.24}$$

$$< \mathbf{X}^{\mathbf{r}} > = \mathbf{0} \tag{5.25}$$

$$< \mathbf{X}^r(0)\mathbf{X}^r(\Delta t) > = 2\Delta\bar{t}\mathbf{I} \tag{5.26}$$

Here $\Delta\mathbf{r}$ is nondimensionalized by the characteristic particle size a; the time by the diffusive time scale a^2/D_t; the imposed velocity $< \mathbf{U} >$ by $\dot{\gamma}a$, where $\dot{\gamma}$ is the magnitude of the shear rate ($\dot{\gamma} = |\dot{\mathbf{\Gamma}}|$). The Peclet number, $Pe = \dot{\gamma}a^2/D_t$, measures the relative importance of shear and Brownian forces. We use periodic boundary conditions for equilibrium suspensions and Lees-Edwards boundary conditions for non-zero Pe.

In this work, we are interested in a monodisperse suspension of hard cubes. The equations of motions described above are similar to that of spherical particles with rough surfaces which have tangential frictional collisional forces acting on them. In this case, collisional torques are generated due to the frictional forces, while collisional torques are generated due to their shape for cubic particles.

We have modified the potential-free algorithm developed by Heyes and Melrose (also used by Schaertl and Sillescu, Brady and Foss) in which the Brownian and affine displacements and rotations are made first. The simulation then checks for particle overlaps and calculates the collision forces and torques based on the degree of overlaps. In a single time step, cubic particles are initially translated and rotated based on the applied shear and Brownian motion. Overlapping pairs of cubes are determined using perpendicular axis theorem. Any overlap between two cubes can either be edge-edge overlap or a corner-face overlap and it depends on the relative orientation and the distance between cubes. The direction, magnitude and the point of contact forces are then determined for each pair. If the overlap is an edge-edge overlap, the direction of contact force is perpendicular to the two overlapping edges, if the overlap is a corner-face overlap, the contact force is perpendicular to the face on which the overlap occurs. If the time step used in the simulations is small, the minimum translating distance required to unoverlap the two cubes will be along the direction for the contact force. The point of application of force on the two cubes is determined from this minimum translating vector. Since the contact force produces both translation and rotation of the cube, the magnitude is iterated such that the net result of application of force over the time step Δt will rotate and translate the two cubes to just unoverlap them. This procedure of application of contact forces retraces their paths to the point of near contact for small Δt. Since the contact forces that are applied are pair-wise in nature, repeated application of contact forces over all the particle pairs resolves almost all the overlaps. Similar procedure was used to calculate the contact forces for slender rods[x3].

The bulk stress (σ_{ij}) in the medium is a combination of hydrodynamic (σ^h_{ij})and collisional stresses (σ^c_{ij}) in the medium. Since we have neglected the

inter-particle hydrodynamic interactions, the hydrodynamic contribution to the stress reduces to the first order volume fraction correction and the direct Brownian contribution to the stress is zero without hydrodynamic interactions.$\sigma^h_{ij} = -nkT\delta_{ij} + 2\eta E_{ij} + n\eta_{ijkl}E_{kl}$). Therefore, the bulk stress in the medium is given by

$$\sigma_{ij} = -p\delta_{ij} - nkT\delta_{ij} + 2_{ij} + n[\eta_{ijkl}]) < E_{kl} > -n < x_i F^p_j > \tag{5.27}$$

Here p is the pressure, n is the number of particle per unit volume, ϕ is the volume fraction and x_i is the inter-particle center to center distance. Here $[\eta_{ijkl}]$ is a forth order viscosity tensor given by given by

$$[\eta_{ijkl}] = 2.7(\delta_{ik}\delta_{jl}+\delta_{il}\delta_{jk}-\frac{2}{3}\delta_{ij}\delta_{kl})+2.2(n_i n_j n_k n_l+m_i m_j m_k m_l+p_i p_j p_k p_l-\frac{1}{3}\delta_{ij}\delta_{kl}) \tag{5.28}$$

Therefore, interesting results are present in the collisional stresses $\Sigma_{ij} = x_i F^p_j$ obtained from the simulations. Unlike collisions between spherical particles, the contact forces produce torques on the particles. Therefore, cubic particle have a finite angular velocity relative to the fluid which will result in an anti-symmetric collisional stresses in the medium. Therefore Σ_{ij} can be written as

$$\Sigma_{ij} = \Sigma^{sym}_{ij} + \Sigma^{anti-sym}_{ij} \tag{5.29}$$

$$\Sigma^{anti-sym}_{ij} = \epsilon_{ijk}R_\omega(\Omega_k - \omega_k) \tag{5.30}$$

The suspension viscosity due to collisional stresses relative to that of the solvent is defined for simple shear flow from the xy-components of the bulk stress and rate of strain

$$\eta_r = \frac{\Sigma^{sym}_{xy}}{2\eta E_{xy}} \tag{5.31}$$

One of the other important factors in the simulations is the value of the time step Δt. The magnitude of the non-dimensional time step is important in the equation of motion for both low and high Pe. For any non-dimensional time

step, Δt, if N_c is the number of collisions that occur in each time step Δt, the ensemble average of the collisional stress is given by

$$< \sigma >=< N_c >< \mathbf{x}\mathbf{F}^p > \tag{5.32}$$

Here $\mathbf{F}^p$ and $\mathbf{x}$ are the contact forces and displacement vector between the two particles in the collisions. The magnitude of the contact force $\mathbf{F}^p$ is proportional to the overlapping distance between particles.The dominant contribution to this distance is the Brownian displacement (scales as $\Delta t^{(1/2)}$) for low Pe and shear displacement (scales as Δt^1) for high Pe. Therefore, the contact force $\mathbf{F}_p$ scales as $\Delta t^{(1/2)}$ for low Pe and Δt^1 for high Pe. The number of collisions per time step (N_c) is related to the flux of the particles hitting its surface. The flux is related to the relative velocity, which scales as $\Delta t^{(-1/2)}$ for low Pe and $\Delta t^{(-1)}$ for high Pe. Therefore, the ensemble average of total collisional stress should be independent of the value of Δt used in the simulations, provided the number of collisions per time step is small compared to the total number of particles.

Equilibrium osmotic pressure ($\Pi = \frac{\sigma_{xx}+\sigma_{yy}+\sigma_{zz}}{3}$) is a convenient parameter to calculate for various magnitudes of time step. Based on the scaling analysis, it should be feasible to find a maximum value of Δt below which, the osmotic pressure remains almost constant. The dependence of osmotic pressure(Π) on the magnitude of non-dimensionalized Δt is plotted for 250 cubic particles at volume fraction of 0.2(figure 5.1). It is clear that the value of osmotic pressure is almost constant after $\Delta t = 10^{-5}\frac{a^2}{D_t}$. At this Δt, the number of collisions per time step (N_c) is 15. We chose appropriate values of Δt by maintaining approximately the same number of collisions per time step. We have verified that the osmotic pressure remains approximately constant when the number of collisions per time step N_c is less than or equal to 15 for $\phi = 0.45$ with 250 cubic particles.

We have also varied the number of cubic particles to study its dependence of osmotic pressure at the same Δt. As the number of particles increase, the computational time needed to resolve the inter-cube collisions increases. Furthermore, as the volume fraction increases, we would need more particles to simulate bulk flow behavior. Figure 5.2 shows the variation of osmotic pressure for 250 and 1000 particles over a range of volume fractions. It is clear from the figure that the percentage change in the osmotic pressure is very small even at higher volume fractions. Therefore all the simulations were carried out with 250 cubic particles in the system.

5.3 Results

A large number of simulations have been performed over a range of volume fractions (ϕ = 0.1 to 0.4) and Peclet numbers (Pe = 0 to 10000). For equilibrium suspensions, all the runs for volume fractions less than 0.2 were started from a random configuration of particles. For higher volume fractions, they were initialized with random orientation at ϕ = 0.2 and the particle size is slowly increased by five percent and allowed to reach equilibrium before it is increased further again. The procedure is repeated until we reach the desired volume fraction. The system was allowed to reach equilibrium at the desired volume fraction by running it for more than $100a^2/D_t$ steps. For non-zero Peclet numbers, simulations were started from the equilibrium configuration of cubic particles. Many of the long runs were divided into statistically independent subintervals in order to determine the statistical variation in the properties.The value of time step used is $\Delta t = k * max(1, Pe)$ here, Δt is non-dimensionalized by a^2/D_t. All simulations are for simple shear flow with the flow, velocity-gradient, and vorticity

directions, respectively, along the three axes (x, y, z) of the cubic unit cell.

5.3.1 Equilibrium suspensions

The suspension microstructure plays an important role in determining the bulk properties of the suspensions. Previously, equilibrium configuration of cubic particles was studied using Monte Carlo simulations. It has been shown that cubic particles exists in different phases based on the volume fraction of particles. For volume fractions(ϕ) lower than 0.45, they exist in isotropic phase wherein, the cubes have no translational and rotational order. For $\phi > 0.52$ and < 0.74, they exist in cubatic phase. In this phase, cubes have rotational order but no translational order. For $\phi > 0.74$, cubes are in crystalline phase. In this case, they have both translational and rotational order. $\phi > 0.45 and < 0.52$ is a coexisting region between isotropic and cubatic phases. Using Brownian dynamics, the time required to reach equilibrium increases as the volume fraction of cubes increases. Specifically, it is difficult to obtain phase transitions because the particles get stuck in the glassy phase. Therefore, our study is restricted to volume fractions less than 0.45.

The equilibrium pair probability distribution ($g(r)$, r is the non-dimensionalized distance) for cubic particles at various volume fractions is shown in the figure 5.3. $g(r) = 0$ for $r < 1$ because $r = 1$ is the minimum separation distance between the cubes. As it is clear from the figure, the height of the first peak position increases as the volume fraction increases. The position of the peak decreases gradually with the volume fraction. As the volume fraction increases, cubes tend to become translationally more layered, which is

indicated by the enhancement in the second and third peaks. As the volume fraction increases, the number of nearest neighbors increases which is indicated by the area under the curve.

The osmotic pressure in a suspension is given by

$$\Pi = -\frac{1}{3}(\sigma_{xx} + \sigma_{yy} + \sigma zz) - nkT \tag{5.33}$$

When nondimensionalized by nkT, the particle contribution to the suspension pressure at equilibrium is equal to the collisional stress that arises from the xF_p term in governing equation. Figure 5.4 shows the equilibrium suspension pressure as a function of volume fraction ϕ. These results have been plotted relative to the Carnahan-Starling equation, valid for hard sphere suspensions. As it is clear from the figure, the values of osmotic pressure for spheres is larger than that of cubes at lower volume fractions. However, as the volume fraction increases the osmotic pressure for cubes increases much more rapidly than spherical particle suspensions. This is because, as the volume fraction increases the number of nearest neighbors increases which would hinder the rotational freedom of cubes resulting in much more rapid increase in the osmotic pressure compared to the spherical particles. As we approach $\phi = 0.5$, the increase in the osmotic pressure is attributed to the system reaching a phase transition region.

Comparisons are also made with the osmotic pressure of an inscribed sphere and having hard sphere interactions. This will be the lower limit of osmotic pressure for cubic particles. As it is clear from the figure 5.4, the value of osmotic pressure for inscribed spheres is always less than that of cubic particles. We have used the pair probability distribution of cubic particles at very low concentrations to obtain the potential of mean force, which is then used as a soft interaction potential between inscribed spheres. The pair probability distri-

bution function at very low concentrations is initially calculated. It was fitted with a sixth order polynomial function with the correct boundary conditions (i.e $g(r) = 0$ when $r = 1$ and $g(r) = 1$ when $r = \sqrt{(3)}$. The potential of mean force $U(r)$ is calculated as $U(r) = -kT \log(g(r))$. Metropolis monte carlo simulations were carried out to obtain the equilibrium configurations of spherical particles interacting through the above mentioned soft potential at various volume fractions. The osmotic pressure for these soft spheres is then calculated $\Pi = \frac{2\pi}{3} n^2 \int_0^\infty r^3 g(r) \frac{dU}{dr} dr$. Here n is the number of particles per unit volume.

In order to better understand the dependence of osmotic pressure of cubic particles, we have compared it with the osmotic pressure for an inscribed spheres interacting with the above mentioned soft potential. This method preaverages the orientation dependence and approximates the cube as an inscribed sphere interacting with orientationally averaged soft potential. As it is clear from the figure 5.4, at low volume fractions, the osmotic pressure for cubic particles matches well with that of the inscribed spheres interacting through soft potential. As the volume fraction increases, cubes start to lose their orientational freedom, thereby resulting in the increase of osmotic pressure.

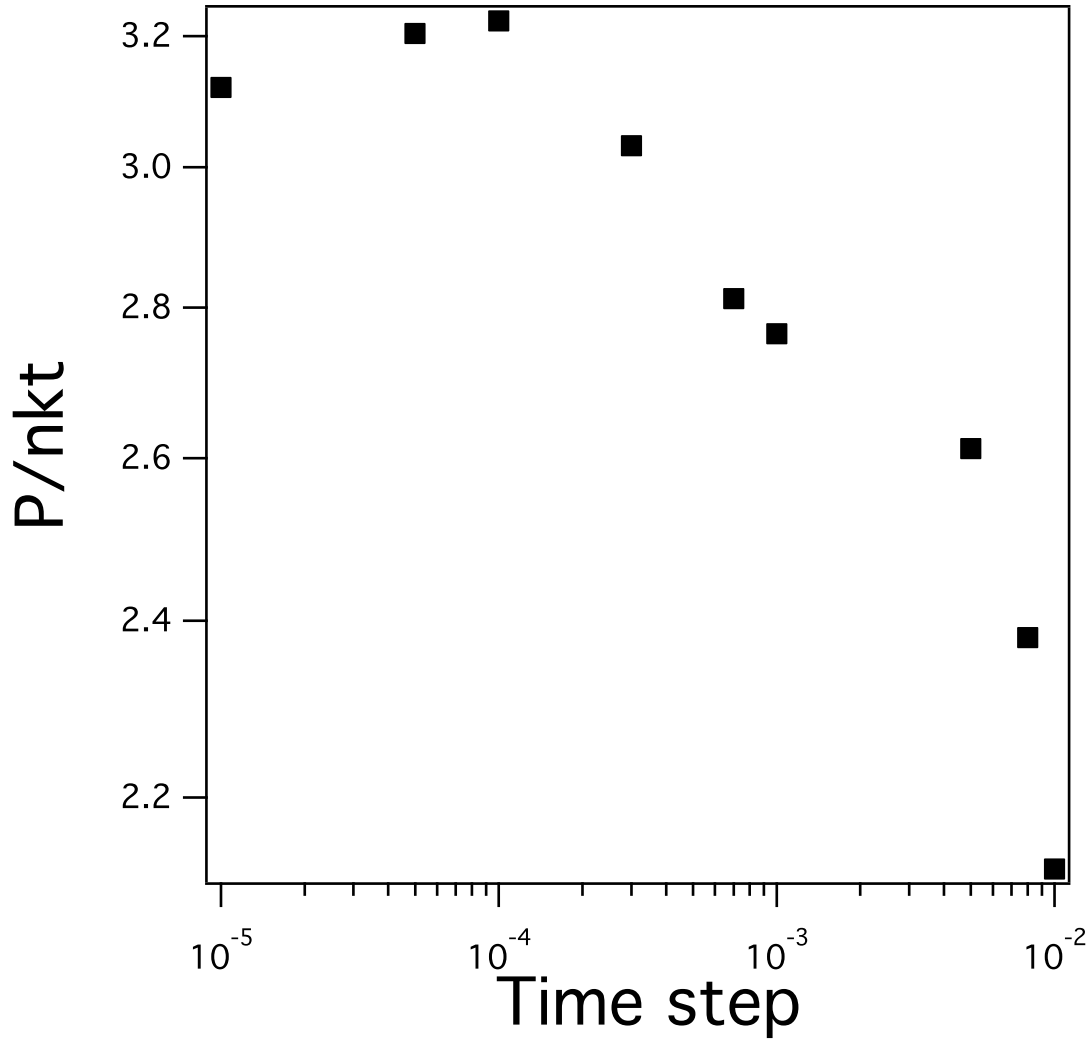

Figure 5.1: Variation of Osmotic pressure with the size of the time step. As the time step decreases, the value of osmotic pressure almost remains constant

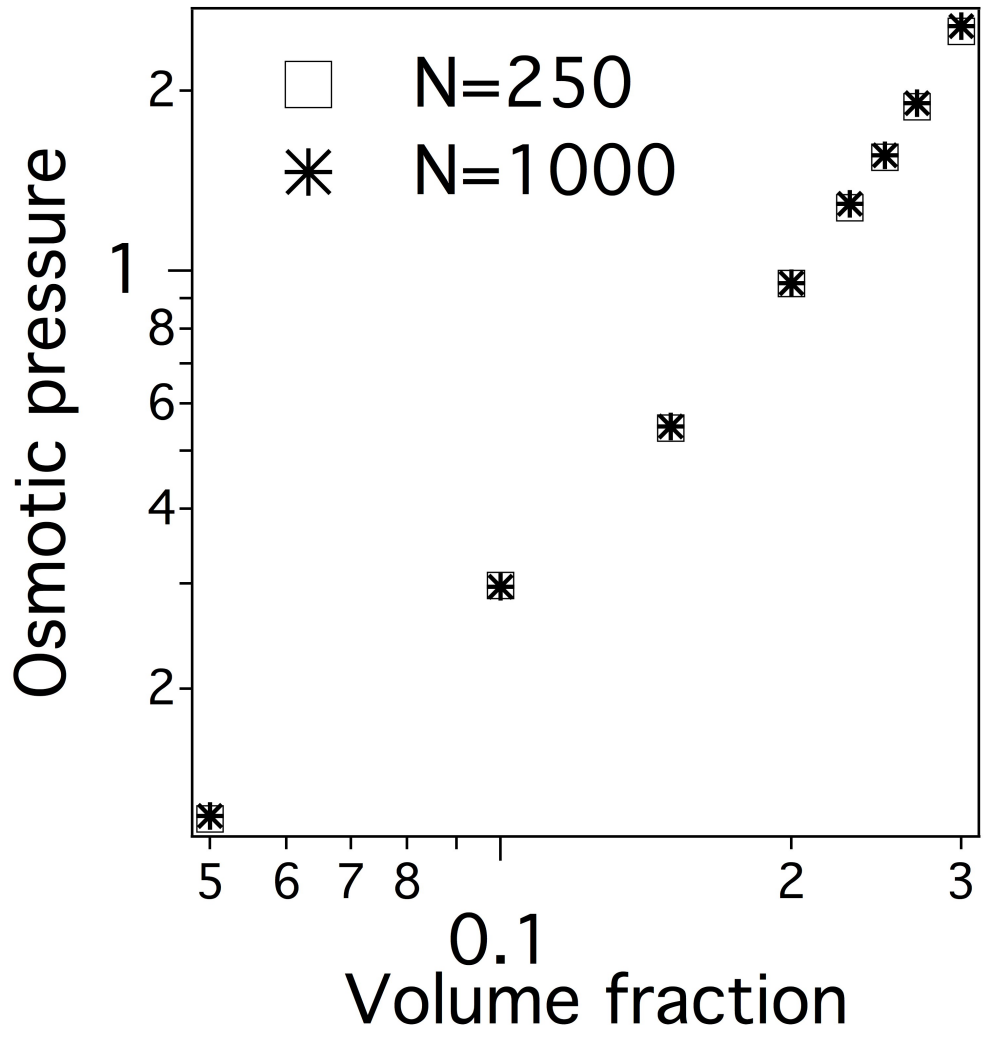

Figure 5.2: Variation of Osmotic pressure with the volume fraction for 250 and 1000 cubic particles.

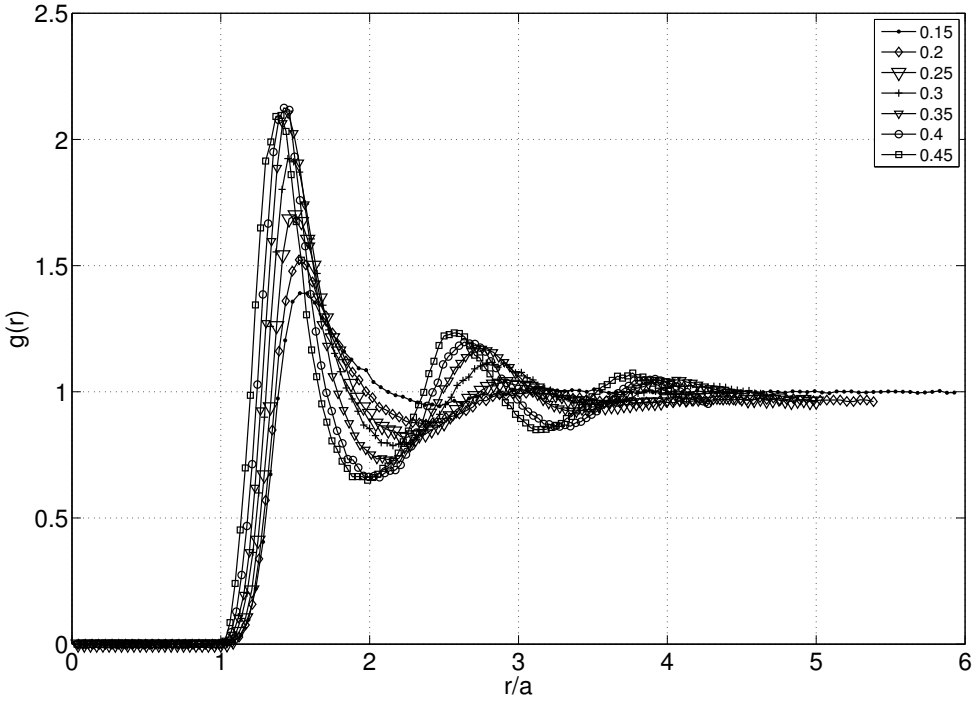

Figure 5.3: Equilibrium pair probability distribution of cubic particles as a function of volume fraction

The short-time translational self-diffusivity in the absence of hydrodynamic interactions is the average instantaneous particle mobility. This is always equal to D_t and does not vary with ϕ or Pe. The long-time translational self-diffusivity is defined as

$$D^{\infty}{}_{t} = \lim_{t\to\infty} \frac{1}{2} \frac{d(r(t) - x(0))^2}{dt} \tag{5.34}$$

These are calculated from mean-square displacement data evaluated during the simulation runs. At each time step, the mean-square displacements are calculated and is plotted with time. After long time, the mean-square displacement increases linearly with time. The slope of this line gives the long time diffusivity. The variation of translational diffusivity with the volume fraction is plotted in the figure 5.5. These results are compared with the translational diffusivities of spherical particles without hydrodynamic interactions. We found that the translational diffusivity for cubes and spheres are almost equal to each other.

In order to calculate the rotational diffusivity, we chose one of the normal vectors as the principle director (p_i). In a time step Δt, if the director rotates to another direction $p_i(t)$, we define a net rotational displacement vector $\delta\varphi_i$ as

$$\delta\varphi_i = \cos^{-1}(p_i(t).p_i(0))\epsilon_{ijk}p_j(t)p_k(0) \tag{5.35}$$

Thus the vector $\varphi_i(t) = \int_0^t \delta\varphi_i(x)dx$ defines the rotational trajectory of the particle. We calculated the rotational diffusivity as

$$D_r = \lim_{t\to\infty} \frac{1}{4t} < (\varphi(t) - \varphi(0))^2 > \tag{5.36}$$

It is important to note that $\varphi_i(t)$ is not a unit vector. This results in the finite value for the rotational diffusivity. Mazza et. al.. used similar procedure to calculate the rotational diffusivity of water molecules. [12]

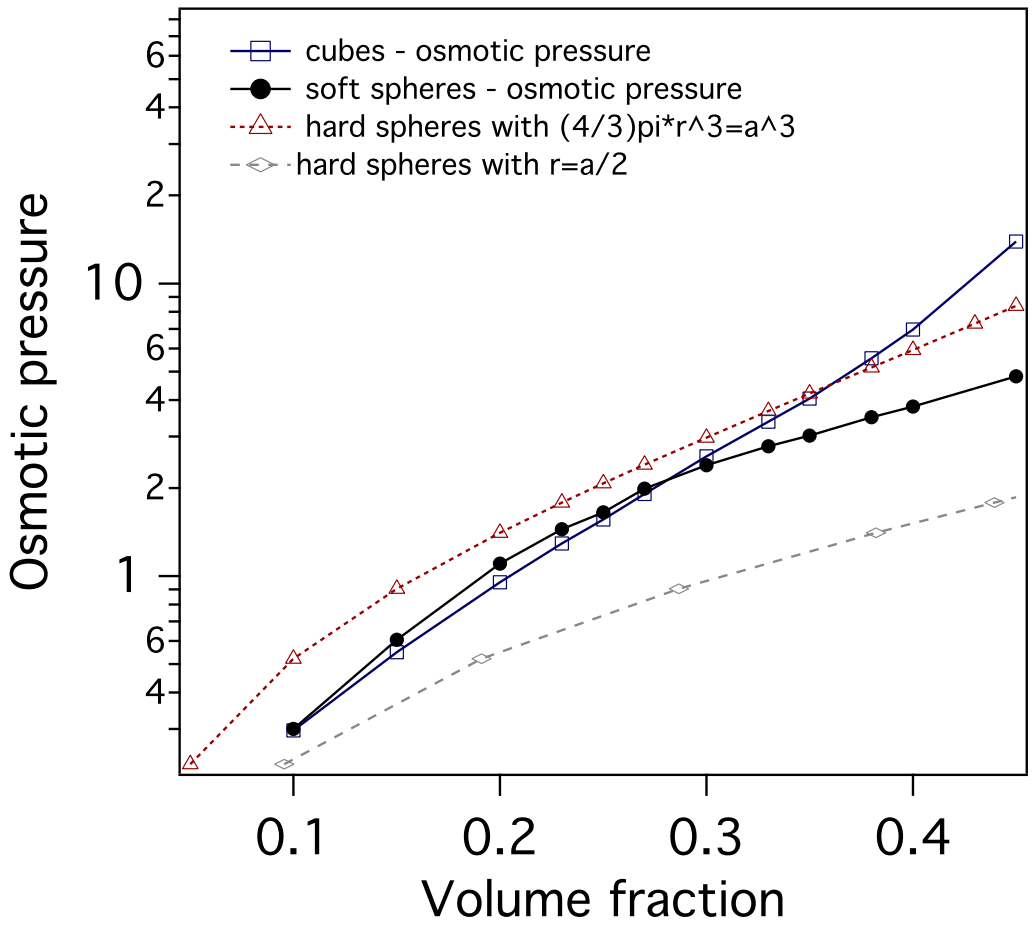

Figure 5.4: Variation of Osmotic pressure with the volume fraction of particles. The figure compares the values of osmotic pressure of cubic particles with that of equivalent spheres, inscribed spheres and inscribed spheres interacting through soft potential

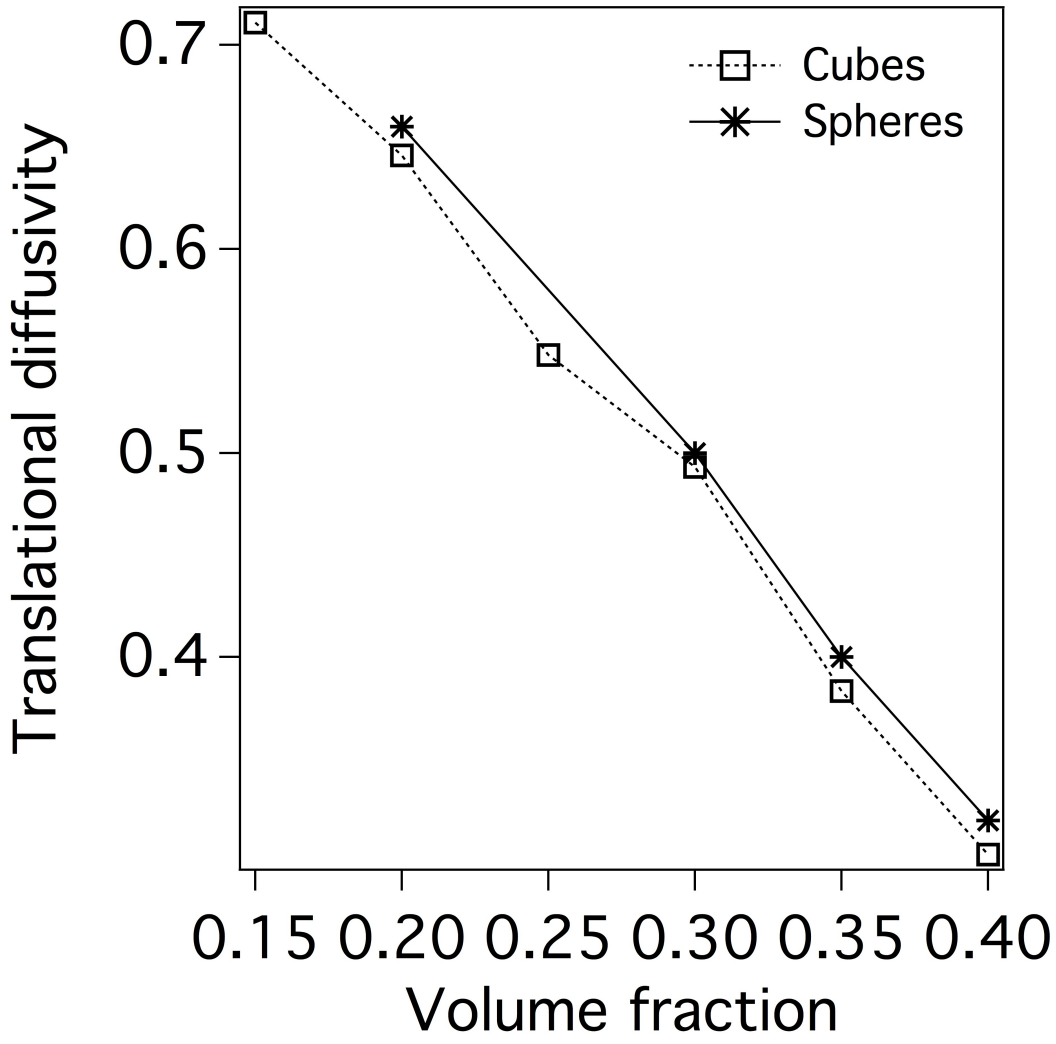

Figure 5.5: Variation of translational diffusivity with the volume fraction of cubes.

When the non-dimensional rotational and translational diffusivities are plotted on the same graph(figure 5.6), it is interesting to note that the rotational diffusivity decays faster than the translational diffusivity. The particles reach cubatic phase when the rotational diffusivity is almost zero and the translational diffusivity is still finite.

For non-zero *Pe* numbers, the anti-symmetric component of collisional stresses is non-zero and is given by

$$\Sigma_{ij}^{anti-sym} = \epsilon_{ijk} R_{\omega}(\Omega_k - \omega_k) \tag{5.37}$$

The variation of the angular velocity relative to the fluid with the *Pe* is plotted over a range of volume fractions. As it is clear from the figure 5.8 that the angular velocity($|\mathbf{\Omega}|/|\omega - 1|$) is almost constant with *Pe* and is only dependent on the volume fraction. Figure below shows the plot of mean $|\mathbf{\Omega}|/|\omega - 1|$ as a function of volume fraction (ϕ). It is clear that the relative angular velocity increases with the increase in volume fraction. This is due to the increase in the number of collisions between the cubic particles. As they collide more, the collision torque increases, as a result, relative angular velocity increases.

Zero shear viscosity is defined as the value of apparent viscosity in the limit of zero shear rate. This can be calculated using both directly and indirectly. The instantaneous stress at any time t is given by $\sigma(t)$. For equilibrium suspensions, the average value of σ_{xy} is zero. However, the shear stress autocorrelation function $< \sigma_{xy}(0\sigma_x y(t)) >$ has a finite value which depends on the microstructure of the suspension. The relaxation of these fluctuations is related to the zero shear viscosity given by the Green-Kubo relationship.

$$\eta_0 = \eta_{\infty} + \frac{V}{kT} \int_0^{\infty} < \sigma_{xy}(t)\sigma_{xy}(0) > dt \tag{5.38}$$

Here η_∞ is the high frequency viscosity contribution. When hydrodynamic interactions are neglected, the value of η_∞ is equal to the first order correction to the solvent viscosity $\eta(1 + 3.1\phi)$. We have also calculated the zero shear viscosity from the non-equilibrium suspensions. At low Pe, the suspensions were found to be Newtonian with constant viscosity. In this case, the viscosity evaluated at Pe =0.03 was considered as the zero shear viscosity of the medium.

Figure 5.9 shows the variation of zero shear viscosity with the volume fraction of cubic particles. Zero shear viscosity data for Brownian hard spherical particles was taken from Brady and Foss[10]. Zero shear viscosity for a suspension of cubes is marginally larger than the corresponding value for spherical particles at low volume fractions. However, when the volume fraction increases cubes were found to have a higher viscosity. Since cubic particles slowly lose their orientational freedom as the volume fraction increases, the system takes longer time to relax when compared with spherical particles.

5.3.2 Variation of viscosity at with *Pe*

Figure 5.10 shows results for the suspension viscosity as a function of Pe over a range of volume fraction between 0.1 to 0.4. The curves show shear thinning behavior that is characteristic of any Brownian suspensions. We have also compared the data with the corresponding viscosities for spheres. It is interesting to note that in the case of spherical particles, there is a abrupt drop in the viscosity at around $Pe = 100$. This matches with the structural transition from layered structure to a more ordered string phase. For cubic particles, viscosity is shear-thinning gradually and unlike spherical particles, we do not notice any sudden

drop in the viscosity. We have also found that the cubic particles do not phase transition to a string like structure and will always remain in a layered structure. This could be due to the fact that the rotating cubic particles will not allow them to reach a more ordered phase due to increase in the number of collisions between adjacent cubes.

The first and the second normal stress differences are given by

$$N_1 = < \sigma_{xx} > - < \sigma_{yy} > \tag{5.39}$$

$$N_2 = < \sigma_{yy} > - < \sigma_{zz} > \tag{5.40}$$

The normal stress differences normalized by $\eta\dot{\gamma}$ is plotted in the figure shown below. Both the normal stress difference decrease at low Pe and then remains constant.

5.4 Conclusions

Brownian dynamic simulations interactions for hard cubic particles in a suspension were carried out to understand stresses in the medium for both equilibrium and sheared suspensions. These numerical simulations include contact stresses developed between two randomly oriented cubes colliding with each other. Cubic particles can be assumed as spheres interaction with a soft potential, which produces the same probability distribution as cube at very low volume fractions. The rotational diffusivity for cubes decreases much more faster than the translational diffusivity. As the volume fraction increases, we may expect to see zero rotational diffusivity and non-zero translation diffusivity. This will happen when particles enter into cubatic phase. Further study needs to be carried

out to verify this result. The translational diffusivity for cubes is lower than the translational diffusivity for spheres. The edges and corners hinder the motion of cubic particles in isotropic phase which leads to lesser translational diffusivity. We also find that the zero shear viscosity for cubic particles is slightly larger than that of spherical particles and the difference between their viscosities increases as the volume fraction increases.

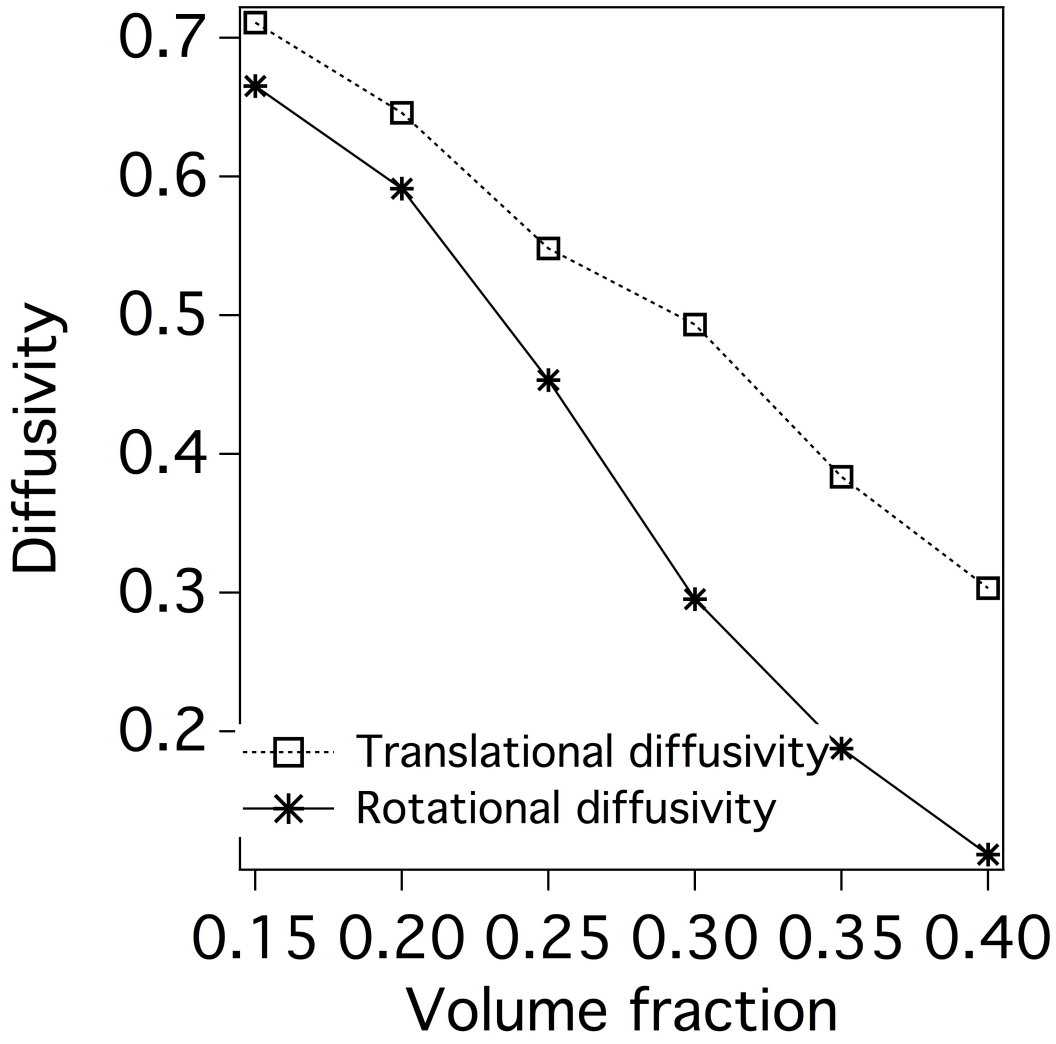

Figure 5.6: Comparison of rotational and translational diffusivity with the volume fraction of cubes.

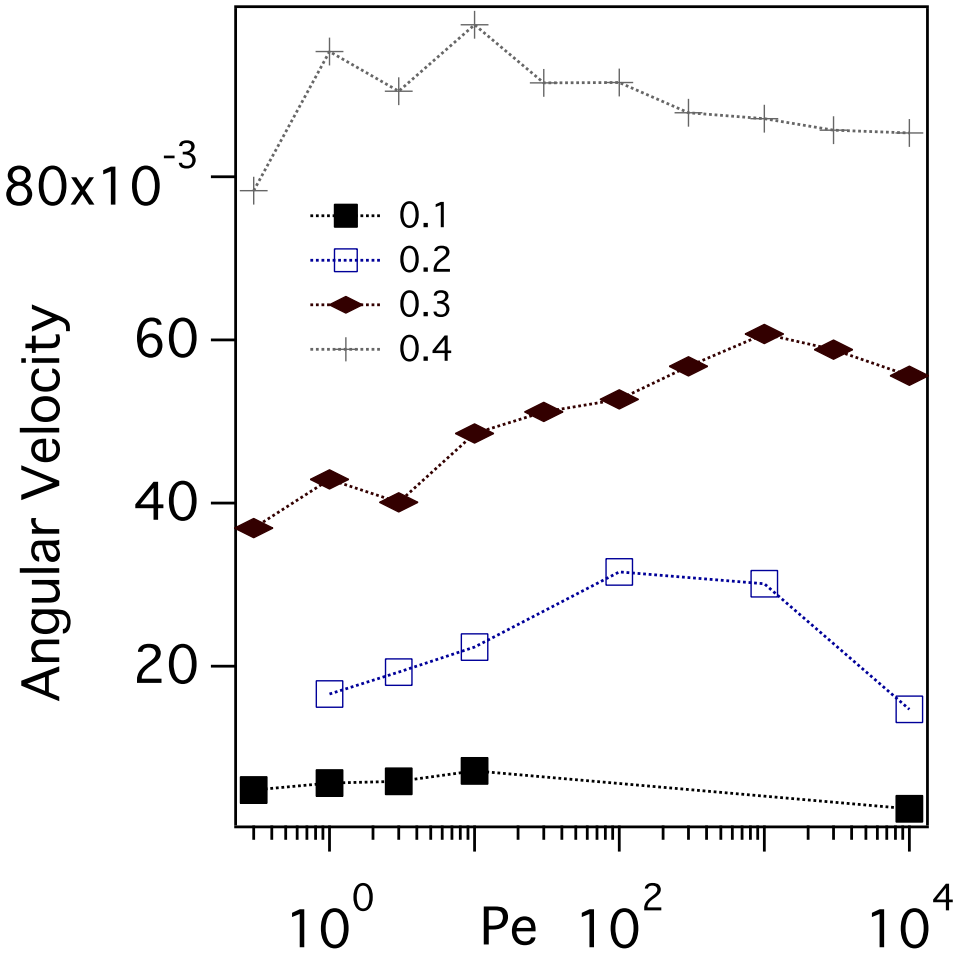

Figure 5.7: Dependence of angular velocity on the *Pe* for various volume fractions.

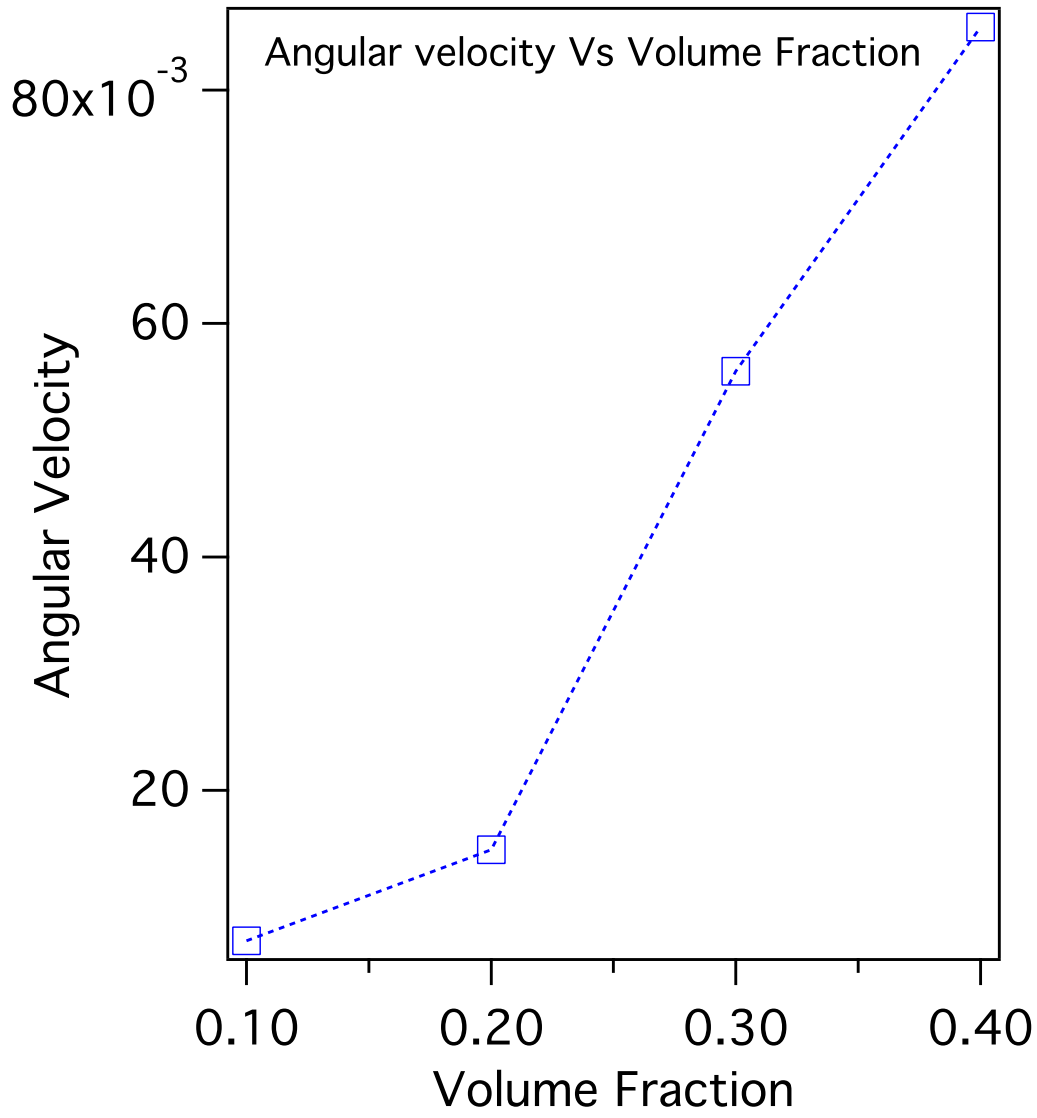

Figure 5.8: Variation of mean angular velocity with the volume fraction of the particles.

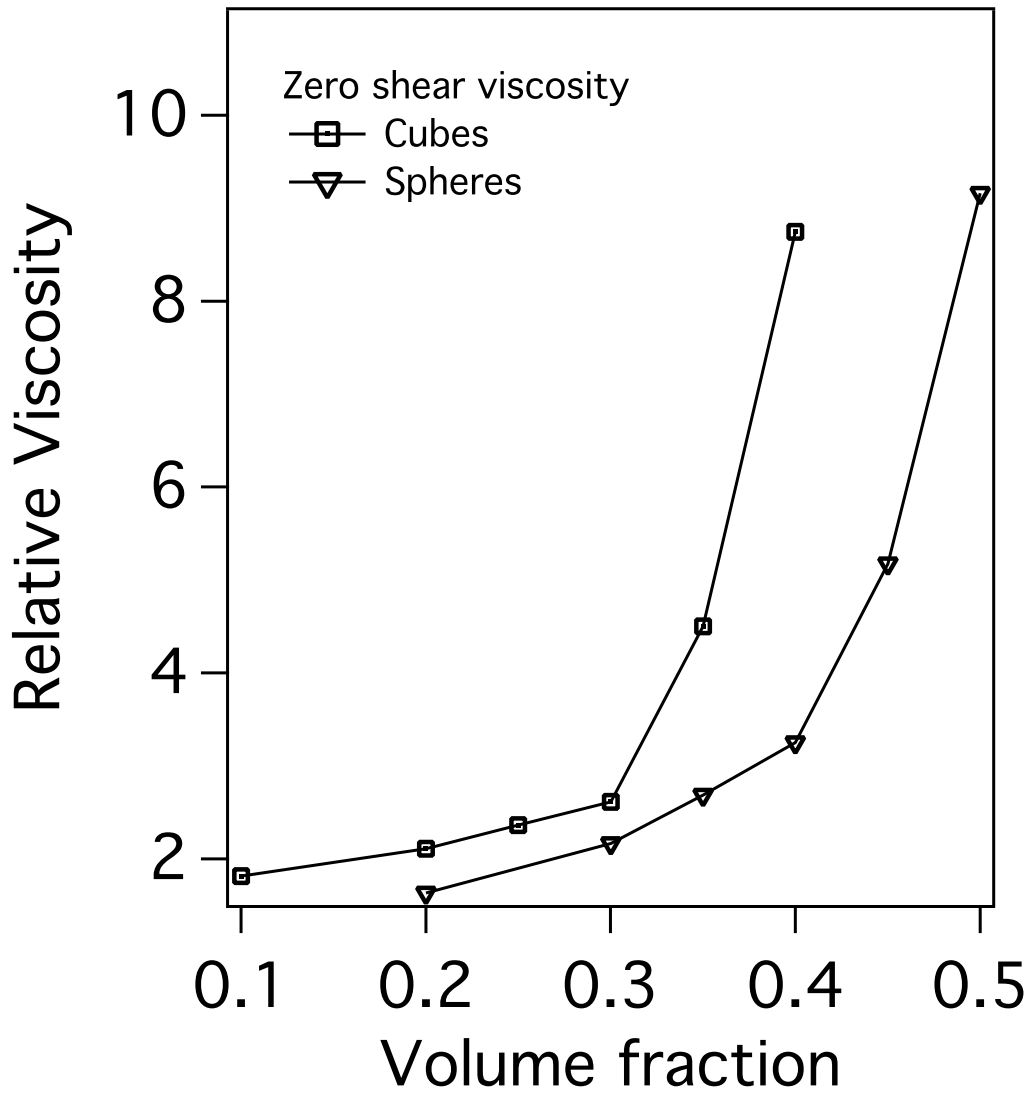

Figure 5.9: Dependence of zero shear viscosity on the volume fraction of cubes. The squares are the simulated data points for cubic particles. The spheres are the zero shear viscosity data for suspension of spheres.

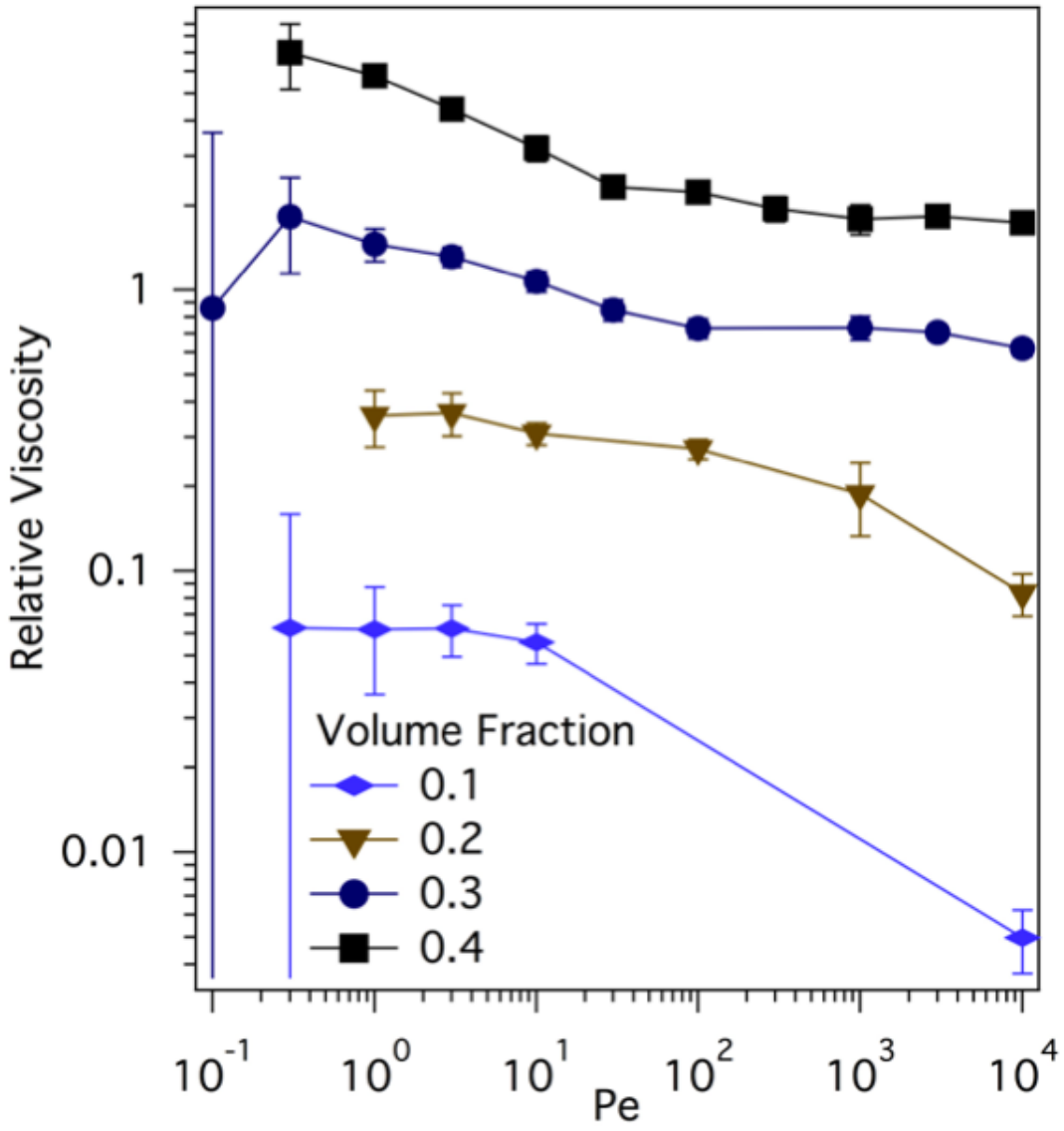

Figure 5.10: The plot shows the variation of collision contribution to the suspension viscosity with the Peclet number. At low volumes, we see a zero shear viscosity regime which matches well with the results obtained from Green-Kubo relationship

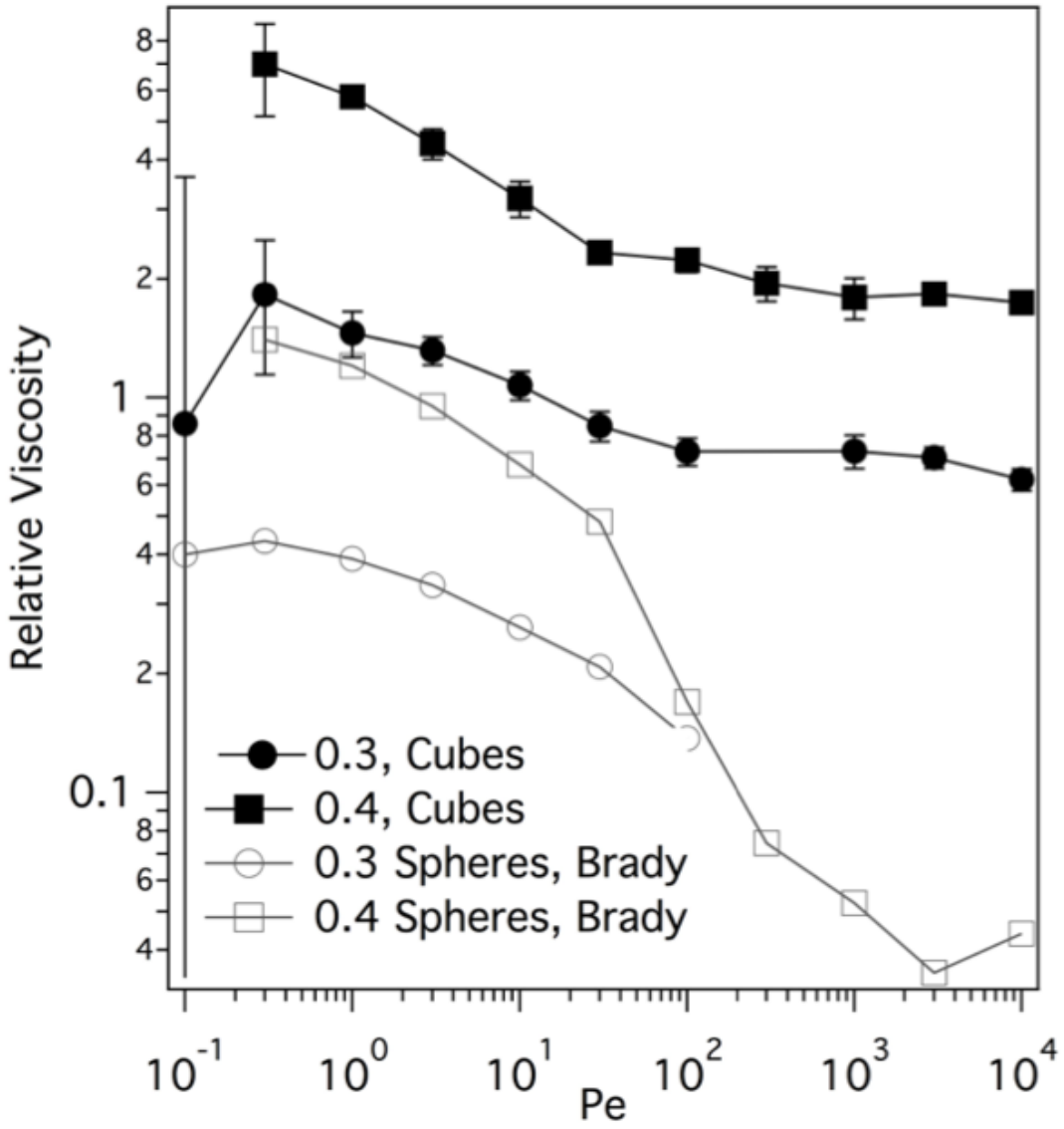

Figure 5.11: Comparison of collision contribution to viscosities for a suspension of spheres and cubes. At high shear rates, unlike spheres there is no sudden drop in the viscosity for cubic particle suspensions

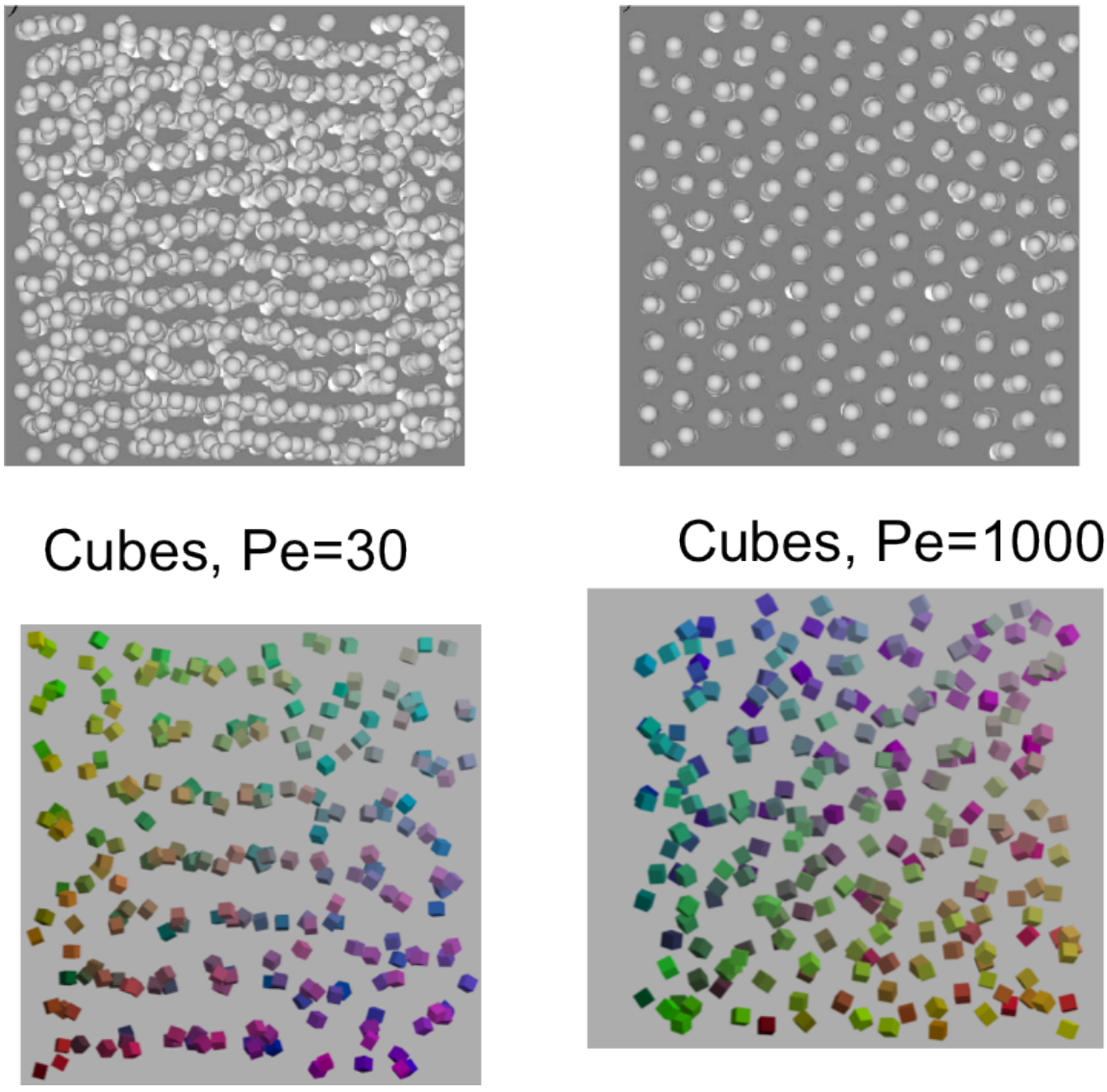

Figure 5.12: Comparison of snap shots of particle locations for spheres and cubes. The size of the particles was deliberately decrease for convenience

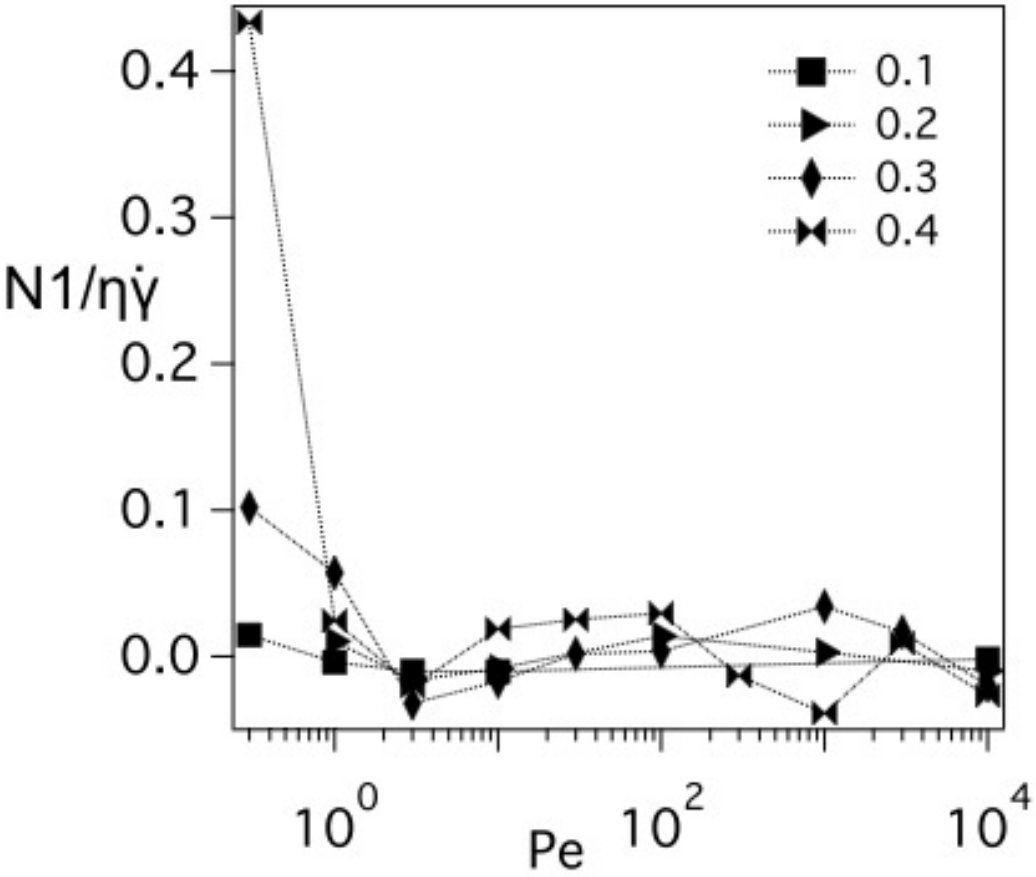

Figure 5.13: Non-dimensionalized first normal stress difference as a function of *Pe* and the volume fraction

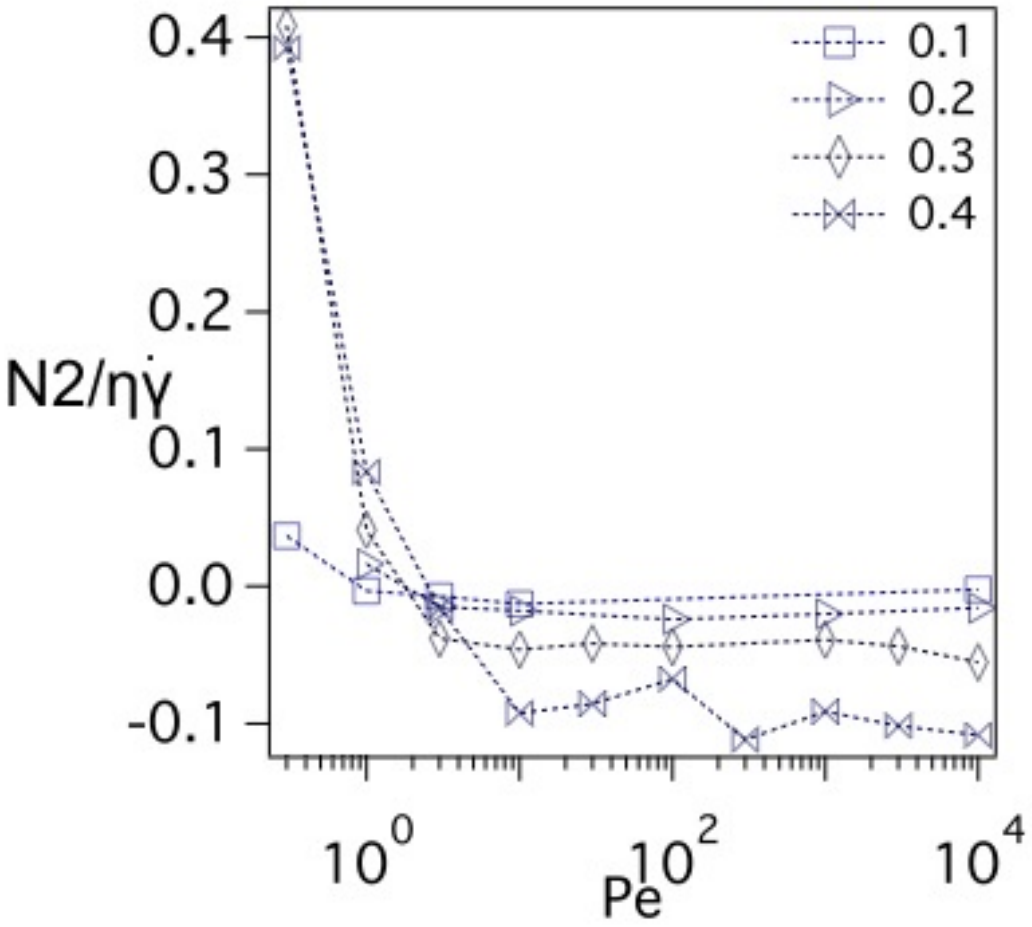

Figure 5.14: Non-dimensionalized second normal stress difference as a function of *Pe* and the volume fraction

BIBLIOGRAPHY

[1] A Einstein. *Investigation on the theory of the Brownian movement*. Dover Publications, 1956.

[2] W. B. Russel. *Colloidal Dispersions*. Cambdrige University Press, 1999.

[3] G. K. Batchelor. The stress system in a suspension of force-free particles. *Journal of Fluid Mechanics*, 41:545–570, 4 1970.

[4] Donald L. Ermak and J. A. McCammon. Brownian dynamics with hydrodynamic interactions. *Journal of Chemisty and Physics*, 69(4):1352, 1978.

[5] D.M Heyes and J.R. Melrose. Brownian dynamics simulations of model hard-sphere suspensions. *Journal of Non-Newtonian Fluid Mechanics*, 46:1, 1993.

[6] Weige Xue and Gary S. Grest. Shear-induced alignment of colloidal particles in the presence of a shear flow. *Physical Review Letters*, 64:419–422, 1990.

[7] SR Rastogi, NJ Wagner, and SR Lustig. Rheology, self-diffusion, and microstructure of charged colloids under simple shear by massively parallel nonequilibrium brownian dynamics. *Journal of Chemical Physics*, 104(22):9234–9248, 1996.

[8] L. Durlofsky, J. F. Brady, and G. Bossis. Dynamic simulation of hydrodynamically interacting particles. *Journal of Fluid Mechanics*, 180:21–49, 7 1987.

[9] David R. Foss and John F. Brady. Structure, diffusion and rheology of brownian suspensions by stokesian dynamics simulation. *Journal of Fluid Mechanics*, 407:167, 2000.

[10] David R. Foss and John F. Brady. Brownian dynamics simulation of hard-sphere colloidal dispersions. *Journal of Rheology*, 44(3):629, 2000.

[11] w Schaertl and h Sillescu. Brownian dynamics simulations of colloidal hard-spheres - effects of sample dimensionality of self-diffusion. *Journal of Statistical Physics*, 74(3-4):687–703, 1994.

[12] Marco G. Mazza, Nicolas Giovambattista, Francis W. Starr, and H. Eugene Stanley. Relation between rotational and translational dynamic heterogeneities in water. *Physical Review Letters*, 96:057803, 2006.

CHAPTER 6

CUBIC PARTICLES IN SUSPENSIONS: SYNTHESIS AND RHEOLOGY

6.1 Introduction

Nanoparticles with a spectrum of sizes, shapes, mass distributions (e.g. hollow, rattle-type, coreshell particles), and compositions are today routinely synthesized by a growing set of techniques involving wet chemtistry: solgel, solvothermal, ionothermal, and soft and hard templating approaches, to name a few [1, 2, 3, 4, 5]. It is now possible to synthesize nanoparticles of a specific shape and size in bulk quantities. It has been shown using theory and simulations that the shape plays an important role in the structure and rheology of the suspensions. The goal of this chapter is to measure the rheological properties of cubic particles in suspensions and compare these results with the theoretical results. Suspension of spherical particles were also prepared to compare them with suspension of cubic particles. This chapter is divided into two sections. The first section describes the procedures followed to synthesize cubic particles of desired sizes and chemistries. These particles are characterized to understand the kind of interactions that exists between particles. The second section deals with the measurement and analysis of rheological properties of the cubic suspensions. We then make a critical comparison between the results obtained from theory and experiments to gain more insights into the rheological properties.

6.2 Synthesis of cubic particles

Currently, cube shaped nanoparticles can be synthesized using many compounds, including but not limited to cobalt oxide(Co3O4), silver, gold, lead sulfide, sodium magnesium fluoride and copper sulfide [6, 7, 8, 9, 10, 11]. Most of the techniques used either use soft template method or sacrificial template method. Soft template method uses liquids or gases (medium) as templates while reactants act as templates in the sacrificial template method.

We have synthesized four different types of cubic particles: 1) Lead telluride nanocubes (PbTe, 10 nm) 2) Iron oxide nanocubes (Fe3O4, 20 nm) 3) Iron oxide nanocubes (Fe3O4, 100 nm) and 4) Manganese carbonate microcubes (MnCO3, 5.3 μm). Manganese carbonate microspheres (MnCO3, 4.8μm were also synthesized using the procedures described in the literature [12, 13, 14, 15]. Synthesis procedures and characterization of these particles is briefly described below. Unless otherwise stated, all the chemicals were purchased from Sigma-Aldrich and were used as received.

In order to synthesize PbTe nanocubes, 0.5 mmol of lead acetate trihydrate (99.99%), 1.0 mL of oleic acid (90%), and 10 mL of oleylamine (70%) were loaded into a 50 ml three-neck round-bottom flask equipped with a condenser. The mixture was then degassed by bubbling argon gas into the flask for an hour. The solution mixture was heated to 200 C with vigorous stirring. Once a clear light-yellow solution was formed, 0.5 mL of 1.0 M Tellirium in triocylphosphine (90%) was pre-pared and was rapidly injected into the system. The reaction was then stopped 1 min after the injection by quickly transferring the container to an ice bath. The synthesized nanocubes were isolated by precipitating them

from the reaction system using ethyl alcohol (200 proof) followed by repeated centrifugation. Standard size-selection post-treatment using a pair- solvent mixture of ethyl alcohol and anhydrous hexane (98.5%) to obtain PbTe nanocubes with narrow size distribution.

This approach leads to PbTe nanocubes with a mean side length of 10 nm. The images from transmission electron microscope shown in figure 6.1. These nanoparticles have very high surface areas and so they are covered with short oligomer chains to provide steric stabilization.

Fe_3O_4 nanocubes of size 20 nm were synthesized by mixing 0.5 mmol of Iron(III) acetyl acetonate $Fe(acac)_3$, 4 mmol of 1,2- hexadecandiol, 8 mmol of oleic acid, 2 mmol of oleyl amine, and 10 ml of benzyl ether was heated in a 100ml three neck flask. Initially, the solution mixture was degassed by bubbling Argon has into the mixture at 110C for about an hour. The temperature was then raised to 200C and maintained at this temperature for 30 minutes. The solution mixture was then heated to about 290C at a heating rate of 15C per minute. The temperature of the mixture was then maintained at this temperature for one hour. The solution mixture was then cooled down to room temperature, and the synthesize nanocubes were purifed by repeated centrifugation using ethanol.

During this reaction, oleic acid acts as a capping agent, since it binds itself to selective surface of the crystal. This is because the surface energies of facets differ from each other. As a result the nucleation growth is non-isotropic and leads to various shaped based on the binding preferences of oleic acid. By carefully controlling the temperature and the time of the reaction, which controls the nucleation and the growth dynamics, we can obtain narrowly dispersed cubic

particles.

The transmission electron microscope images are show in the figure 6.1. These particles also have short chain oleic acid chains attached on the surface. We have also synthesized cubic particles with polyethylene glycol chains attached on the surface by replacing the attached oleic acid chains with poly ethylene glycol trimethoxy silane (MW: 250). In the reaction, about 0.1 gms of purified oleic acid capped cubic particles were dispersed in 100 ml chloroform and about 0.2 gms of polyethylene glycol trimethoxy silane was added to the solution. The mixture was then heated at 40C, with closed cap for about 7 hours. The resultant mixture was then purified using repeated centrifugation to obtain poly ethylene glycol capped nanocubes.

100 nm Fe3O4 nanocubes are a soft ferrimagnetic particles, which were synthesized by mixing iron(III) acetylacetonate (0.71 g), oleic acid (1.13 g) and benzyl ether (10.4 g) in a 100 ml three neck flask. The mixture solution was degassed at room temperature for one hour using Argon gas. The solution mixture was then heated to 290 C at the rate 20 C/min under vigorous magnetic stirring. The reaction mixture was maintained at this temperature for thirty minutes. After cooling to room temperature, the solution was then centrifuged using a mixture of toluene and hexane to precipitate the Fe3O4 nanocubes. The separated precipitate was washed repeatedly using chloroform and hexane.

Both manganese carbonate cubes and spheres were synthesized using a simple mixing method. To synthesize cubic particles, 1 mmol of manganese sulfate and 10 mmols of ammonium sulfate were dissolved in 70 ml water. Also, 10 mmols of ammonium hydrogen carbonate was also dissolved in 70 ml of water in a separate beaker. About 7 ml of ethanol was added to the manganese

sulfate solution. The two solutions were mixed and aged for 7 hours in water bath maintained at 50C. The product obtained was separated using repeated centrifugation with water and ethanol. The final product was vacuum dried to get the desired microcubes.

Manganese carbonate microspheres were synthesized using a similar procedure. 1 mmol of manganese sulfate and 10 mmols of ammonium hydrogen carbonate were separately dissolved in 70 ml of water each. About 7 ml of ethanol was added to manganese sulfate solution. The two solutions were mixed at room temperature and the reaction was allowed for 3 hours. Microspheres were obtained by repeated centrifugation with water and ethanol.

The transmission electron microscope images for both spheres and cubes are shown below. Density is one of the important parameters which needs to be accurately calculated, since density is needed to convert weight fractions to volume fractions. We have used Anton-paar densitymeter to calculate its density of PbTe and Fe3O4 cubes. Known weight fractions of the PbTe particles were dispersed in chloroform and the overall density of the solution was measured. Assuming that there are no interactions between the solvent and the particles, the mixing is considered as an ideal mixing. Therefore $\rho_1 V_1 + \rho_2 V_2 = \rho_{eff}(V_1 + V_2)$. Here ρ_1 and ρ_2 are the densities of PbTe particles and chloroform respectively. V_1 and V_2 are the volumes of $PbTe$ and chloroform respectively. Since, we know the density of chloroform and the density of dispersed solution ρ_{eff}, we use the above mentioned relation to calculate the density of the particles. Using this procedure, the densities of PbTe (10 nm cubes) , Fe3O4 (20 nm cubes) and Fe3O4 (100 nm cubes) were found to be 6.6 gm/cc, 3.7 gm/cc and 4.1 gm/cc respectively. We have used 1ml and 5 ml pycnometer to measure the density of

manganese carbonate particles. We found that the density of microcubes is 3.2 gm/cc while for micospheres, the density is 3.0 gm/cc.

6.3 Rheological measurements for the suspensions of cubic nanoparticles

Polyethylene glycol (PEG) with molecular weight 400 was used as a suspending medium for Fe_3O_4 nanoparticles while PEG (MW 2000) was used for manganese carbonate particles. PEG is a clear liquid at room temperature which shows Newtonian behavior. Suspensions were made over a large range of volume fractions to study the variation of viscosity with the volume fraction. Anton-Paar MCR 501 rheometer was used to measure the viscosity of the suspensions. We have used cone-plate geometry with cone diameter 25 mm and 1^o cone angle at 30C for both MnCO3 cubes and spheres. The viscosities were measured between shear rate of $10s^{-1}$ and 100 s^{-1}. At these shear rates, the Pe ranges from 10^3 to 10^4.

The table below shows the various kinds of interaction forces that exists in these suspensions. They are all non-dimensionalized with respect to the viscous forces

Table 6.1: Comparison of interaction forces with respect to the viscous forces

Description	PbTe cubes (10nm)	Fe3O4 cubes (20nm)	Fe3O4 cubes (100nm)	MnCO3 cubes (5.4μm)	MnCO3 spheres (4.8μm)
Vanderwaals force (without retardation)	$0.07/Pe < F < 0.66/Pe$	$0.07/Pe < F < 0.66/Pe$	$0.07/Pe < F < 0.66/Pe$	$0.07/Pe < F < 0.66/Pe$	$0.07/Pe < F < 0.66/Pe$
Buoyancy	$10^{-3}/Pe$	$0.009/Pe$	$1.1/Pe$	$75/Pe$	$66/Pe$
Magnetic force	-	$O(10)/Pe$	$O(500)/Pe$	-	-
Shear rate for $Pe = 1$	$10^3 s^{-1}$	$125 s^{-1}$	$1 s^{-1}$	$10^{-7} s^{-1}$	$8 * 10^{-6} s^{-1}$

PbTe nanocubes are the most ideal hard cubic particles to study rheology. However, very small yields of the product limits the study to very dilute concentrations. Also, because of very small size of PbTe particles, it is difficult to reach high Pe. The magnetic interaction forces for iron oxide nanocubes are calculated by measuring the variation of magnetic moment with the applied magnetic field. The hysteresis loops for these two particles are clearly visible in the figure 6.2. It is clear that, even when there is no applied magnetic field, these nanoparticles may have non-zero magnetic moments which leads to magnetic interactions between the particles. These forces are large that they tend to form clusters at equilibrium. We would need to go to high Pe to start breaking these clusters. The rheology of these suspensions will mask the properties specific to the cube shape. As expected, (figure 6.3) the rheology of Fe_3O_4 cubic nanoparticle suspensions shows shear thinning behavior even at very low volume fractions. The viscosity of the suspension decreases as the clusters breakdown with the increase in shear. Manganese carbonate particles will sediment down in the suspension due to large buoyancy forces. We had over come this problem by

carrying out measurements at high *Pe* so that the particles are resuspended due to applied shear. We have assumed that manganese carbonate cubic particles as the hard cubes due to ease of synthesizing this product in required quantities. Manganese carbonate microspheres are similar in size and identical in chemistry. They were used to make comparisons between the rheological properties of spheres and cubes experimentally.

For $MnCO_3$ particles, Newtonian behavior is observed for all volume fractions less than 0.3. For volume fractions below 0.18, we have used quadratic fit for the variation of relative viscosity with the volume fraction as shown in the figure 6.4. Since the measured intrinsic viscosity, which is the first order correction was found to be 3.02 ± 0.329 which is very close to the theoretical prediction, we have fixed the first order coefficient as 3.1 and the ϕ^2 coefficient was calculated. This value was found to be 6.54 (shown in the figure 6.5). This is very close to 6.3, which is the ϕ^2 coefficient for Brownian spherical particles as calculated by Batchelor. The measurements were compared with the high shear viscosity results from Brownian dynamics simulations. Since, inter-particle hydrodynamic interactions were not considered, Brownian dynamics simulations regularly underestimates thevalue of relative viscosity.

Figure 6.6 below compares the viscosity for the suspension of manganese carbonate spheres with the cubes. We find that the viscosity for cubic particles is marginally higher than that of spherical particles at low volume fractions which is consistent with the Brownian dynamics simulation results. As the volume fraction increases, the difference between the viscosity for cubes and spheres appears to be increasing. Further study needs to be carried out to ascertain this trend.

6.4 Conclusions

This chapter addresses the synthesis and characterization of cubic particles. We have synthesized cubic particles of varying sizes (10nm to 5 micron sized cubes) and chemistries ($PbTe$,Fe_3O_4, and $MnCO_3$). Comparison of all the interparticle interactions was carried out. Manganese carbonate cubes and spheres were found to be ideal to study the rheology. Measurements were carried out at high Pe and Newtonian behavior was observed. The variation in the viscosity for manganese carbonate cubic particles was compared with both Brownian dynamics simulation results and with rheological measurements of manganese carbonate spheres. It was found that the results from the Brownian dynamics regularly underestimate the viscosity of the medium. This may be because hydrodynamic interactions were not considered in the Brownian dynamics simulations. The viscosities for cubic suspensions was observed to be marginally higher than spherical particle suspensions. Further study at higher volume fractions needs to be carried this effect.

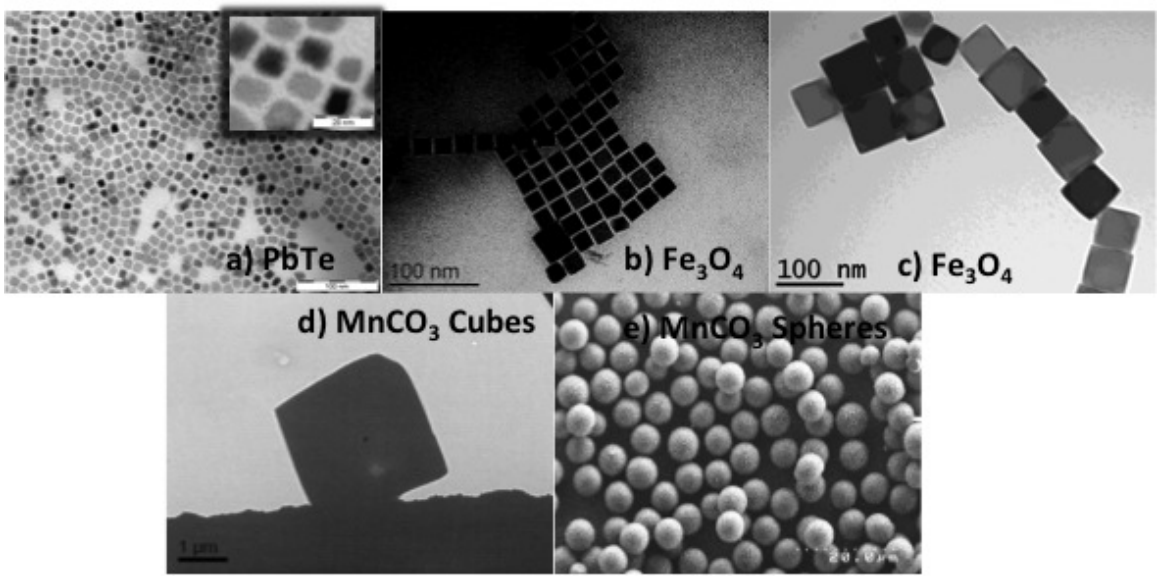

Figure 6.1: TEM images of (a) PbTe nanocubes 10 n, (b)Fe3O4 nanocubes- 20nm (c) Fe3O4 nanocubes- 100nm (d) MnCO3 microcubes MnCO3 microcubes 5.4 μm (e) MnCO3 microcubes MnCO3 microspheres 4.8μm

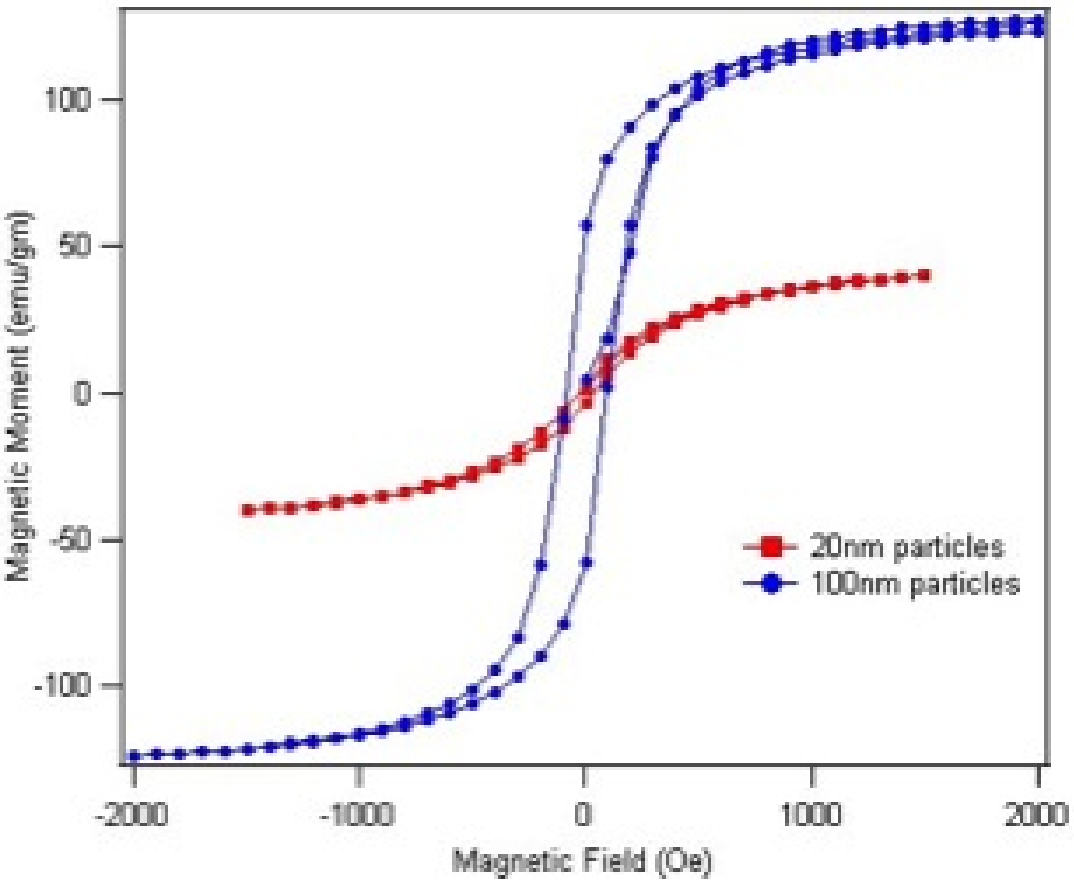

Figure 6.2: Variation of magnetic moment with applied magnetic field for Iron oxide nanoparticles (20 nm) and 100nm. The plot shows a hysteresis loop, indicating that the particles have a non-zero magnetic moment when there is no applied magnetic field. This leads to large magnetic interactions between particles. As a result, cubes tend to form clusters for low to moderate volume fractions

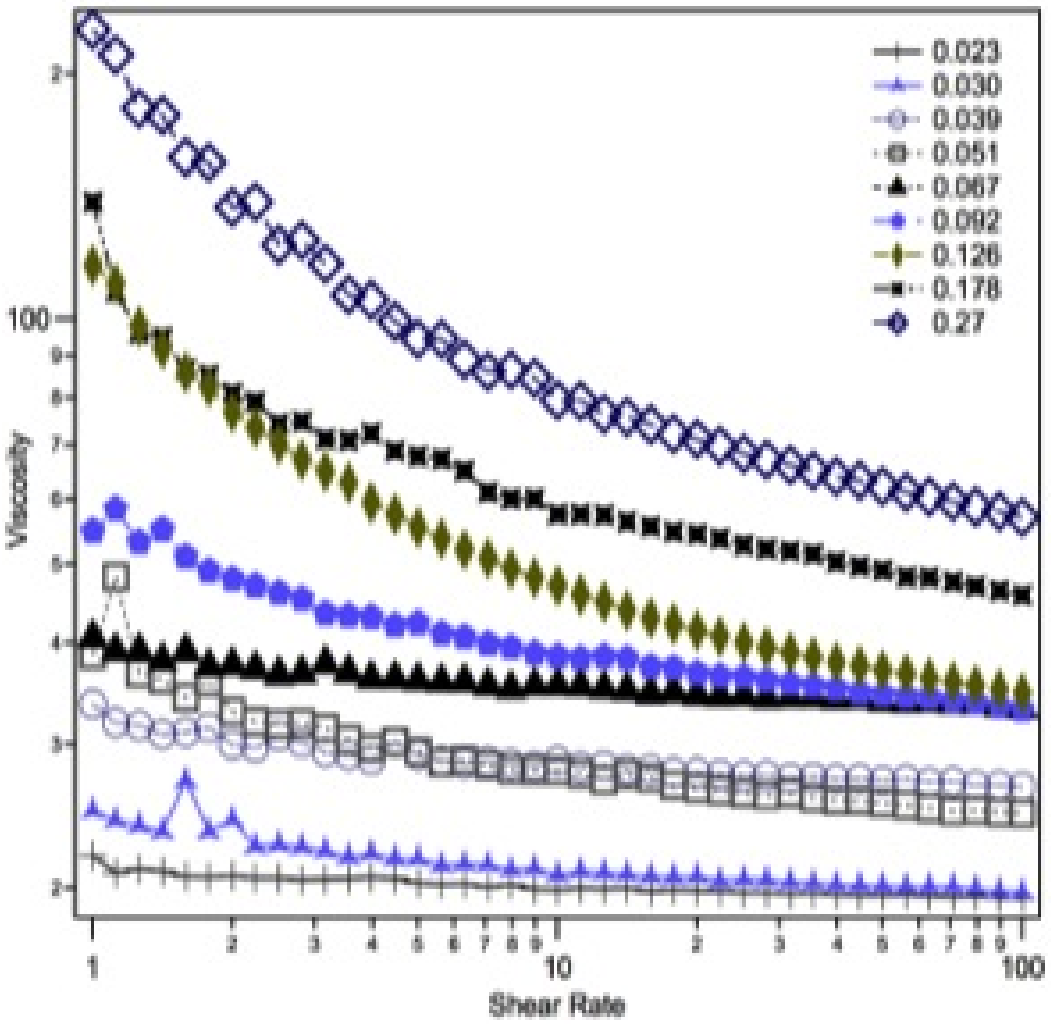

Figure 6.3: Relative viscosity as a function of volume fraction for the suspension of iron oxide nanoparticles (100nm). These materials show shear thinning behavior due to the breakdown of clusters with higher shear rates.

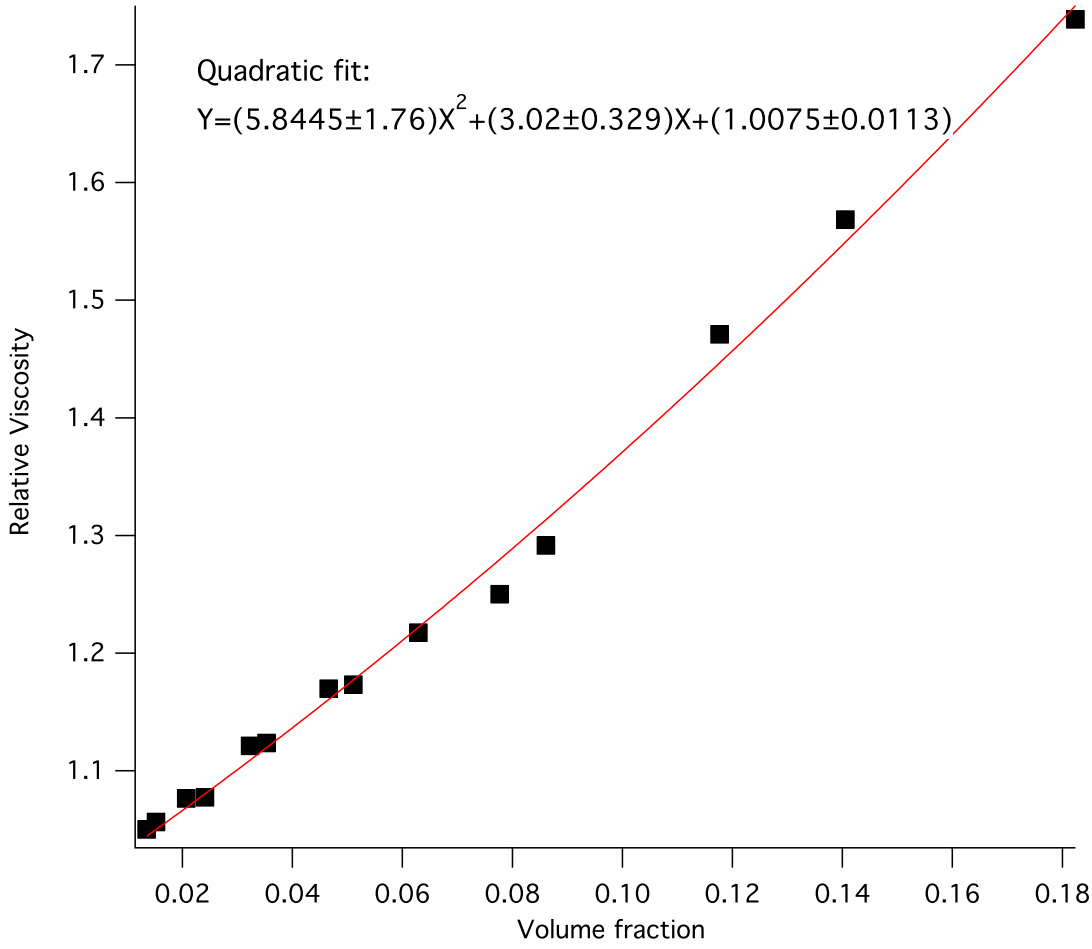

Figure 6.4: Relative viscosity of a suspension of manganese carbonate microcubes

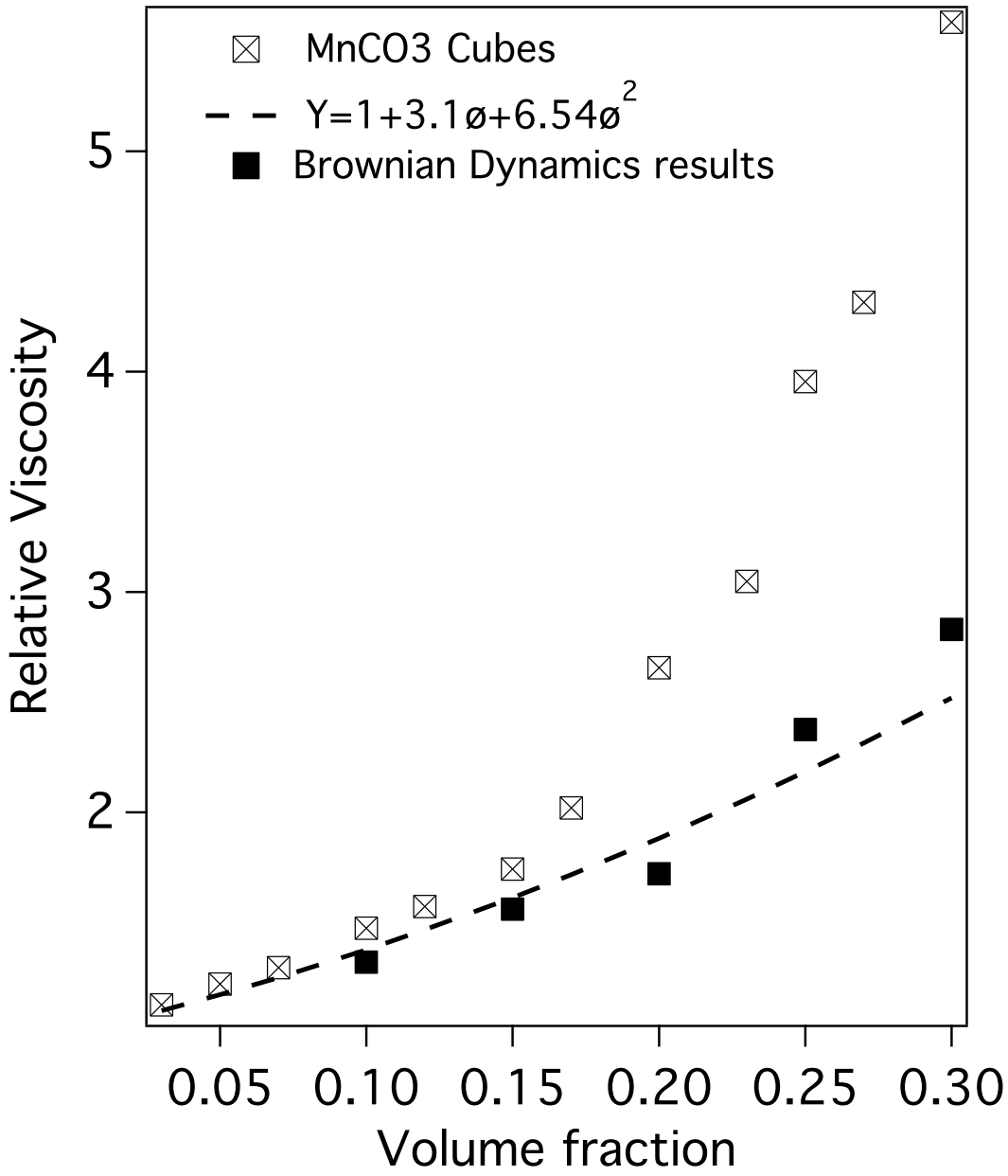

Figure 6.5: Relative viscosity of a suspension of manganese carbonate microcubes and its comparison with Brownian Dynamics results

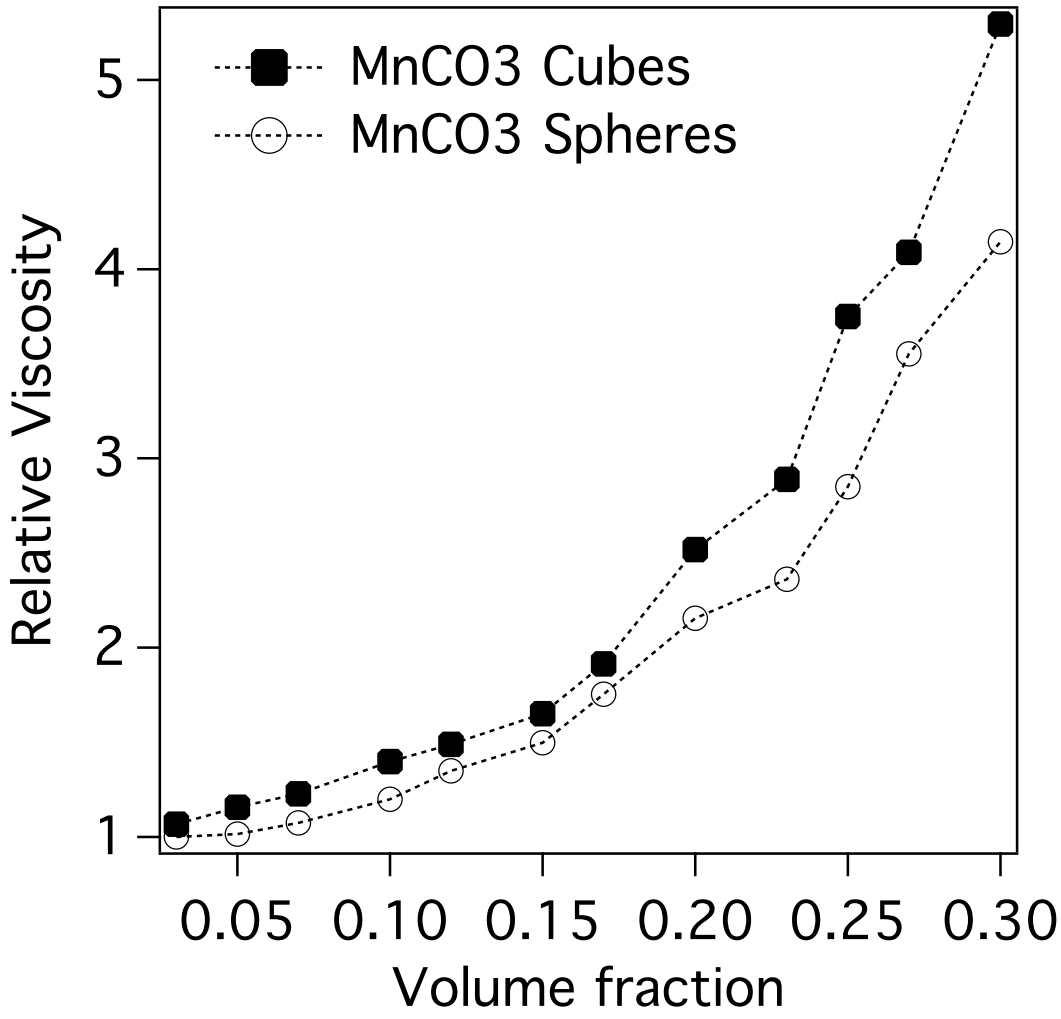

Figure 6.6: Comparison of relative viscosity for spheres and cubes

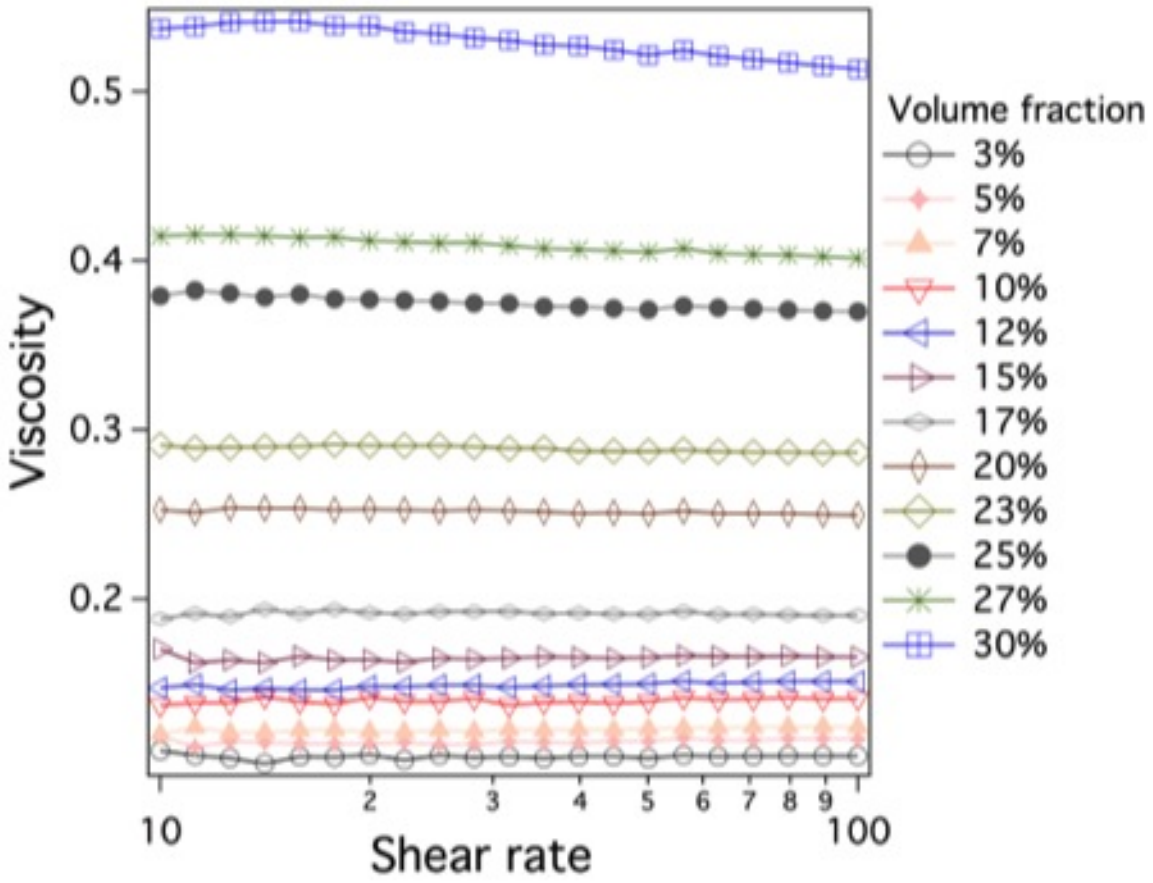

Figure 6.7: Flow curves for the suspension of manganese carbonate microcubes

BIBLIOGRAPHY

[1] L Manna, DJ Milliron, A Meisel, EC Scher, and AP Alivisatos. Controlled growth of tetrapod-branched inorganic nanocrystals. *Nature Materials*, 2(6):382–385, 2003.

[2] J. Park, K. J. An, Y. S. Hwang, J. G. Park, H. J. Noh, J. Y. Kim, J. H. Park, N. M. Hwang, and T. Hyeon. Ultra-large-scale syntheses of monodisperse nanocrystals. *Nature Materials*, 3(12):891–895, 2004.

[3] J. Joo, S. G. Kwon, J. H. Yu, and T. Hyeon. Synthesis of zno nanocrystals with cone, hexagonal cone, and rod shapes via non-hydrolytic ester elimination sol-gel reactions. *Advanced Materials*, 17(15):1873, 2005.

[4] Clemens Burda, Xiaobo Chen, Radha Narayanan, and Mostafa A. El-Sayed. Chemistry and properties of nanocrystals of different shapes. *Chemical Reviews*, 105(4):1025–1102, 2005.

[5] G. M. Whitesides and M. Boncheva. Beyond molecules: Self-assembly of mesoscopic and macroscopic components. *Proceedings of the National Academy of Sciences of the United States of America*, 99(8):4769–4774, 2002.

[6] Q.; X. Shen; Chen and H. Gao. Formation of solid and hollow cuprous oxide nanocubes in water-in-oil microemulsions controlled by the yield of hydrated electrons. *Journal of Colloid and Interface Science*, 312:272, 278 2007.

[7] J. Feng. Size controlled growth of co3o4 nanocubes, in chem. mater. 2003, american chemical society. *Chem. Mater*, page 2829, 2003.

[8] He. at. al. Co3o4 nanoboxes: Surfactant-templated fabrication and microstructure characterization. 18(1078), 2006.

[9] Im. S. H. Large-scale synthesis of silver nanocubes: The role of hcl in promoting cube perfection and monodispersity13. *Angewandte Chemie International Edition*, 18(1078), 2005.

[10] 14.Sun Y.; B.T. Mayers and Y. Xia. Template-engaged replacement reaction: A one-step approach to the large-scale synthesis of metal nanostructures with hollow interiors. nano letters, 2002. 2(5): p. 481-485. *Nano Letters*, 2(5):481, 2002.

[11] J. Xie, C. Xu, N. Kohler, Y. Hou, and S. Sun. Controlled pegylation of monodisperse fe3o4 nanoparticles for reduced non-specific uptake by macrophage cells. *Advanced Materials*, 19(20):3163–3166, 2007.

[12] Jun Zhang, Amar Kumbhar, Jibao He, Narayan Chandra Das, Kaikun Yang, Jian-Qing Wang, Howard Wang, Kevin L. Stokes, and Jiye Fang. Simple cubic super crystals containing pbte nanocubes and their core?shell building blocks. *Journal of the American Chemical Society*, 130(45):15203–15209, 2008.

[13] D. Kim, N. Lee, M. Park, B. H. Kim, K. An, and T. Hyeon. Synthesis of uniform ferrimagnetic magnetite nanocubes. *Journal of the American Chemical Society*, 131(2):454, 2009.

[14] H. T. Yang, T. Ogawa, D. Hasegawa, and M. Takahashi. Synthesis and magnetic properties of monodisperse magnetite nanocubes. *Journal of Applied Physics*, 103(7), 2008.

[15] Jinbo Fei; Yue Cui; Xuehai Yan; Wei Qi; Yang Yang; Kewei Wang; Qiang He and Junbai Li. Controlled preparation of mno2 hierarchical hollow nanostructures and their application in water treatment. *Advanced Materials*, 20(452), 2008.